

Advances in Development of Novel Ultra-High Performance Concrete

Yu Su

Master of Engineering Science (Civil & Structural)

Thesis submitted for the degree of Doctor of
Philosophy at The University of Adelaide, Australia

The School of Civil, Environmental and
Mining Engineering

February 2017

TABLE OF CONTENTS

TABLE OF CONTENTS	I
LIST OF FIGURES	III
LIST OF TABLES	V
ABSTRACT	1
STATEMENT OF ORIGINALITY	3
LIST OF PUBLICATIONS	4
ACKNOWLEDGEMENTS	5
CHAPTER 1: INTRODUCTION	6
BACKGROUND	6
RESEARCH GOALS	10
OUTLINE.....	11
REFERENCES	12
CHAPTER 2: INFLUENCES OF NANO-PARTICLES ON DYNAMIC STRENGTH OF ULTRA-HIGH PERFORMANCE CONCRETE	16
ABSTRACT	16
2.1 INTRODUCTION	17
2.2 UHPC COMPOSITION	19
2.3 STATIC TESTS.....	21
2.3.1 Uniaxial compression test.....	21
2.3.2 Split tensile tests	23
2.4 SHPB TEST	24
2.4.1 Test apparatus	25
2.4.2 Equilibrium check.....	27
2.4.3 Compression test results	28
2.4.4 Split tensile results.....	32
2.5 MICROSCOPY ANALYSIS.....	36
2.5.1 SEM analysis of UHPC after SHPB split tensile tests	37
2.5.2 X-Ray Fluorescence (XRF) and Diffraction (XRD) Analysis	39
2.5.3 Influence of nano additives on the properties of UHPC.....	40
2.6 CONCLUSIONS	42
REFERENCE	42
CHAPTER 3: EFFECTS OF STEEL FIBRES ON DYNAMIC STRENGTH OF UHPC	47
ABSTRACT	47
3.1 INTRODUCTION	47
3.2 UHPC SAMPLE PREPARATION	50
3.3 STATIC TESTS.....	53
3.3.1 Uniaxial compression test.....	53
3.3.2 Split tensile test.....	56
3.4 SHPB TESTING PROGRAM	58
3.4.1 SHPB – Compression	61
3.4.2 SHPB – Tension	65
3.5 CONCLUSIONS	68

ACKNOWLEDGEMENTS.....	69
REFERENCES	69
CHAPTER 4: DEVELOPMENT OF NOVEL ULTRA-HIGH PERFORMANCE CONCRETE: FROM MATERIAL TO STRUCTURE	72
ABSTRACT	72
4.1 INTRODUCTION	73
4.2 EXPERIMENTAL PROGRAM.....	75
4.2.1 Materials	75
4.2.1.1 Mix design.....	76
4.2.2 Material Testing.....	77
4.2.2.1 Compressive testing	78
4.2.2.2 Flexural Tensile Tests	78
4.3 RESULTS AND DISCUSSIONS.....	79
4.3.1 Compressive tests	79
4.3.1.1 Results from compression tests	80
4.3.2 Flexural Tensile Tests.....	83
4.4 MICROSCOPY ANALYS	87
4.5 LABORATORY AND FIELD BLAST TESTS ON UHPC COMPONENTS	87
4.5.1 Specimen geometry	88
4.5.2 UHPC component subjected to static bending	88
4.5.3 UHPC component subjected to blast loads.....	91
4.6 CONCLUSIONS	94
ACKNOWLEDGEMENTS.....	95
REFERENCES	95
CHAPTER 5: MESOSCALE STUDY OF NOVEL ULTRA-HIGH PERFORMANCE CONCRETE UNDER STATIC AND DYNAMIC LOADS.....	99
ABSTRACT	99
5.1 INTRODUCTION	100
5.2 MATERIALS AND SINGLE FIBRE PULL-OUT TEST	102
5.2.1 Single fibre full out test	103
5.2.2 Numerical study of single fibre pull out test and model validation.....	106
5.2.2.1 Material model	106
5.2.2.2 Contact algorithm.....	107
5.2.2.3 Contact parameters and modelling results	109
5.3 STATIC SPLIT TENSION TEST	110
5.4 SPLIT HOKINSON TENSION TEST	113
5.4.1 SHPB test setup	113
5.4.2 Numerical study.....	115
5.5 CONCLUSION.....	122
REFERENCES	122
CHAPTER 6: CONCLUDING REMARKS AND SUGGESTIONS TO FUTURE STUDY	125
6.1 MAJOR FINDINGS	125
6.2 FUTURE WORKS	126

LIST OF FIGURES

Figure 1: Testing set-up for compression tests of cubic specimens.....	22
Figure 2: Stress-strain curves from quasi-static compressive tests.....	22
Figure 3: Split tensile tests.....	23
Figure 4: SHPB experimental system.....	25
Figure 5: Typical waveform of compression test.....	26
Figure 6: Stress equilibrium checks.....	27
Figure 7: Failure patterns of specimens with different nano materials.....	28
Figure 8: Comparison of stress-strain curves at different strain rates of different nano particles.....	29
Figure 9: Dynamic strength of UHPC under various strain rates.....	30
Figure 10: Comparison of DIF curves between NSC and UHPC.....	31
Figure 11: SHPB split tensile test.....	32
Figure 12: High speed camera results of sample damage.....	34
Figure 13: Comparison of DIF curves between NRC and UHPC.....	35
Figure 14: Dynamic increase factors influenced by the volume of Nano-CaCO ₃ in Split Tension SHPB tests.....	36
Figure 15: Pictures of motor matrix and ITZ from SEM analysis.....	38
Figure 16: XRD analysis of UHPC with and without nano additives.....	40
Figure 17: Different types of steel fibres.....	52
Figure 18: Concrete wooden moulds.....	53
Figure 19: Testing set-up for compression tests of cubic specimens.....	54
Figure 20: Stress-strain curves from quasi-static compressive tests.....	54
Figure 21: Influence from fibre aspect ratio on UHPC compressive strength.....	55
Figure 22: Compressive stress-strain curves for different fibre volume fractions.....	56
Figure 23: Split tension tests.....	57
Figure 24: Stress-strain curves from static split tensile tests.....	57
Figure 25: Tensile strength of UHPC with different fibre volume fractions.....	58
Figure 26: SHPB experimental system.....	59
Figure 27: Typical waveform of compression test.....	59
Figure 28: Stress equilibrium checks.....	60
Figure 29: Failure patterns of different type fibre.....	61
Figure 30: Comparison of stress-strain curves at different strain rates of different type fibre.....	62
Figure 31: Strain rate-stress curves of UHPC with various types of fibres.....	63
Figure 32: Dynamic increase factor curves of UHPC with various types of fibres.....	63
Figure 33: Dynamic increase factors of UHPC and normal strength concrete.....	65
Figure 34: Damage modes of UHPC specimens under SHPB tension test.....	67
Figure 35: Dynamic increase factors of UHPC with different types of fibres in SHPB tests.....	67
Figure 36: Dynamic increase factors influenced by the volume of MF15 in Split Tension SHPB tests.....	68
Figure 37: Different types of steel fibres.....	75
Figure 38: Testing set-up for compression tests of cubic specimens.....	78
Figure 39: Setup of the flexural tensile tests.....	79
Figure 40: Failure of specimens from the compression tests.....	80

Figure 41: Comparison of compressive stress-strain curves of UHPC specimens (1 Vol-% TF and 2 Vol-% TF) with mixtures of (a) Nano-CaCO ₃ , (b) Nano-Al ₂ O ₃ (c) Nano-TiO ₂ and (d) Nano-SiO ₂	82
Figure 42: Failure modes of the UHPC specimens in flexural tension tests	84
Figure 43: Flexural tensile tests results.....	84
Figure 44: Pictures of mortar matrix from SEM analysis.....	87
Figure 45: Specimen configuration and reinforcement	88
Figure 46: Instrumentation and setup in the static bending tests	89
Figure 47: Crack propagation on the UHPC component under bending.....	90
Figure 48: Load deflection curve	91
Figure 49: Field blast test setup	92
Figure 50: Blast pressure time-histories	93
Figure 51: Structural column performance after field tests	94
Figure 52: Setup of fibre pull-out test.....	104
Figure 53: Load versus end-slip curves for different fibre embedding depths.....	104
Figure 54: General fibre pull-out load versus end slip curve.....	105
Figure 55: Fictitious spring between fibre and concrete matrix	107
Figure 56: Bond shear stress-slip relationship for the one-dimensional slide line model	108
Figure 57: Comparison between test and simulation.....	110
Figure 58: Split tensile tests.....	111
Figure 59: 3D mesoscale model establishment.....	111
Figure 60: Comparison of the damage mode.....	112
Figure 61: Split stress - Displacement curve	112
Figure 62: SHPB split tensile test setup.....	113
Figure 63: Set-up for SHPB split tension test.....	114
Figure 64: Finite element model of SHPB split tensile test.....	115
Figure 65: Dynamic Increase Factor (DIF) for the tension strength of different concretes and UHPC in comparison	117
Figure 66: Comparison of stress histories from test and simulation.....	118
Figure 67: Comparison of stress-time curves obtained in the test and 3D Mesoscale model	119

LIST OF TABLES

Table 1: Mix proportions of different UHPC formula (unit: kg)	20
Table 2: Experimental results of different formula UHPC under static load	23
Table 3: Static split tensile strength of different UHPC	23
Table 4: Number of SHPB compression and split tensile tests	24
Table 5: Material semi-quantitative analysis from XRF for UHPC with nano additives.....	39
Table 6: Calcium Hydroxide (CH) measurement based on XRD analysis at 28 days	41
Table 7: Calcium Hydroxide (CH) measurement based on XRD analysis at 28 and 500 days	42
Table 8: Mix proportion of UHPC (unit: kg).....	51
Table 9: Material Properties of Fibres	52
Table 10: Experimental results of different formula UHPC under static compressive load ...	56
Table 11: Split tensile strength of different formula UHPC under static load.....	58
Table 12: Material properties of steel fibres	76
Table 13: Mix proportions of UHPC (unit: kg/m ³).....	77
Table 14: Compression strength of UHPC with different nano-additives (unit: MPa)	81
Table 15: Compression strain energy of UHPC with nano-additives (unit: MJ/m ³)	82
Table 16: Flexural tensile testing results (unit: MPa).....	85
Table 17: Fracture energy of UHPC with different nano-particles (unit: J/m ³).....	86
Table 18: Mix proportions of different UHPC formula (unit: kg)	103
Table 19: Parameters used in numerical model	106
Table 20: Parameters used in the contact definition	110
Table 21: Comparison of simulation results with high speed camera observation.....	120
Table 22: Crack and axial force development in the numerical model	121

ABSTRACT

The rising of terrorism activities has promoted fast development of new construction materials to enhance the resistance and resilience of buildings and infrastructure against blast loads. As a notable representative, ultra-high performance concrete (UHPC) has now been widely investigated by government agencies and universities. UHPC inherits positive aspects of ultra-high strength concrete (UHSC) and it is equipped with improved ductility as a result of fibre addition. These features make it an ideal construction material for bridge decks, storage halls, thin-wall shell structures, and other infrastructure against seismic, impact and blast loads.

In the thesis, development of novel UHPC material is presented. The new concrete material is distinguished from previous development by the inclusion of the nanoparticles. It was noticed that addition of nanoscale size particles results in significantly improved material properties without much change of the material composition. The present study focuses on influence of fibre material addition and nanomaterial addition on mechanical properties of UHPC material. In total, three kinds of steel fibre material with varying volume fraction are considered in the material design, in combination with four different nano materials at varying weight dosages. Discussion is carried out on fibre material geometry and fraction as well as nano particle effect.

Static material tests are carried out to understand material strength and ductility. Uniaxial compressive tests and flexural tensile tests reveal the exceptional material strength, ductility as well as energy absorption capability. Since the material aims at improving the structural performance under extreme loading conditions, dynamic material properties are also of significant importance. Split Hopkinson Pressure Bar (SHPB) tests are conducted on UHPC samples, dynamic compression tests and split tensile tests are studied and compared with static material strength to obtain the dynamic increase factor which is critical in the design of material and structures against dynamic loads.

All the above tests can be used to qualitatively and quantitatively examine the material performance with nano material and steel fibre material addition at macroscale. To further study the influence of these materials, microscopy analysis was conducted to provide explanation of macroscopic failure phenomenon at micro-scale. Morphology of the samples was observed by Scanning Electron Microscopy (SEM). X-Ray Diffraction (XRD) instrument was used for phase analysis and semi-quantitative analysis. Elemental analysis

was conducted by X-Ray Fluorescence (XRF). In SEM tests on post-damage UHPC samples, different damage modes at ITZ are identified, XRD and XRF analysis confirmed the filling and pozzolanic effect of nano particles addition.

In most cases, UHPC material can be treated as homogeneous at macroscopic scale, when observed at a smaller length scale, UHPC is heterogeneous and consists of constituents including aggregate, CH crystals, C-S-H gel, water and fibre material. It is impractical to consider all the phases in the microstructure of SFRC. In general, to investigate the interfacial transition zone (ITZ) effect on the fibre bonding properties, UHPC is described as multi-phase material consisting of the cement paste, aggregates, fibres and ITZs among them. The existence of ITZs weakens the bonding between the fibres and concrete matrix. The bonding performance of UHPC is influenced by the fibre geometry, fibre orientation, and also the strength of the matrix, it is therefore critical to consider the ITZ effect in the performance of UHPC. In the current study, the bonding effect between the fibre material and matrix is investigated firstly by single fibre pull-out tests in which different fibre embedding depths are considered. The experimental results are then used to establish the bond-slip relationship in the numerical model. Three dimensional mesoscale model with consideration of both the concrete matrix and fibre phase is established. Model calibration is conducted with comparison to static material tests, further validation is obtained through SHPB split tensile test simulation. The proposed 3D mesoscale model can effectively model the material behaviour especially the post yielding ductility.

With the understanding of the new material, field blast tests are carried out on concrete components constructed with this UHPC. Comparison is made against conventional concrete component and high strength concrete components, and the exceptional performance reveals its potentiality in the protective structural design.

STATEMENT OF ORIGINALITY

I certify that this work contains no material which has been accepted for the award of any other degree or diploma in my name, in any university or other tertiary institution and, to the best of my knowledge and belief, contains no material previously published or written by another person, except where due reference has been made in the text. In addition, I certify that no part of this work will, in the future, be used in a submission in my name, for any other degree or diploma in any university or other tertiary institution without the prior approval of the University of Adelaide and where applicable, any partner institution responsible for the joint-award of this degree.

I give consent to this copy of my thesis when deposited in the University Library, being made available for loan and photocopying, subject to the provisions of the Copyright Act 1968.

The author acknowledges that copyright of published works contained within this thesis resides with the copyright holder(s) of those works.

I also give permission for the digital version of my thesis to be made available on the web, via the University’s digital research repository, the Library Search and also through web search engines, unless permission has been granted by the University to restrict access for a period of time.

.....

Print Name

.....

Signature

.....

Date

LIST OF PUBLICATIONS

1. Su, Y., Li, J., Wu, C.Q., Wu, P.T. and Li, Z.X. 2016. Influences of nano-particles on dynamic strength of ultra-high performance concrete. *Composites Part B: Engineering*, 91, pp.595-609.

Status: Published

2. Su, Y., Li, J., Wu, C.Q., Wu, P.T. and Li, Z.X. 2016. Effects of steel fibres on dynamic strength of UHPC. *Construction and Building Materials*, 114, pp.708-718.

Status: Published

3. Su, Y., Wu, C.Q., Li, J., Li, Z.X., and Li, W.G. 2017. Development of novel ultra-high performance concrete: from material to structure. *Construction and Building Materials* 135, pp. 517-528.

Status: Published

4. Su, Y., Li, J., Wu, C.Q., Wu, P. T, M. and Li, X.B. Mesoscale study of novel ultra-high performance concrete under static and dynamic loads. Accepted by *Materials and Design* on the 10th Oct 2016.

Status: Accepted

ACKNOWLEDGEMENTS

The author would like to express his sincere gratitude to his supervisors, Prof. Chengqing Wu for his invaluable guidance and supervision during this study. His good nature, patience, frankness, and technical expertise had a profound impact on the author's academic experience and personal goals. Special thanks are given to the author's team, Dr. Jun Li, Mr Jian Liu and Mr. Pengtao Wu, for helping with definitely improving the quality of the author's work.

The author extends his sincerest thanks to his family for the support, especially his father Guozhi Su and mother Xiulan Peng. Also, his friends Mr. Ron Seidel and Mr. Yuemin Yuan deserve lots of thanks and much more, for their patience and help. Finally, the author dedicates this thesis to his fiancée Ms. Guanzhen Li who has provided with the confidence and on-going support to the author to complete the thesis with the best of his abilities.

CHAPTER 1: INTRODUCTION

BACKGROUND

Over the past several decades, a fast development is seen on high compressive strength concrete and high ductility concrete. High strength concrete is designed to achieve a size efficiency of large structures and also provide extra strength safety margin. High ductility concrete, on the other hand, is mainly designed to overcome the material brittleness, ensure the ductility and energy absorption capability of structural members under dynamic loads. The decoupled development of both resulted in exclusion of each other's desirable properties. A considerable effort has been devoted to development of new concrete with both benefits from high compressive strength and high material ductility.

Fibre material is known to be beneficial to ductility enhancement in cementitious matrix. The concept of using fibres as material reinforcement is not new. Fibres have been used as reinforcement since the mighty time of ancient Roman. Modern version of concrete fibres did not come into use until 1960s when steel fibres, glass fibres and synthetic fibres took the stage. Use of fibre in concrete matrix can reduce the concrete permeability and enhance its crack control ability. Investigation of the influence from varying fibre reinforcement type on the concrete performance had been conducted in the recent studies. Among all fibre types, steel fibres are known to have higher modulus of elasticity than the concrete matrix which means they can enhance the load carrying capacity, thus increase tensile strength of the material. Concrete with steel fibre reinforcement has better impact, shatter and abrasion resistance.

Nowadays steel fibres are widely used as reinforcement in industrial floor slabs, standard reinforcing cage for tunnel segments, shotcrete and prefabricated concrete products. Ye et al. [1] experimentally investigated the mechanical behaviour of concrete reinforced by hybrid different shapes of steel fibres. The largest fracture energy and bending toughness were obtained with hybrid-fibres, where the volume ratio of long ultra-fine fibre was 1.5%, and the ratio of long end-hooked fibre was 0.5%. The hybrid-fibres had generated positive intermixing effect. Kim et al. [2] examined the effects of twisted steel fibre on concrete flexural toughness, and three types of twisted fibre with different lengths and diameters were considered. Ryu et al. [3] found that concrete with twisted fibre reinforcement exhibited

significantly improved mechanical characteristics compared to control concrete containing conventional straight fibre. Bindiganavile and Banthia [4] pointed out that under both static and low-rate impact loads, the predominant failure mode of steel fibre reinforced concrete material was the steel fibre pull-out. To increase the bonding between the concrete and steel fibre material, Xu et al. [5] proposed spiral shaped steel fibres, and the impact tests had demonstrated that fibre reinforced concrete specimens reinforced with this spiral shaped fibres displayed the largest ultimate compressive strength, the largest post-failure strength and the largest energy-absorption capacity amongst specimens reinforced with seven other types of fibres tested.

For steel fibre reinforced concrete, two of the most important factors that affect the concrete properties are fibre aspect ratio (ratio of steel fibre length over diameter) and volume fraction. Increasing fibre aspect ratio helps increasing the probability of heterogeneous distribution and flocculation in concrete. Fibre volume fraction significantly affects the workability of concrete. Yazıcı et al. [6] tested hooked-end bundled steel fibres reinforced concrete, and the influence of different aspect ratios and fibre volumes were discussed. They noted that split tensile strength, flexural strength of SFRC are improved with increasing aspect ratio and fibre volume fraction. Wang et al. [7] conducted experimental analysis on effect of fibre aspect ratio on mechanical properties of steel fibre reinforced concrete, and the results revealed that the aspect ratio had an optimal value for strengths in every concrete batch. Beyond this value, the addition of steel fibres into concrete may have an effect of increasing the ductility rather than the strengths.

With the combination of reactive powder concrete and steel fibre reinforcement, ultra-high performance concrete (UHPC) can be formulated. UHPC has unique material composites: typically fine-grained sand, silica fume, small steel fibers, and special blends of high-strength Portland cement. UHPC is characterized with remarkable ductility, durability and strength properties [8]. First use of ultra-high strength concrete in civil construction was in Canada. The Shawnessy Light Rail Transit (LRT) Station, constructed during fall 2003 and winter 2004, forms part of a southern expansion to Calgary's LRT system and is the world's first LRT system to be constructed with ultra-high performance concrete [9]. Later applications of this material on pedestrian bridge in Germany [10], a cable stayed bridge in Korea [11] and a series of pedestrian bridge in New Zealand [12] have impressed the world with its great mechanical performance and durability. In the recent years, UHPC had been used in structural elements to resist extreme earthquake effects [13], and explosive loads [14, 15]. In

modern society, with the rising of terrorism activities, construction material concerning infrastructure protection is under fast developing. UHPC is now widely investigated by government agencies and universities.

In the first part of the present study, different fibres with varying geometries and volume fractions are considered in the ultra-high performance concrete design, and the static and dynamic material properties are investigated based on experimental studies.

Recently, development of nanotechnology has attracted great scientific attention. It was observed that several phenomena including statistical mechanical effects and quantum mechanical effects become pronounced as size of the system decreases. Due to their ultra-fine size, addition of nanoscale particles results in significantly improved material properties without much change of the material composition. As a consequence, researchers and engineers are exploring feasibility of re-engineering many existing materials like concrete by adding nanoscale particles into the matrix to get new and novel material which has unprecedented performance. The experimental results showed that the compressive strengths of mortars with nano-SiO₂ particles were all higher than those of mortars containing silica fume at 7 and 28 days [16], [17]. Liu et al. [18] added nano-CaCO₃ into cement paste and the experimental results showed that nano-CaCO₃ (NC) had no effect on water requirement of normal consistency of cement. However, with the increase of NC content, its flowability decreased and setting time of fresh cement paste was shortened. Flexural strength as well as compressive strength increased with the addition of NC at the age of 7 days and 28 days. Nazari and his colleagues conducted series of experimental tests on different nanoscale additives mixed into concrete matrix [19-24]. Although their work had only been demonstrated in small samples, it was believed that if only it can scale up to larger quantities, it is possible to produce concrete four times stronger than the strongest existing commercial concrete mixes. Despite great advantages and potentials, concerns remain for wide utilization of nanoscale particles in structural construction. Firstly, toxicity and environmental impact of nanomaterials should be well addressed [25]. It is also well acknowledged that most of the nanoscale materials are expensive which limits their use with concrete in industry.

In the second part of the present study, effect from nano material addition on the mechanical performance of UHPC is investigated. Static tests including uniaxial compression, third-point bending as well as dynamic compressive tests using SHPB are conducted. Dynamic compressive strength and tensile strength of UHPC samples with varying nano addition are

compared and discussed. Dynamic Increase Factors which are important describing the material under high loading rate are generated and plotted in charts, and the influences of different nano material additions and dosages on the dynamic properties of UHPC material are discussed. Furthermore, UHPC samples after SHPB tests are analysed under microscopy Scanning Electron Microscope (SEM) Analysis to explain the macro failure in micro scale. X-Ray Diffraction (XRD) Analysis and X-Ray Fluorescence (XRF) Analysis are carried out to further understand the failure element composition and strength development of this novel material.

Although concrete material can be treated as homogeneous at macroscopic scale, when observed at a smaller length scale, concrete like UHPC is heterogeneous and consists of constituents including aggregate, CH crystals, C-S-H gel, water and fibre material. Existence of ITZs weakens the bonding between the fibres and concrete matrix. The bonding performance of SFRC is influenced by the fibre geometry [26-28], fibre orientation [29, 30], and also the strength of the matrix, it is therefore critical to consider the ITZ effect in the performance of UHPC.

In general, to investigate the interfacial transition zone (ITZ) effect on the fibre bonding properties, UHPC can be described as multi-phase material consisting of the cement paste, aggregates, fibres and ITZs among them. As can be noted in the literature, the mechanical behaviour of SFRC is mainly investigated through experimental and associated analytical studies. Over the past several decades, with the development of computer power and computational mechanics, numerical simulation of material and structural behaviour under both static and dynamic conditions are becoming increasingly popular. Fibre reinforced concrete is studied as homogeneous material [31-36]. Besides these homogeneous models, mesoscale study considering the heterogeneity of concrete under static and dynamic loads can also be found in the literature. Research was carried out on plain concrete in mesoscale under dynamic loads [37-39]. Fang and Zhang [40] conducted three-dimensional modelling of steel fibre reinforced concrete material under intense dynamic loading, and their model well reproduced SFRC failure under contact detonations. Xu et al. [41] developed an axisymmetric mesoscale model with components of fibre, aggregate and mortar to investigate the dynamic failure behaviour of SFRC material under impact loading.

The mesoscale modelling of UHPC material is studied in the present research, single fibre pull-out tests are firstly carried out to provide information about the interfacial bonding

between the fibre and concrete matrix. Then the bonding is modelled with sliding contact algorithm in the numerical model, the numerical model is then calibrated through static split tensile tests, and SHPB tests are finally investigated with the mesoscale model.

The above experimental and numerical study demonstrated the exceptional mechanical properties of the novel UHPC material. In the next stage study, structural components made with selected fibre and nano composition are casted. Static bending tests on beams are carried out to study structural ultimate bending capacity.

As aforementioned, the development of this novel UHPC material aims at mitigating the structural damage and increasing the structural redundancy and robustness in extreme loading environment such as impact and blast. After studying the material properties, and also the structural component under static loading condition, field blast tests are carried out to demonstrate the feasibility of utilizing such material against close-in explosions. Previous study had demonstrated that flexural designed component may fail in brittle shear mode [42, 43] under short duration high intensity blast loads, and such damage is not desired as less blast energy can be absorbed. With the novel UHPC material which has significantly enhanced tensile strength and material ductility, it is anticipated less shear damage would occur on UHPC component and the crack propagation can be confined by fibre, also the fibre pull-out process would consume large amount of blast energy leading to less structural damage.

RESEARCH GOALS

The study was undertaken with the aim of developing novel ultra-high performance concrete material with exceptional loading carrying capacity and much improved tensile strength as well as material ductility. The specific topics reported in the thesis consist of:

- 1) Development of a novel UHPC material with addition of high performance steel fibre material and nano material.
- 2) Experimental study on material static compressive and tensile strength, the influence from varying fibre material addition and nano material addition are studied.
- 3) Experimental study on material dynamic compressive and tensile strength, the influence from varying fibre material addition and nano material addition are studied.
- 4) Development of numerical model based on experimental results, and the heterogeneity of the material is studied, the material is modelled as a two-phase material with concrete

matrix and fibre phase. Bonding between the two phases are modelling with sliding contact algorithm.

- 5) Conducting a numerical study based on three-dimensional mesoscale numerical model, static material tests and dynamic SHPB tests are simulated to validate the feasibility of the model and contact algorithm.

OUTLINE

This thesis comprises six chapters. The five chapters following this introductory chapter are arranged as follows:

Chapter 2 demonstrated the development of novel Ultra-high performance concrete, and the major target focuses on the nano material influence. Material performances under both static and dynamic loading condition are investigated, and microscopy study is conducted to reveal the benefits from nano material addition.

Chapter 3 after confirming the positive effects from nano particles addition, material composition is further studied with consideration of the fibre material influence. Varying fibre materials at different volume fraction are studied in the experimental tests. Ageing the static and dynamic material tests are conducted. Comparison and discussion about the fibre addition is presented

Chapter 4 focuses on the study of numerical model establishment, with information from single fibre pull-out tests, numerical model is established and extensive numerical studies concerning the material static performances are conducted.

Chapter 5 conducted further study on UHPC material, the flexural tensile strength and fracture energy absorption of UHPC with different nanoscale materials and steel fibres are compared and discussed. Laboratory static bending tests and field blast tests on structural components made of selected UHPC material composition, and the results highlighted the material ductility and blast resistant capacity of UHPC material developed in the present study.

Chapter 6 summarizes the main outcomes of this research, along with suggestions for future studies.

REFERENCES

- [1] B. Daio, S. Hu, Y. Ye, S. Yang, Z. Liu, Mechanical Behavior of Ultra-High Performance Concrete Reinforced with Hybrid Different Shapes of Steel Fiber, in: CICTP 2012, pp. 3017-3028.
- [2] S.H. Kim, G.S. Ryu, K.T. Koh, Flexural Behavior Characteristics of UHPC According to Twisted Steel Fiber, *Advanced Materials Research*, 652 (2013) 1499-1504.
- [3] G.S. Ryu, S.H. Kim, G.H. Ahn, K.T. Koh, Evaluation of the Direct Tensile Behavioral Characteristics of UHPC Using Twisted Steel Fibers, *Advanced Materials Research*, 602 (2013) 96-101.
- [4] V. Bindiganavile, N. Banthia, Polymer and Steel Fiber-Reinforced Cementitious Composites under Impact Loading? Part 1: Bond-Slip Response, *ACI Materials Journal*, 98 (2001).
- [5] Z. Xu, H. Hao, H. Li, Experimental study of dynamic compressive properties of fibre reinforced concrete material with different fibres, *Materials & Design*, 33 (2012) 42-55.
- [6] Ş. Yazıcı, G. İnan, V. Tabak, Effect of aspect ratio and volume fraction of steel fiber on the mechanical properties of SFRC, *Construction and Building Materials*, 21 (2007) 1250-1253.
- [7] Z.L. Wang, J. Wu, J.G. Wang, Experimental and numerical analysis on effect of fibre aspect ratio on mechanical properties of SRFC, *Construction and Building Materials*, 24 (2010) 559-565.
- [8] C. Wu, D.J. Oehlers, M. Rebstroff, J. Leach, A.S. Whittaker, Blast testing of ultra-high performance fibre and FRP-retrofitted concrete slabs, *Engineering Structures*, 31 (2009) 2060-2069.
- [9] V. Perry, D. Zakariassen, First use of ultra-high performance concrete for an innovative train station canopy.
- [10] E. Fehling, K. Bunje, M. Schmidt, Gärtnerplatz – Bridge over River Fulda in Kassel: Multispan Hybrid UHPC-Steel Bridge, in: *Designing and Building with UHPFRC*, John Wiley & Sons, Inc., 2013, pp. 0-136.
- [11] W.J.C.Y.J.K.J.-R.C.J.S. Park, Dynamic Characteristics Evaluation of Innovative UHPC Pedestrian Cable Stayed Bridge, *Engineering*, Vol. 4 No. 12 (2012) 869-876.
- [12] M. Rebstroff, G. Wight, Perspective on UHPCs from a Specialist Construction Company, in: *Designing and Building with UHPFRC*, John Wiley & Sons, Inc., 2013, pp. 189-208.
- [13] G.J. Parra-Montesinos, S.W. Peterfreund, S.-H. Chao, Highly damage-tolerant beam-column joints through use of high-performance fiber-reinforced cement composites, *ACI Structural Journal*, 102 (2005).
- [14] J. Magnusson, M. Hallgren, Reinforced high strength concrete beams subjected to air blast loading, in: *Structures under shock and impact VIII*, Wit Press, 2004, pp. 53-62.
- [15] M. Zhang, M. Sharif, G. Lu, Impact resistance of high-strength fibre-reinforced concrete, *Magazine of Concrete research*, 59 (2007) 199-210.
- [16] B.-W. Jo, C.-H. Kim, G.-h. Tae, J.-B. Park, Characteristics of cement mortar with nano-SiO₂ particles, *Construction and Building Materials*, 21 (2007) 1351-1355.
- [17] Y. Qing, Z. Zenan, K. Deyu, C. Rongshen, Influence of nano-SiO₂ addition on properties of hardened cement paste as compared with silica fume, *Construction and Building Materials*, 21 (2007) 539-545.
- [18] X. Liu, L. Chen, A. Liu, X. Wang, Effect of Nano-CaCO₃ on Properties of Cement Paste, *Energy Procedia*, 16, Part B (2012) 991-996.

- [19] A. Nazari, S. Riahi, The effects of SiO₂ nanoparticles on physical and mechanical properties of high strength compacting concrete, *Composites Part B: Engineering*, 42 (2011) 570-578.
- [20] A. Nazari, S. Riahi, The effects of zinc dioxide nanoparticles on flexural strength of self-compacting concrete, *Composites Part B: Engineering*, 42 (2011) 167-175.
- [21] A. Nazari, S. Riahi, The effect of TiO₂ nanoparticles on water permeability and thermal and mechanical properties of high strength self-compacting concrete, *Materials Science and Engineering: A*, 528 (2010) 756-763.
- [22] A. Nazari, S. Riahi, The effects of ZrO₂ nanoparticles on physical and mechanical properties of high strength self compacting concrete, *Materials Research*, 13 (2010) 551-556.
- [23] A. Nazari, S. Riahi, The effects of limewater on flexural strength and water permeability of Al₂O₃ nanoparticles binary blended concrete, *Journal of Composite Materials*, 45 (2011) 1165-1172.
- [24] A. Nazari, S. Riahi, The effects of ZnO₂ nanoparticles on split tensile strength of self-compacting concrete, *Journal of Experimental Nanoscience*, 7 (2012) 491-512.
- [25] C. Buzea, I.I. Pacheco, K. Robbie, Nanomaterials and nanoparticles: Sources and toxicity, *Biointerphases*, 2 (2007) MR17-MR71.
- [26] Y. Su, J. Li, C. Wu, P. Wu, Z.-X. Li, Effects of steel fibres on dynamic strength of UHPC, *Construction and Building Materials*, 114 (2016) 708-718.
- [27] K. Holschemacher, T. Mueller, Y. Ribakov, Effect of steel fibres on mechanical properties of high-strength concrete, *Materials & Design*, 31 (2010) 2604-2615.
- [28] R.S. Olivito, F.A. Zuccarello, An experimental study on the tensile strength of steel fiber reinforced concrete, *Composites Part B: Engineering*, 41 (2010) 246-255.
- [29] S.-T. Kang, J.-K. Kim, Investigation on the flexural behavior of UHPCC considering the effect of fiber orientation distribution, *Construction and Building Materials*, 28 (2012) 57-65.
- [30] S.J. Barnett, J.-F. Lataste, T. Parry, S.G. Millard, M.N. Soutsos, Assessment of fibre orientation in ultra high performance fibre reinforced concrete and its effect on flexural strength, *Materials and Structures*, 43 (2010) 1009-1023.
- [31] L. Mao, S. Barnett, D. Begg, G. Schleyer, G. Wight, Numerical simulation of ultra high performance fibre reinforced concrete panel subjected to blast loading, *International Journal of Impact Engineering*, 64 (2014) 91-100.
- [32] Z.L. Wang, L.P. Wu, J.G. Wang, A study of constitutive relation and dynamic failure for SFRC in compression, *Construction and Building Materials*, 24 (2010) 1358-1363.
- [33] J. Li, C. Wu, H. Hao, Investigation of ultra-high performance concrete slab and normal strength concrete slab under contact explosion, *Engineering Structures*, 102 (2015) 395-408.
- [34] J. Li, C. Wu, H. Hao, An experimental and numerical study of reinforced ultra-high performance concrete slabs under blast loads, *Materials & Design*, 82 (2015) 64-76.
- [35] J. Li, C. Wu, H. Hao, Residual Loading Capacity of Ultra-High Performance Concrete Columns After Blast Loads, *International Journal of Protective Structures*, 6 (2015) 649-670.
- [36] Z.L. Wang, H. Konietzky, R.Y. Huang, Elastic-plastic-hydrodynamic analysis of crater blasting in steel fiber reinforced concrete, *Theoretical and Applied Fracture Mechanics*, 52 (2009) 111-116.
- [37] X.Q. Zhou, H. Hao, Mesoscale modelling and analysis of damage and fragmentation of concrete slab under contact detonation, *International Journal of Impact Engineering*, 36 (2009) 1315-1326.
- [38] Y. Lu, Z. Song, Z. Tu, Analysis of dynamic response of concrete using a mesoscale model incorporating 3D effects, *International Journal of Protective Structures*, 1 (2010) 197-217.

- [39] X. Wang, M. Zhang, A.P. Jivkov, Computational technology for analysis of 3D meso-structure effects on damage and failure of concrete, *International Journal of Solids and Structures*, 80 (2016) 310-333.
- [40] Q. Fang, J. Zhang, Three-dimensional modelling of steel fiber reinforced concrete material under intense dynamic loading, *Construction and Building Materials*, 44 (2013) 118-132.
- [41] Z. Xu, H. Hao, H.N. Li, Mesoscale modelling of fibre reinforced concrete material under compressive impact loading, *Construction and Building Materials*, 26 (2012) 274-288.
- [42] J. Li, H. Hao, A Simplified Numerical Method for Blast Induced Structural Response Analysis, *International Journal of Protective Structures*, 5 (2014) 323-348.
- [43] g. Hao, Predictions of Structural Response to Dynamic Loads of Different Loading Rates, *International Journal of Protective Structures*, 6 (2015) 585-605.

Statement of Authorship

Article Name: Influences of Nano-particles on Dynamic Strength of Ultra-High Performance Concrete

Su, Y., Li, J., Wu, C., Wu, P. and Li, Z.X. 2016. Influences of nano-particles on dynamic strength of ultra-high performance concrete. *Composites Part B: Engineering*, 91, pp.595-609.

Status: Published

Su, Y. (candidate)

Contribution: helped conduct tests, processed and analysed test data and prepared manuscript

I hereby certify that the statement of contribution is accurate.

Signed..... Date 27/08/2016

J, L.

Contribution: supervised research and tests, provided critical manuscript evaluation and acted as corresponding author.

I hereby certify that the statement of contribution is accurate and I give permission for the inclusion of the paper in the thesis.

Signed..... Date 24/8/2016

Wu, C.

Contribution: supervised research and tests, provided critical manuscript evaluation and acted as corresponding author.

I hereby certify that the statement of contribution is accurate and I give permission for the inclusion of the paper in the thesis.

Signed..... Date 24/8/2016

Wu, P.

Contribution: helped design and conduct tests.

I hereby certify that the statement of contribution is accurate and I give permission for the inclusion of the paper in the thesis.

Signed..... Date 2016.8.24

Li, Z.X.

Contribution: provided critical manuscript evaluation.

I hereby certify that the statement of contribution is accurate and I give permission for the inclusion of the paper in the thesis.

Signed..... Date Aug. 25, 2016

CHAPTER 2: INFLUENCES OF NANO-PARTICLES ON DYNAMIC STRENGTH OF ULTRA-HIGH PERFORMANCE CONCRETE

Yu Su^{1,2}, Jun Li^{1,2}, Chengqing Wu^{1,2,*}, Pengtao Wu¹, Zhong-Xian Li¹

¹TCU-UA (Tianjin Chengjian University-University of Adelaide) Joint Research Centre on
Disaster Prevention and Mitigation

²School of Civil, Environmental and Mining Engineering, the University of Adelaide, SA,
Australia 5005

ABSTRACT

Known for its high strength, ductility and durability, ultra-high performance concrete (UHPC) is a topic of interest in recent years for scientists and civil engineers. Great potential application of UHPC has driven increasingly more investments and research into this industry. In recent studies, taken advantage of the nanotechnology, novel UHPC material with nano material addition was developed. Great static performance improvement was observed when compared with normal strength concrete. To obtain full understanding of material properties, especially dynamic performance, Split-Hopkinson Pressure Bar (SHPB) tests were conducted on this new concrete material. For comparison purpose, static properties from uniaxial compression and split tensile tests are obtained and discussed. In this paper, effects of nano materials on behaviour of UHPC are assessed through group comparison. Dynamic increase factor (DIF) values for both the dynamic compressive strength and tensile strength are generated. It is found that the strength of UHPC increases with the rising of strain rates and dosage of nano material influences UHPC dynamic properties. However, UHPC is noted to be less rate sensitive compared to normal strength concrete. Microscopy analysis including Scanning Electron Microscope (SEM) Analysis, X-Ray Diffraction (XRD) Analysis and X-Ray Fluorescence (XRF) Analysis are conducted to understand the macroscopic failure phenomenon, element composition and concrete hydration process.

KEYWORDS: A. Fibres; A. Particle-reinforcement; D. Mechanical testing.

2.1 INTRODUCTION

Ultra-High Performance Concrete (UHPC), also known as reactive powder concrete (RPC), is a relatively new material formulated by combining Portland cement, silica fume, quartz flour, fine silica sand, high-range water reducer, water, and steel or organic fibres. Compared with normal strength concrete material, UHPC is known for its high strength, high ductility and high durability. It allows construction of sustainable and economic buildings with extraordinary slim design. Its high strength and ductility makes it an ideal building material for bridge decks, storage halls, thin-wall shell structures, and highly loaded columns. Some pioneering applications of this material such as a hybrid (steel and UHPC) pedestrian bridge in Germany [1], a cable stayed bridge in Korea [2] and a series of pedestrian bridge in New Zealand [3] have impressed the world with its great capacity and potentiality. Although UHPC has been developed for decades, its performance and functions can still be further improved.

Fibre reinforcement is one of the most important composites of UHPC. The concept of using fibres is not new. In the ancient time, horse hairs were used in mortar and straw to construct mud bricks. Modern versions of concrete fibre were not widely used until 1960s when steel, glass and synthetic fibres took the stage. After mixing with fibrous material, material integrity increases. Some types of fibres like steel fibres produce great impact, abrasion and shatter resistance in concrete [4-6], thus reduce flexural, shear and spall damage which are quite common in normal strength concrete [7, 8]. Steel fibres can also increase concrete flexural strength, provide better crack control and energy absorption capacity. As reported by Xu and Wille [9], the fracture energy of UHPC is influenced by fibre factor which is a function of the fibre volume fraction and slenderness. Comprehensive research on steel fibre reinforced concrete can be found in the open literature [10-13].

Recently, development of nanotechnology has attracted great scientific attention. It was observed that several phenomena including statistical mechanical effects and quantum mechanical effects become pronounced as size of the system decreases. Due to their ultra-fine size, addition of nanoscale particles results in significantly improved material properties without change of the material composition. As a consequence, researchers and engineers are exploring feasibility of re-engineering many existing materials like concrete by adding nanoscale particles into the matrix to get new and novel material which has unprecedented performance. Li et al. [14] investigated the properties of cement mortars blended with

nanoparticles nano-SiO₂ or nano-Fe₂O₃ to explore their super mechanical and smart (temperature and strain sensing) potentials. Jo et al. [15] experimentally investigated properties of cement mortars with nano-SiO₂ addition. The experimental results showed that the compressive strengths of mortars with nano-SiO₂ particles were all higher than those of mortars containing silica fume at 7 and 28 days. They concluded that it was plausible to add nano-SiO₂ particles in order to make high-performance concrete. Qing et al. [16] made similar observations and they noticed that comparing with cement paste with silica fume addition, the cement paste mixed with nano-SiO₂ particles had obvious higher compressive strength, especially at early age. Nano-SiO₂ was believed to accelerate cement hydration process. Liu et al. [17] added nano-CaCO₃ (NC) into cement paste and the experimental results showed that NC had no effect on water requirement of normal consistency of cement. However, with the increase of NC content, its flowability decreased and setting time of fresh cement paste was shortened. Flexural strength as well as compressive strength increased with the addition of NC at the age of 7 days and 28 days. Nazari and his colleagues conducted series of experimental tests on different nanoscale additives mixed into concrete matrix [18-23]. Although their work had only been demonstrated in small samples, it was believed that if only it can scale up to larger quantities, it is possible to produce concrete four times stronger than the strongest existing commercial concrete mixes. Najjigivi et al. [24] assessed workability and compressive of binary blended concretes mixed with different types of SiO₂ nanoparticles. It was concluded that SiO₂ nanoparticles played significant roles in mechanical properties of concrete by formation of additional calcium silicate hydrate gel during treatment, which played an important role in raising highly the compressive strength of binary blends.

Despite great advantages and potentials, concerns remain for wide utilization of nanoscale particles in structural construction. Firstly, toxicity and environmental impact of nanomaterials should be well addressed [25]. It is also well acknowledged that most of the nanoscale materials are expensive which limits their use with concrete in industry.

In recent research, a newly designed UHPC material with both steel fibre reinforcement and nano material addition was experimentally tested. The nano materials used in the concrete had been applied in industry for years because of their reasonable price. Static material tests such as uniaxial compression test and split tensile tests were conducted to get basic material properties of the newly developed UHPC. It was noted that the UHPC with nano-additives has much improved compressive strength as well as tensile strength which indicates good potential of utilizing such material in protective design against dynamic loads such as blast

load, seismic load and impact load. However, it is commonly acknowledged that concrete material is sensitive to rate of loading. Both compressive strength and tensile strength of concrete increase with loading rate. Under this condition, it is imperative to conduct dynamic tests on the newly developed UHPC to obtain complete knowledge of material constitutive relationship including both the static and dynamic properties.

Conventional screw-driven or servo-hydraulic methods of material testing had been utilized in determining the material property at high strain rate. However, these methods may not be perfectly adequate as the strain rates in the test is limited and oscillations and emerging stress wave exist in the testing apparatus [26]. Such oscillations and stress waves impair the transducer load reading, thus making the data obtained more complex to interpret reliably. To overcome such limitations, testing method namely Split-Hopkinson Pressure Bar (SHPB) was developed [27] and extended [28, 29]. SHPB method can be favourably used in both the dynamic compressive and tensile tests. In previous study concerning material dynamic performance, this method was widely adopted [30-32].

In the present study, SHPB test results of 94 UHPC samples including 41 compressive tests and 53 split tensile tests are summarized. Dynamic compressive strength and tensile strength of these samples are compared and discussed. Dynamic Increase Factors which are important describing the material under high loading rate are generated and plotted in charts, and the influences of different nano material additions and dosages on the dynamic properties of UHPC material are discussed. Furthermore, UHPC samples after SHPC tests are analysed under microscopy Scanning Electron Microscope (SEM) Analysis to explain the macro failure in micro scale. X-Ray Diffraction (XRD) Analysis and X-Ray Fluorescence (XRF) Analysis are carried out to further understand the failure element composition and strength development of this novel material.

2.2 UHPC COMPOSITION

In the current research, nano materials including Nano-CaCO₃, Nano-SiO₂, Nano-TiO₂ and Nano-Al₂O₃ are added into the base mix of UHPC at the same weight fraction of 3%. All specimens in the current research are reinforced by micro steel fibre namely MF15. Micro steel fibre MF 15 has a diameter of 0.12 mm and a length of 15 mm, and its yielding strength is 4200 MPa.

Nano material in the current study was mixed at a constant weight dosage of 3%, and this amount of mixture was determined in order to achieve a balance of performance and cost-effectiveness. The addition of nano material affects material hydration process. When a small quantity of the nano-particles were uniformly dispersed in the cement paste, the nano-particles located in the cement will promote and accelerate cement hydration due to their high activity. However, when the nano-particles cannot be well dispersed, as in the case of extensive nano-particles content addition, these nano-particles will create weak zones. Consequently, the homogeneity of microstructure cannot be reached, and low strength will be expected. In a relevant study [16] , it was reported that concrete strength increases with nano content up to 4 wt.% and then decreases. Considering high cost of nano materials, a weight dosage of 3% is made in the present study for all nano materials additions to achieve a balance of performance and cost-effectiveness.

Table 1 shows the complete mix proportions of different UHPC formula.

Table 1: Mix proportions of different UHPC formula (unit: kg)

Constituents	Micro Steel Fibre MF15			
52.5 Cement	750			
Silica Fume	225			
Silica Flour	190			
Sand	1030			
Superplasticizer	16			
Water	190			
Water/Cement	25.30%			
Steel Fibre	191			
Nano-CaCO ₃	63.1	-	-	-
Nano-SiO ₂	-	63.1	-	-
Nano-Al ₂ O ₃	-	-	63.1	-
Nano-TiO ₂	-	-	-	63.1

All UHPC samples were produced by mixing silica fume, fine sand and powder materials which consisted of cement and nanoparticles, in a laboratory concrete mixer. They were firstly dry mixed for 5 minutes before any water addition. Then 70% water was added and mixed for 3 minutes to fluidise the mix. Superplasticizer was added before the other 30% water was finally mixed. The mixing process was then continued for another 5 minutes before steel fibres were added and manually dispersed in order to avoid clumping and guarantee the fibres were uniformly distributed and randomly oriented.

Slump tests were carried out to assess the workability of the UHPC material immediately after concrete mixing. It was noted the concrete in the current study had good workability with a slump exceeding 250 mm and slump spread exceeding 900 mm diameter.

After proper curing in wooden moulds, specimens are prepared by cutting them to the specified length and are thereafter grinded and measured. There are high requirements on the flatness of end surfaces in order to obtain an even load distribution in the load tests. The specimens used for static compression test were 100 mm cubes, and the samples used in the following split tensile and SHPB tests were cylinders with 75 mm diameter and 37.5 mm height.

2.3 STATIC TESTS

Uniaxial compression tests and split tensile tests were conducted to determine static uniaxial compressive strength and split tensile strength of UHPC.

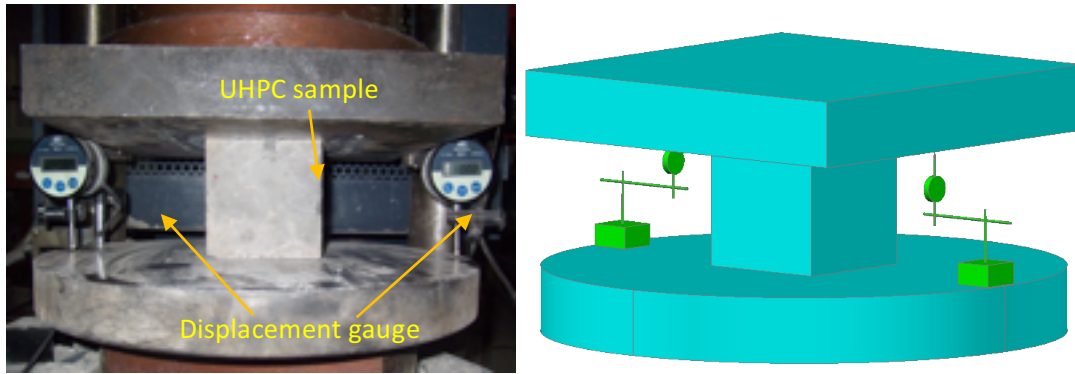
2.3.1 Uniaxial compression test

The experiments were carried out on a number of 100 mm*100 mm*100 mm UHPC cubes using a 3000 kN capacity computer-controlled electromechanical servo hydraulic pressure testing machine as shown in Figure 1a.

Figure 1b illustrates the testing setup. At both sides of the loading plate, there was an axially oriented displacement gauge to record the test data. In total there were 68 specimens tested. Testing procedure conformed to the China Standard GB/T 50081-2002. In the uniaxial compression test, the specimens were tested under a uniform loading rate of 10 kN/s.



(a) YAW-3000 computer controlled servo pressure testing machine



(b) Testing samples and displacement gauges installation

Figure 1: Testing set-up for compression tests of cubic specimens

Static compressive stress-strain curves obtained from samples with different nano additions are shown in Figure 2. It can be observed that when the same steel fibres i.e. micro steel fibre MF15 were used as UHPC reinforcements, different nano material additions had influence on the concrete compressive strength. UHPC with 3% of Nano-TiO₂ had the highest strength which is about 14% higher than the lowest compressive strength measured from UHPC with Nano-Al₂O₃. Addition of Nano-CaCO₃, Nano-SiO₂ provided slightly higher compressive strength than Nano-Al₂O₃. Among all the nano materials, UHPC mix with Nano-CaCO₃ seemed to yield the lowest material ductility, post peak compressive strength quickly dropped to around 60 MPa and then entered stress plateau. UHPC specimens with addition of other three nano materials exhibited prominent material ductility. Before entering the stress plateau, there was only slight stress loss from the peak.

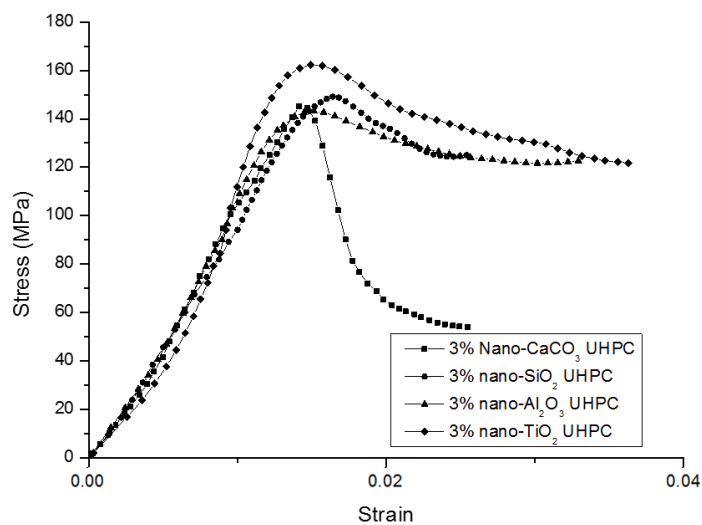


Figure 2: Stress-strain curves from quasi-static compressive tests

The static compressive strengths for UHPC with different nano-additives are averaged and listed in Table 2.

Table 2: Experimental results of different formula UHPC under static load

UHPC	3% Nano-CaCO ₃	3% Nano-SiO ₂	3% Nano-Al ₂ O ₃	3% Nano-TiO ₂
Compressive Strength (MPa)	145.1	149.6	143.5	162.6
Standard Deviation	16.59	17.47	16.15	20.37

2.3.2 Split tensile tests

Static split tensile tests were conducted on cylindrical UHPC specimens with diameter of 75 mm and height of 37.5 mm, as shown in Figure 3.

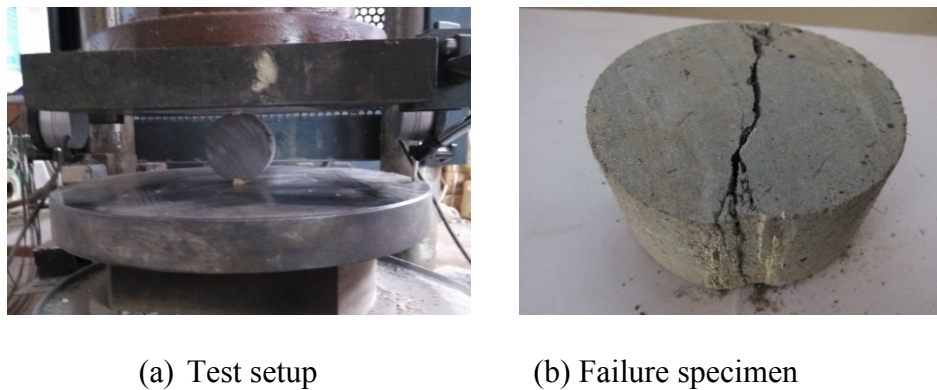


Figure 3: Split tensile tests

The split tensile strength was calculated according to $\sigma = \frac{2P}{\pi DL}$ in which P is the load at failure; D and L are the diameter and length of the specimen, respectively.

The static split tensile strengths for UHPC with different nano-additives are then averaged and listed in Table 3.

Table 3: Static split tensile strength of different UHPC

UHPC	3% Nano-CaCO ₃	3% Nano-SiO ₂	3% Nano-Al ₂ O ₃	3% Nano-TiO ₂
Strength (MPa)	22.2	13.9	15.4	17.7
Standard Deviation	5.31	5.48	7.72	4.35

It is noted that, all UHPC samples have greatly improved split tensile strength compared with their normal strength counterparts. UHPC sample with 3% volume dosage Nano-CaCO₃ addition has the highest split tensile strength and it is about 60% higher than the value obtained from UHPC with 3% Nano-SiO₂. Addition of 3% Nano-TiO₂ gives the UHPC sample with the second highest split tensile strength of 17.7 MPa.

From the uniaxial compressive and split tensile tests shown in the above sections, it is clearly observed that addition of different nano materials has a great influence on the mechanical properties of UHPC, given that UHPC samples have the same steel fibre material and fibre volume dosage. Generally speaking, UHPC material with nanomaterial addition outperforms the conventional strength concrete.

For cement based material like concrete, calcium silicate hydrate (C-S-H) is the main product during the hydration process and is primarily responsible for the material strength. Nano material like CaCO₃ and SiO₂ are typically high effective pozzolanic material and addition of such material into the cement paste will improve the microstructure of the paste and reduce calcium leaching as these materials react with Calcium Hydroxide (CH) and form additional C-S-H gel. The strength of hardened cement paste is thus increased.

2.4 SHPB TEST

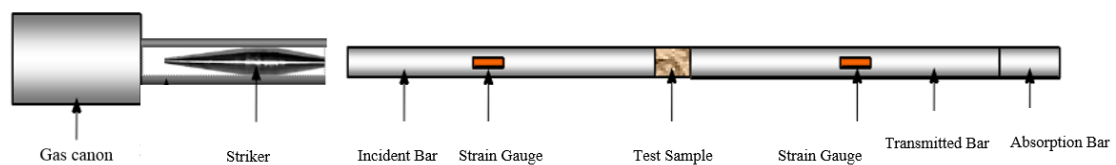
Table 4 summarises the number of SHPB compression and split tensile tests conducted for the current study. In total, 41 compression SHPB tests and 53 split SHPB tests were conducted. Please note, two more group tests were carried out to investigate the influence from different dosages of Nano-CaCO₃.

Table 4: Number of SHPB compression and split tensile tests

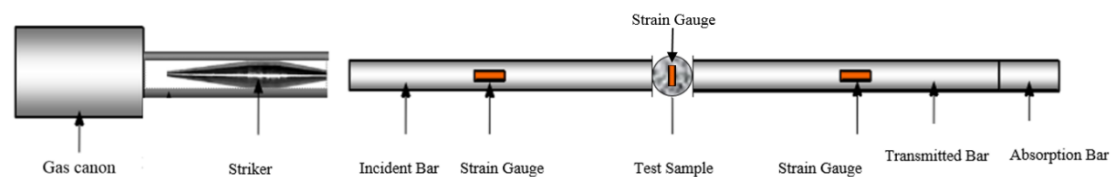
	L/D	Fibre	NANO	L(mm)	Compression test number	Split tensile test number
EFFECTS OF NANO MATERIAL	0.5	MF15	3% CaCO ₃	37.5	12	9
	0.5	MF15	3% SiO ₂	37.5	7	8
	0.5	MF15	3% Al ₂ O ₃	37.5	8	10
	0.5	MF15	3% TiO ₂	37.5	7	10
IMPACT OF NANO-CONTENT	L/D	Fibre	NANO	L(mm)	Compression test number	Split tensile test number
	0.5	MF15	3% CaCO ₃	37.5	12	9
	0.5	MF15	5% CaCO ₃	37.5	4	8
	0.5	MF15	1% CaCO ₃	37.5	3	8

2.4.1 Test apparatus

In the current study, the dynamic tests were conducted on SHPB test specimens with 75 mm diameter and 37.5 mm height. The experimental systems of SHPB compressive and split tensile tests are sketched in Figure 4. It is worth noting that when determining the concrete tensile strength, traditional direct pull out test is considered to be the best suited method. However, the uniform stress-state idea in the specimen is rarely reached, and in practice premature failure due to the stress concentration around grips is often observed. As an alternative and indirect method, SHPB split tensile test as shown in Figure 6b can generate a tensile stress within the specimen by far-end compression, which is easier and more convenient in instrumentation than direct pull out test.



(a) SHPB compression test setup



(b) SHPB split tensile test setup

Figure 4: SHPB experimental system

In SHPB tests, the specimens were placed between the ends of two straight bars, called the incident bar and the transmitted bar. At the end of the incident bar (some distance away from the specimen, typically at the far end), a stress wave is created which propagates through the bar toward the specimen. This wave is referred to as the incident wave, and upon reaching the specimen, split into two smaller waves. One of them, the transmitted wave, travels through the specimen and into the transmitted bar, causing plastic deformation in the specimen. The other wave, called the reflected wave, is reflected away from the specimen and travels back down the incident bar. Strain gages were then placed on the bars to measure strains caused by the waves. Assuming deformation in the specimen is uniform, the stress and strain can be calculated from the amplitudes of the incident, transmitted, and reflected waves. Figure 5 shows typical waves in SHPB compression test.

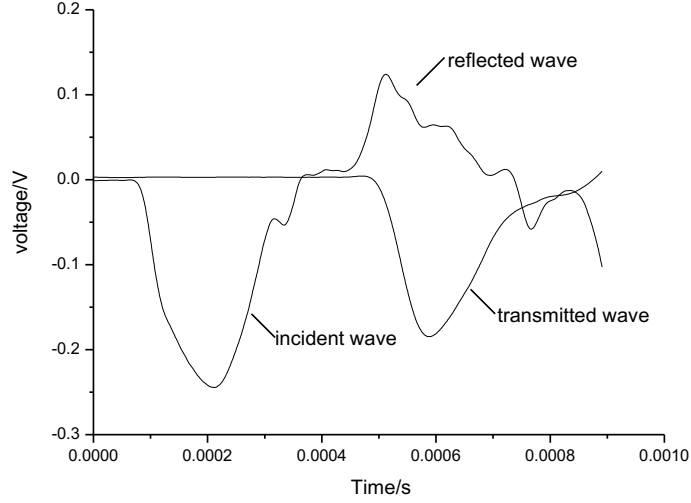


Figure 5: Typical waveform of compression test

Based on one dimensional stress wave propagation theory [33], the stress, strain and strain rate in SHPB compressive test can be calculated using the following equations.

$$\sigma(t) = E \left(\frac{A}{A_s} \right) \varepsilon_T(t) \quad (1)$$

$$\varepsilon(t) = \int_0^T \dot{\varepsilon}(t) dt \quad (2)$$

$$\dot{\varepsilon}_c(t) = -\frac{2c_0}{L} \varepsilon_R(t) \quad (3)$$

where E , A and C_0 are Young's modulus, cross-sectional area and elasticity wave velocity of the SHPB bars; A_s and L are cross sectional area and length of the test samples; ε_T and ε_R are incident strain and reflective strain.

For SHPB split tensile test, the compressive stress along the split bar length direction and tensile stress perpendicular to the bar length direction can also be calculated following the theory of elasticity.

$$\sigma_c = \frac{2P}{\pi DL} \frac{D^2}{r(D-r)} \quad (4)$$

$$\sigma_t = -\frac{2P}{\pi DL} \quad (5)$$

$$\dot{\varepsilon}_t(t) = \frac{\sigma_t}{E_s T} \quad (6)$$

where P is the loading force which can be calculated based on the strain measured on the split bar, D is the diameter, and L is the thickness of the specimen, r is the distance measured from

the loading point, E_s is the quasi-static Young's modulus of specimen, T is the time lag between the start of the transmitted stress wave and the occurrence of the maximum transmitted stress.

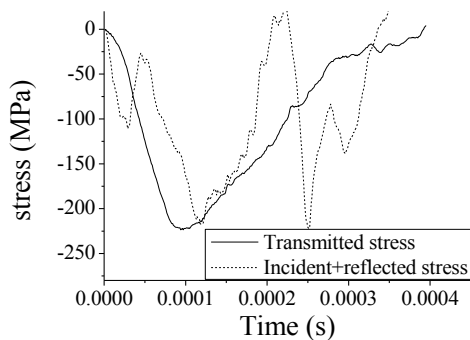
2.4.2 Equilibrium check

In SHPB test, it is critical to conduct longitudinal stress equilibrium check. Equation 7 is used to calculate the stress balance.

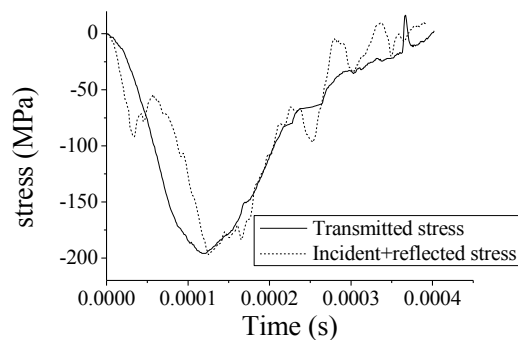
$$\sigma_T = \sigma_I + \sigma_R \quad (7)$$

where σ_T is the transmitted stress; σ_I is the incident stress and σ_R is the reflected stress.

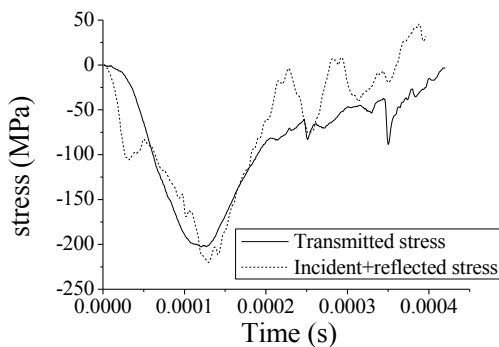
Figure 6 shows stress equilibrium check on UHPC samples with different nano material additions. The strain rates displayed in the figure are the highest strain rate reached in the SHPB tests. It can be concluded that under the highest strain rate, all specimens reached stress balance which verified the accuracy of SHPB tests conducted in the present research.



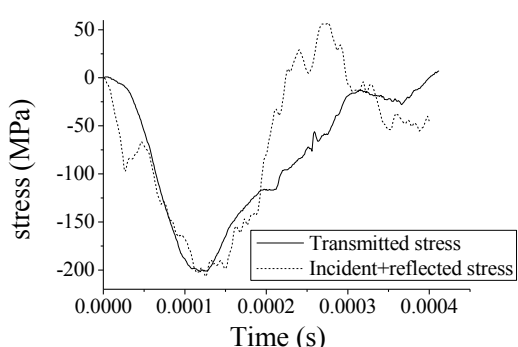
(a) 3% Nano-CaCO₃ (strain rate 93.74 1/s)



(b) 3% Nano-SiO₂ (strain rate 79.72 1/s)



(c) 3% Nano-Al₂O₃ (strain rate 85.45 1/s)



(d) 3% Nano-TiO₂ (strain rate 90.35 1/s)

Figure 6: Stress equilibrium checks

2.4.3 Compression test results

Figure 7 shows the typical failure modes of UHPC samples with different nano material additions after SHPB compression tests. It can be observed that, with the same steel fibre MF15 reinforcement, the samples failure modes are more or less the same regardless of the nano material mixture. Except some visible cracks, most part of the samples remains intact. This could be attributed to the effect of steel fibre which bridges the cracks and retards crack extension.



(a) 3% Nano-CaCO₃



(b) 3% Nano-SiO₂



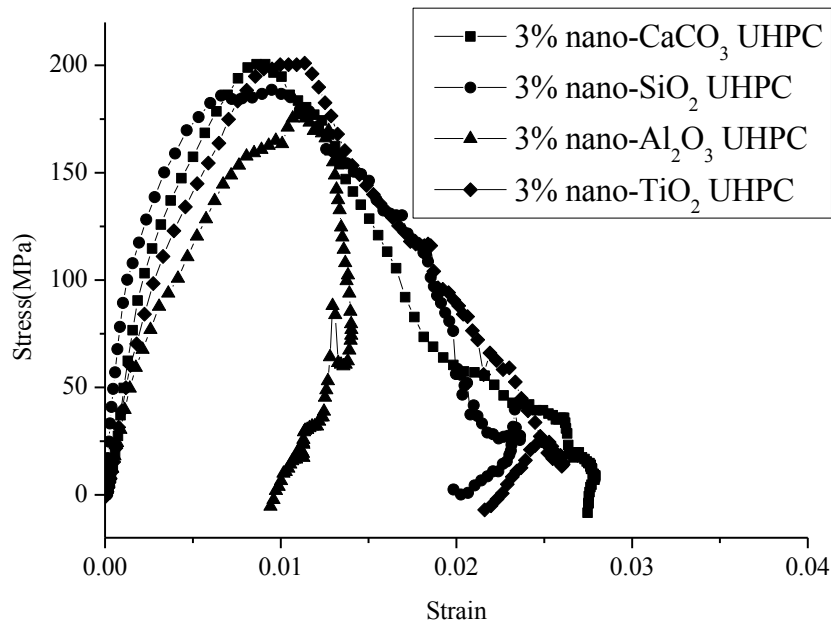
(c) 3% Nano-Al₂O₃



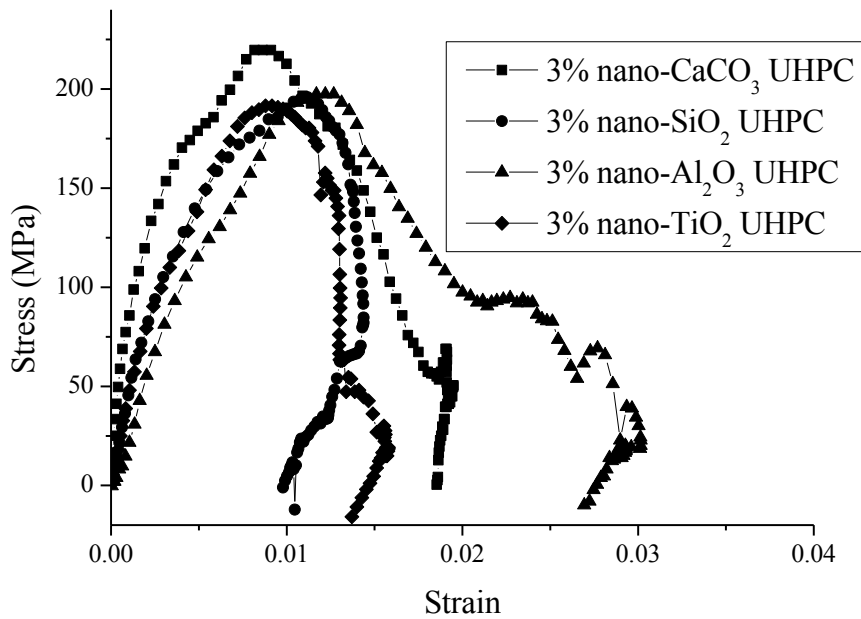
(d) 3% Nano-TiO₂

Figure 7: Failure patterns of specimens with different nano materials

Figure 8 shows dynamic compressive stress-strain curves of UHPC specimens with different nano materials mixes. Comparing with static test results shown in Figure 4, it can be clearly observed that with the increase of strain rate from 0/s to 60/s and then 80/s, all UHPC samples display a strength enhancement. It can also be noticed that, UHPC with Nano-CaCO₃ addition is the most loading rate sensitive which has the highest strength increment during the test.



(a) Strain rate 60/s



(b) Strain rate 80/s

Figure 8: Comparison of stress-strain curves at different strain rates of different nano particles

Dynamic strengths of UHPC samples under various strain rates are plotted in Figure 9. It can be observed all UHPC materials are sensitive to the strain rate ranging from 0/s to 80/s. The increase of loading rate favours the material compressive strength. When the strain rate

exceeds 80/s, although strength increase can still be noticed in the UHPC material, the rate of strength increase gradually slows down.

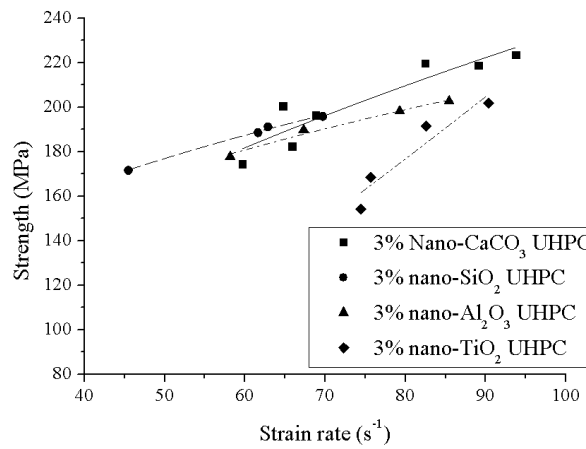


Figure 9: Dynamic strength of UHPC under various strain rates

The dynamic increase factors (DIF) for UHPC compressive strength including all test samples are plotted in Figure 10. It should be noticed that, in the current study, due to the lack of data at low strain rates, there are no DIF values ranging from 0 to 40/s. Further tests are required for a complete DIF curve fitting. In the previous studies, CEB [34] assumed change of slope in DIF curves happens at 30/s for normal strength concrete. Marval et al [35] proposed a formulation for DIF curves which indicates a change of slope happens at 1/s for normal strength concrete. As shown in Figure 10, a DIF of about 1.54 for UHPC with Nano-CaCO₃ is obtained at the highest measured strain rate of 94/s.

Comparison is made between the normal strength concrete (NSC) without fibre reinforcement and nano material addition and UHPC material used in the present study. For comparison purpose, the NSC material has a static compressive strength of 52.5 MPa, and its dynamic increase factors are calculated based on the formula discussed in [35] which is originated from CEB code [34].

For normal strength concrete compressive strength:

$$DIF = \frac{f_c}{f_{cs}} = \begin{cases} \left(\frac{\dot{\epsilon}}{\dot{\epsilon}_s}\right)^{1.026\alpha} & \text{for } \dot{\epsilon} \leq 30s^{-1} \\ \gamma_s \left(\frac{\dot{\epsilon}}{\dot{\epsilon}_s}\right)^{1/3} & \text{for } \dot{\epsilon} > 30s^{-1} \end{cases} \quad (8)$$

where f_c is the dynamic compressive strength at $\dot{\epsilon}$; f_{cs} is the static compressive strength at $\dot{\epsilon}_s$; $\dot{\epsilon}$ is the strain rate in the range of 30×10^{-6} to 300 s^{-1} ; $\dot{\epsilon}_s$ is the static strain rate 30×10^{-6} ; $\log \gamma_s = 6.156 \alpha - 2$; $\alpha = 1/(5 + 9f_{cs}/f_{co})$; $f_{co} = 10 \text{ MPa}$.

As displayed in Figure 10, normal strength concrete material has higher DIF values than UHPC with fibre and nano material addition at the same strain rate. In fibre-reinforced concrete material, the fibres resist the lateral spreading of the cracks by bridging across regions of lower strength. Therefore, the beneficial effect of a restraint on lateral crack growth has already been partially accounted for by fibre reinforcement, resulting in higher failure strength under quasistatic loading. Subsequently, the influence of the higher loading rate on reducing lateral crack development would be lessened.

Low porosity microstructure is another possible reason for low rate sensitivity of UHPC. As listed in Table 1, the water/cement ratio for the current UHPC materials is 0.25 which is significantly smaller than conventional concrete which usually has a water/cement ratio around 0.4. Total porosity of UHPC is lower than normal concrete, although no clear relationship exists linking the DIF with porosity, indirect experimental evidences were noted from previous study proving that the strain rate sensitivity of compressive strength is more obvious for higher porosity specimens [36],[37],[38].

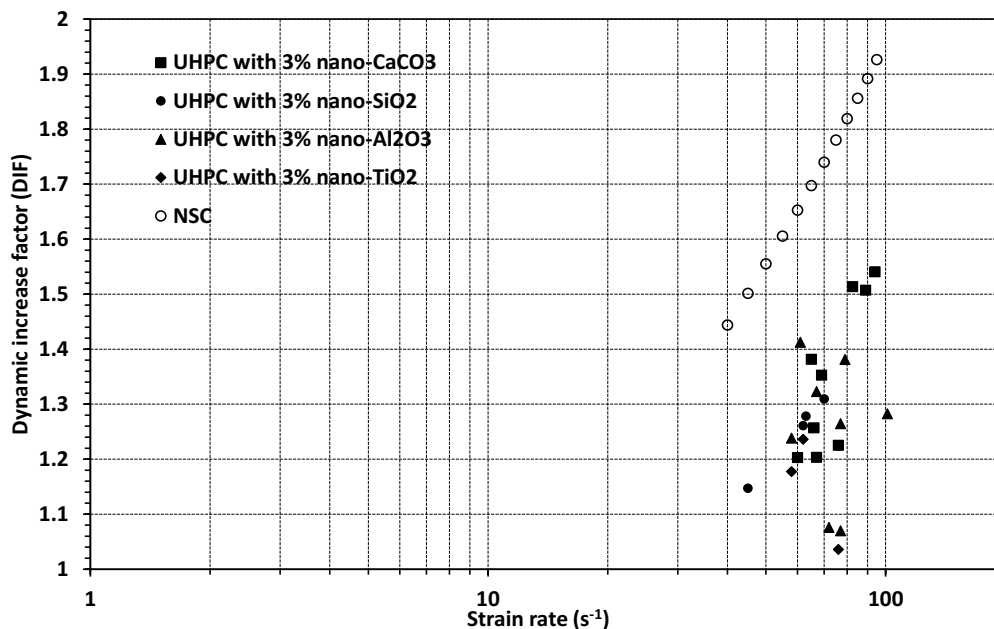
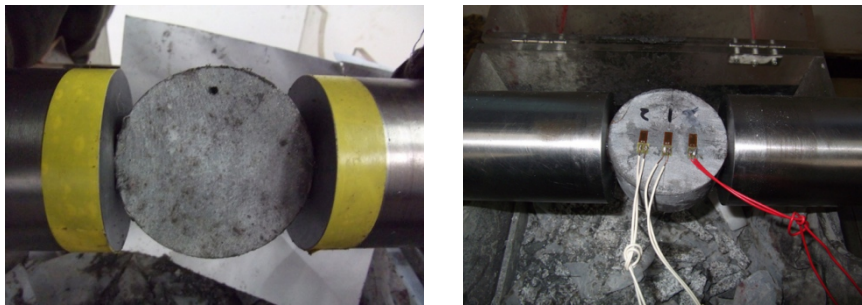


Figure 10: Comparison of DIF curves between NSC and UHPC

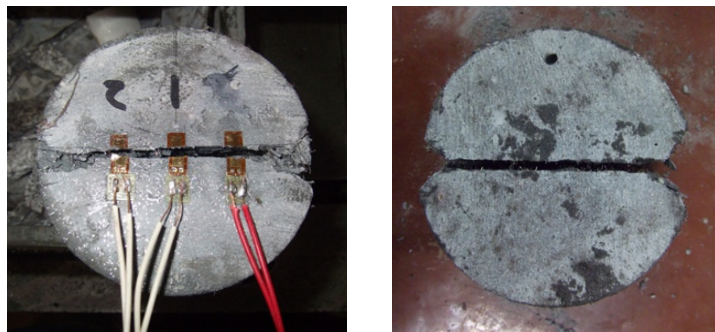
2.4.4 Split tensile results

After dynamic compressive tests, SHPB split tensile tests were carried out. Tension testing in a Split Hopkinson Pressure Bar (SHPB) is more complex due to a variation of loading methods and specimen attachment to the incident and transmission bar [39]. Figure 11a shows the SHPB split tensile test setup, the parallelism of the two flat ends of the UHPC specimen is important and hence should be checked carefully prior to the tests. Three strain gauges are glued perpendicular to the loading direction. Compared with the size of UHPC specimens, the strain gauge glued at the surface of the specimen is very small and thin, so the effects of crack bridging to the splitting crack by the gauges and the glue can be neglected.

Figure 11b shows the typical failure mode of UHPC material. It can be noticed that the crack propagation route and failure path is along the loading diameter at which position the strain can be recorded by the strain gauge attached on the sample surface.



(a) Test setup

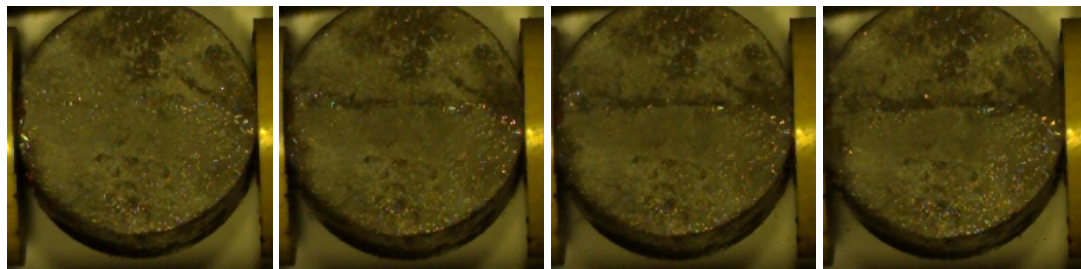


(b) Typical failure mode

Figure 11: SHPB split tensile test

The failure modes of the specimens are investigated from two perspectives. Firstly, it is necessary to check the location of crack initiation, whether the failure is initiated from the centre of the disc is of vital importance. Secondly, the route of crack propagation is important, and the failure path should be along the loading diameter. In order to investigate these two

phenomena, high speed camera was used in the SHPC split tensile tests, and sample responses at 155, 310 and 465 μs were captured. Based on trial tests, at these specified times, samples showed crack initiation, crack propagation and end concrete crush, respectively. As depicted in Figure 12, crack initiated at the sample centre where the maximum tensile stress existed and quickly propagated towards both ends, at about 310 μs , cracks reached the sample ends and end concrete crush started crushing. Generally speaking, the crack paths were all along the loading diameter in which the strain gauges could detect the response with accuracy. The comparison among UHPC with different nano material additions showed that mixture of 3% Nano-SiO₂ resulted in quicker crack generation and larger cracks while samples with Nano-CaCO₃ mixture showed better crack confinement.



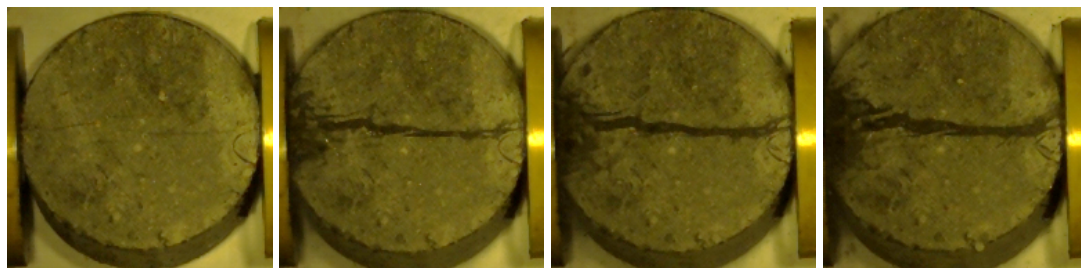
$t=0\mu s$

$t=155\mu s$

$t=310\mu s$

$t=465\mu s$

3% Nano-CaCO₃



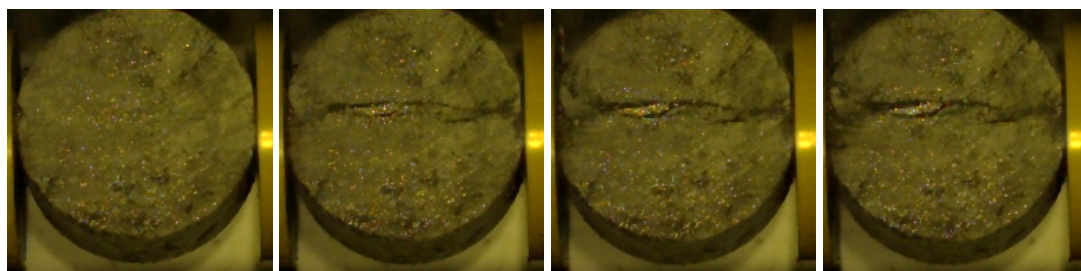
$t=0\mu s$

$t=155\mu s$

$t=310\mu s$

$t=465\mu s$

3% Nano-SiO₂



$t=0\mu s$

$t=155\mu s$

$t=310\mu s$

$t=465\mu s$

3% Nano-Al₂O₃

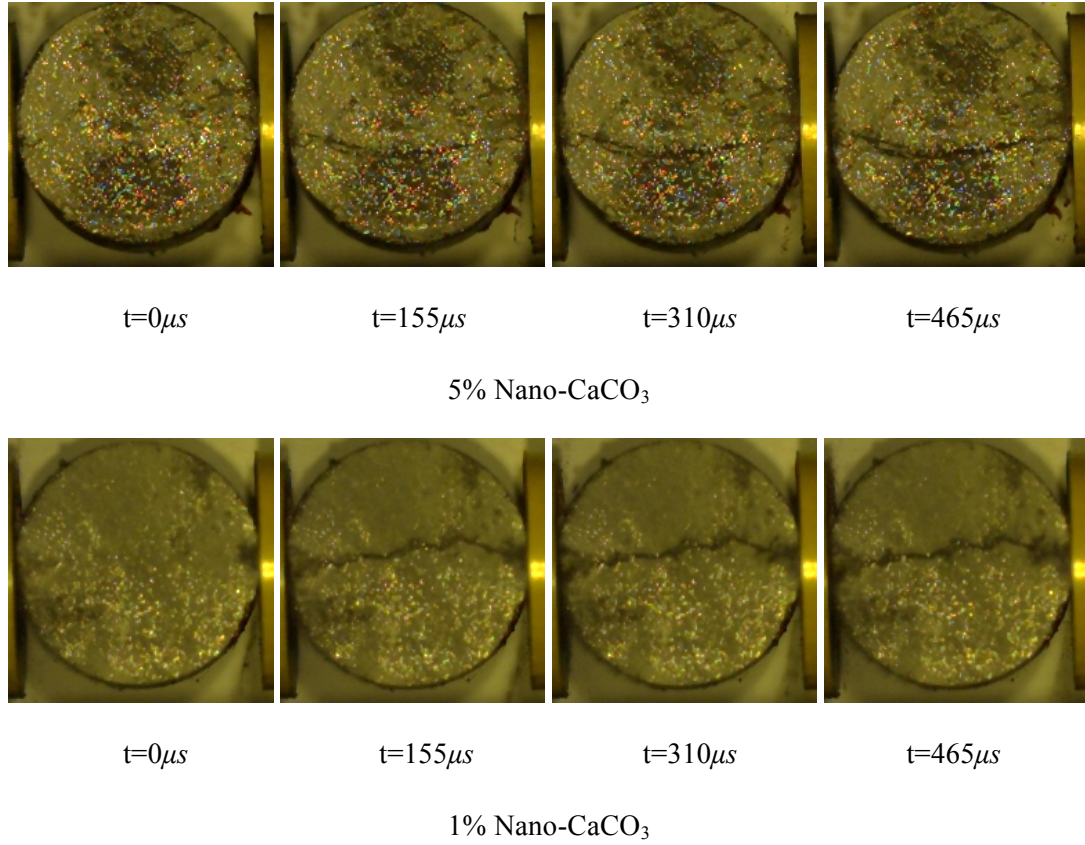


Figure 12: High speed camera results of sample damage

Figure 13 gives the DIF values for dynamic tensile strength of UHPC with different nano material additions. All samples have prominent tensile strength enhancement during the tests. A largest DIF of about 2.55 was obtained in UHPC with Nano-TiO₂ at the strain rate of 14/s. It can also be noted that different from the performance under dynamic compressive test, UHPC with nano-CaCO₃ is relatively insensitive to the high loading rate and its tensile DIF values are quite small around 1.3 even at strain rate of 11/s.

Similar with SHPB dynamic compressive strength, the DIF values of the UHPC materials are compared with those of the normal strength concrete material at the same loading rate. The dynamic increase factors of NSC which are obtained from formulae proposed by Malvar and Crawford [35].

The DIF for normal strength concrete in tension can be calculated as:

$$DIF = \frac{f_t}{f_{ts}} = \begin{cases} \left(\frac{\dot{\epsilon}}{\dot{\epsilon}_s}\right)^\delta & \text{for } \dot{\epsilon} \leq 1s^{-1} \\ \beta \left(\frac{\dot{\epsilon}}{\dot{\epsilon}_s}\right)^{1/3} & \text{for } \dot{\epsilon} > 1s^{-1} \end{cases} \quad (9)$$

where f_t is the dynamic tensile strength at $\dot{\epsilon}$; f_{ts} is the static tensile strength at $\dot{\epsilon}_s$; $\dot{\epsilon}$ is the strain rate in the range of 1×10^{-6} to 160 s^{-1} ; $\dot{\epsilon}_s$ is the static strain rate 1×10^{-6} ; $\log \beta = 6\delta - 2$; $\delta = 1/(1 + 8f_{cs}/f_{co})$; $f_{co} = 10 \text{ MPa}$.

As shown in Figure 13, similar with the observation made in the SHPB compression tests, the DIF of UHPC is constantly lower than the values of NSC. It is considered that the steel fibre reinforcement and nano addition account for the major strength increment of UHPC material and thus the contribution from the strain rate effects are lessened. Also, as aforementioned, the porosity of UHPC is lower than NSC which has been experimentally proved to be influential to the dynamic performance of concrete material.

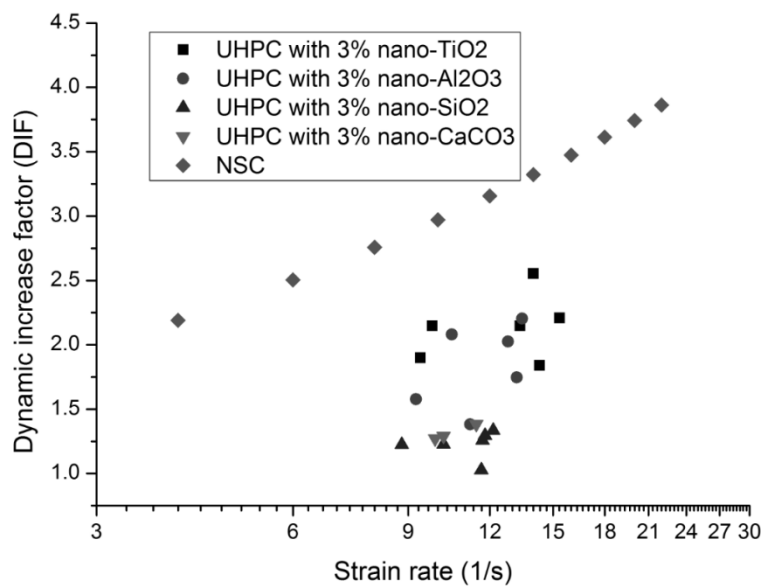


Figure 13: Comparison of DIF curves between NRC and UHPC

In the split tensile test of the current research, two more sets of UHPC samples with the same type of nano particle CaCO_3 addition but different dosages (1% CaCO_3 and 5% CaCO_3) were tested to investigate the influence of volume dosage of nano material on the dynamic tensile strength of UHPC. In Figure 14, influence of different nano material CaCO_3 volume dosages on the dynamic tensile strength is plotted. According to available tests data, UHPC with 1% volume dosage of nano CaCO_3 yields slightly lower DIF values than UHPC with 3% volume dosage of nano CaCO_3 . However, great improvement is observed when the volume dosage increased to 5%. It can thus be concluded that increase of volume dosage could have positive influence on the dynamic tensile strength. However, further investigation is required to find out the optimal value of nano material dosage in order to balance the strength requirement and workability.

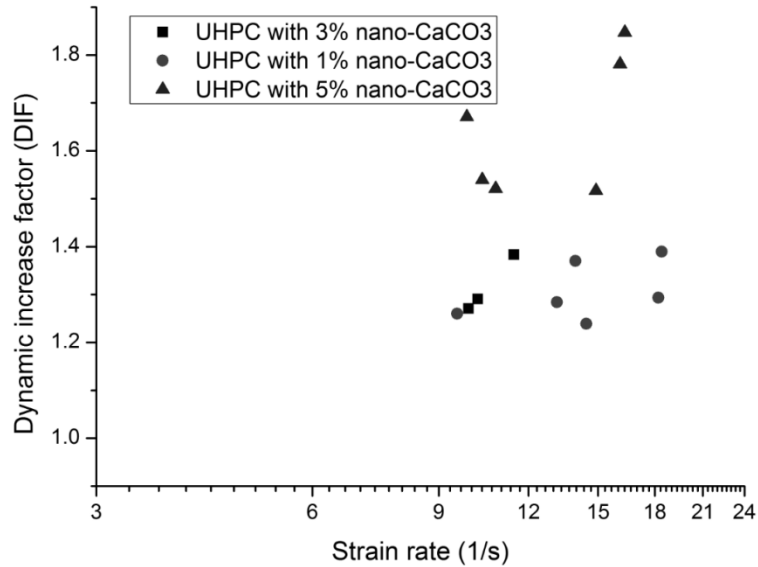


Figure 14: Dynamic increase factors influenced by the volume of Nano-CaCO₃ in Split Tension SHPB tests

After completing the SHPB tensile tests, it can be generally concluded that when compared with normal strength under dynamic tensile loads [35, 39, 40], UHPC with nano material and fibre reinforcement has lower dynamic increase factor, and this observation is consistent with the previous study [41, 42].

2.5 MICROSCOPY ANALYSIS

Microscopy analysis was conducted to provide explanation of macroscopic failure phenomenon at micro-scale. Morphology of the samples was observed by Scanning Electron Microscopy (SEM) using LEO 1550 Scanning Electron Microscope. X-Ray Diffraction (XRD) instrument Bruker D4 ENDEAVOR was used for phase analysis and semi-quantitative analysis. Elemental analysis was conducted by X-Ray Fluorescence (XRF) of Bruker Handheld XRF Spectrometry.

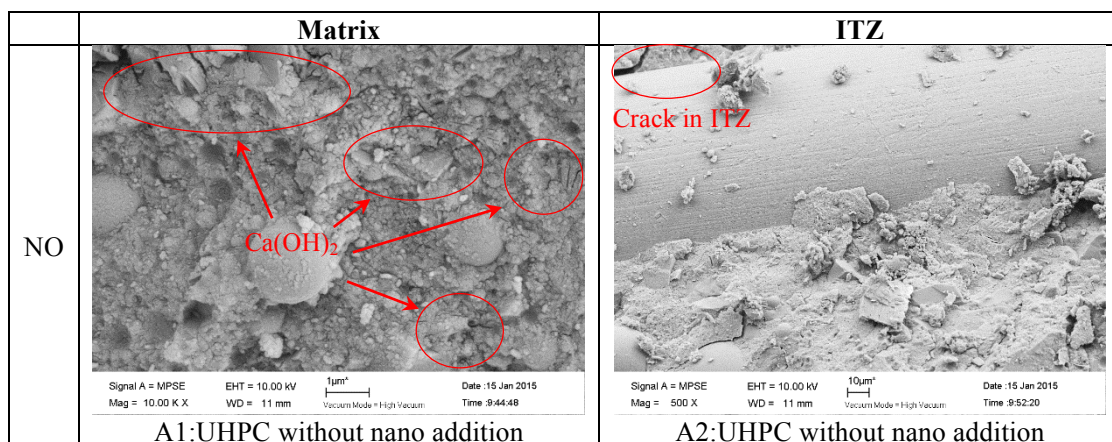
Specimens after SHPB split tensile tests were knocked into small pieces, soaked in ethanol for a week, and ethanol were renewed 3 times in this period; and then were put into a vacuum desiccator (about 40 °C) for drying. Finally samples were stored in a desiccator with limestone inside to keep dry and anti-carbonation.

2.5.1 SEM analysis of UHPC after SHPB split tensile tests

Pictures of matrix and interfacial transition zone (ITZ) taken from the Scanning Electron Microscope (SEM) tests are listed in Figure 15, consisting of four types of samples with different nano additives and one without any nano additive. Please note that all these photos are taken from damaged samples after SHPB split tensile tests.

In Figure 15 A1, large number of well-developed calcium hydroxide $\text{Ca}(\text{OH})_2$ plates can be observed which implies that without nano particles addition, the porosity of the hardened UHPC is relatively large and $\text{Ca}(\text{OH})_2$ has enough space to grow. In UHPC with nano particles addition as shown in Figure 15 B1, C1, D1 and E1, one can observe very dense structures with quite few air pores, and this observation confirmed the filling effect from the ultra-fine nano particles. Furthermore, after a close look into the cement matrix, one can notice that the main hydration product is the foil-like fine C-S-H gel, and no plate-shaped $\text{Ca}(\text{OH})_2$ can be observed. These C-S-H gel are possibly generated from the pozzolanic reactions of nano particles with $\text{Ca}(\text{OH})_2$.

The interfacial transition zones between the steel fibre and cement paste in post-damage UHPC samples are also shown in Figure 15. Two major damage modes can be identified in the figure. In Figure 15 A2, C2 and D2, cement cracks around the ITZ are observed, and these cracks are generated by the stress transferred from steel fibre to the cement in dynamic tests, and cracks initiate in the cement because concrete cement has lower fracture strength than steel fibre. In Figure 15 B2 and E2, besides cement cracks, debonding and pulling out of steel fibre from cement paste can be observed. ITZs in these two figures are damaged and thus their widths are significantly larger than the other three scenarios.



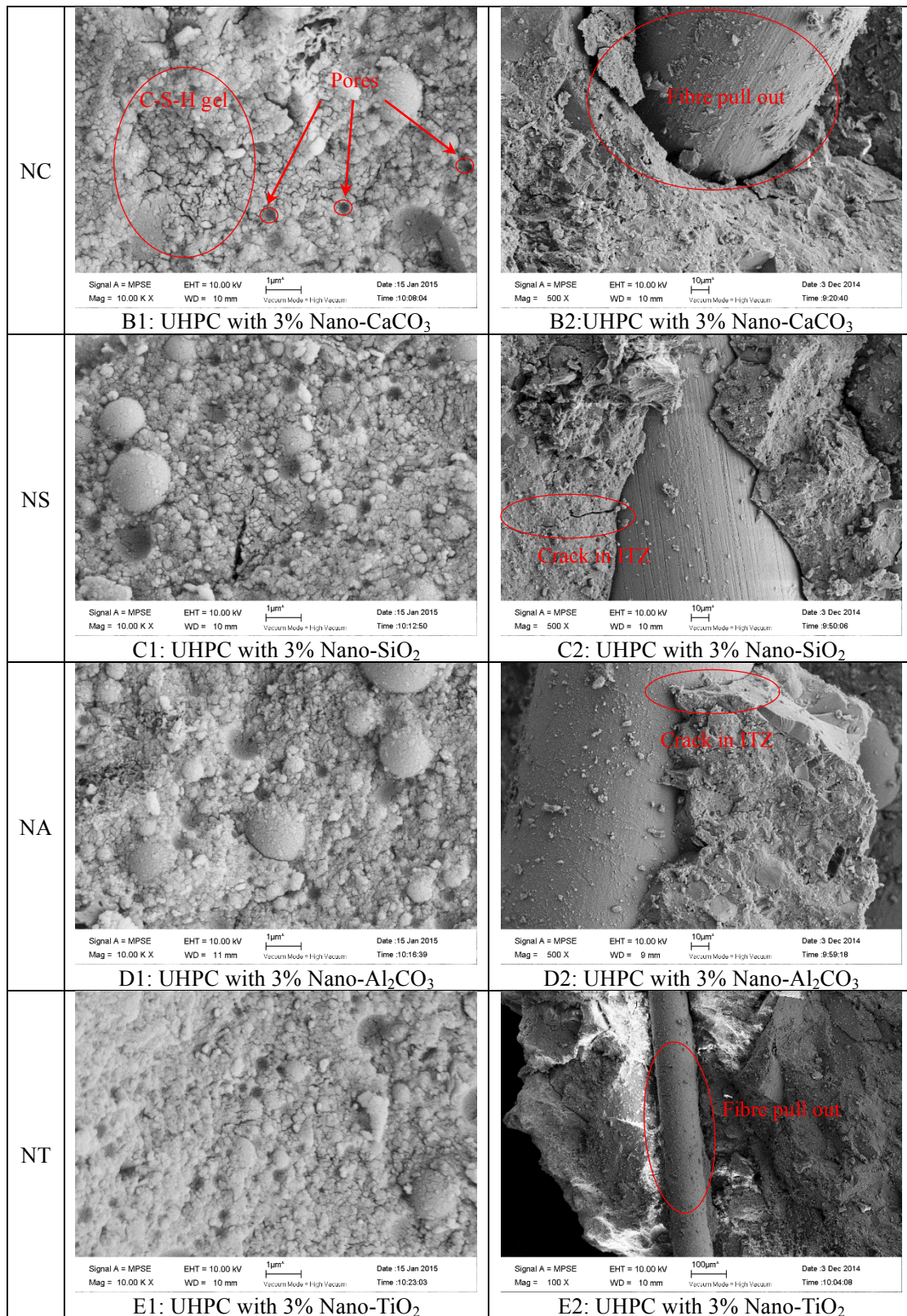


Figure 15: Pictures of motor matrix and ITZ from SEM analysis

2.5.2 X-Ray Fluorescence (XRF) and Diffraction (XRD) Analysis

The X-Ray fluorescence (XRF) test results of UHPC samples are shown in Table 5. It is noted that CaO is the main component in UHPC with or without nano addition, which is followed by SiO₂ and Fe₂O₃.

Table 5: Material semi-quantitative analysis from XRF for UHPC with nano additives

Material	Percentage			
	NC	NS	NA	NT
MgO	0.409	0.432	0.437	0.430
Al ₂ O ₃	2.700	2.780	3.260	2.740
SiO ₂	35.13	39.42	37.54	36.60
P ₂ O ₅	0.783	0.788	0.768	0.746
SO ₃	1.490	1.350	1.220	1.240
Cl	0.036			
K ₂ O	2.430	2.290	2.340	2.390
CaO	46.18	42.22	43.40	42.72
TiO ₂	0.492	0.464	0.475	2.610
Cr ₂ O ₃	0.099	0.129	0.095	
MnO	0.445	0.443	0.379	0.403
Fe ₂ O ₃	8.983	8.209	8.994	9.152
CuO	0.120	0.133	0.135	0.139
ZnO	0.126	0.095	0.085	0.095
SrO	0.164	0.137	0.132	0.150
ZrO ₂	0.037			
BaO	0.150			
WO ₃	0.230	0.907	0.521	0.413

X-Ray Diffraction (XRD) Analysis was used to identify the polycrystalline phases of cement and hardened cement paste through recognition of the X-Ray patterns that are unique for each of the crystalline phases [43]. Comparing with SEM tests, a major advantage of the XRD technique is its speed and ease of measurement. Furthermore and perhaps more importantly, the different phases in the samples can be distinguished [44]. In the current study, besides the investigation of UHPC with different nano material composition, UHPC samples of 28 days and 500 days were analysed to give information of long-term hydration process of UHPC.

Diffraction patterns were collected in the range of 10 - 80° 2θ, 0.02°/step, 2°/min as continuous scans. After data collection, all patterns were processed through Jade 5.0 software.

Diffraction patterns are shown in Figure 16, calcium hydroxide $\text{Ca}(\text{OH})_2$ peaks were identified on diffraction patterns of the UHPC mixture examined. It is noted that ettringite ($\text{Ca}_6\text{Al}_2(\text{SO}_4)_3(\text{OH})_{12}\cdot 26\text{H}_2\text{O}$) characteristic peaks are not seen in the diagram which confirms the SEM observation that ettringite needles are absent in UHPC with high pozzolanic effect. Similar observations were found in the previous UHPC development [45].

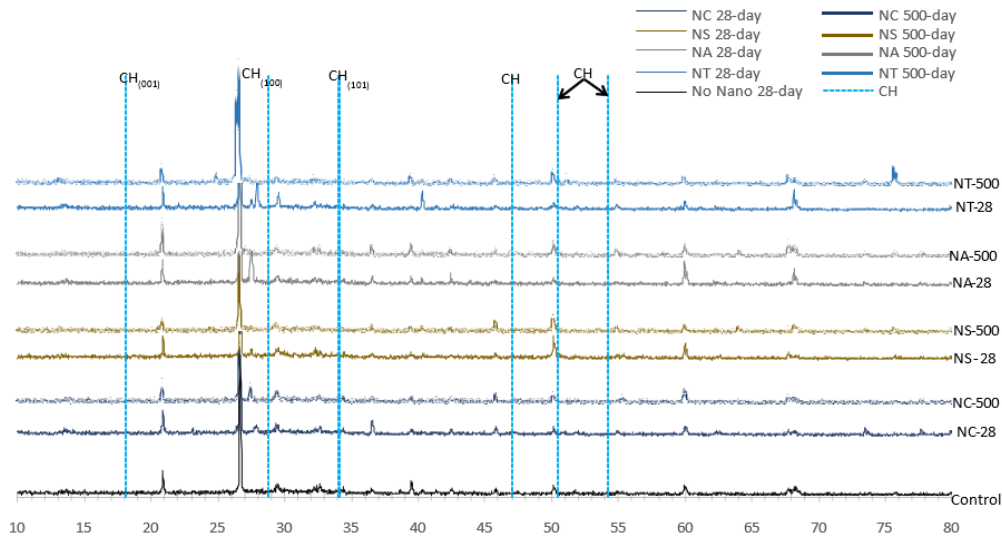


Figure 16: XRD analysis of UHPC with and without nano additives

2.5.3 Influence of nano additives on the properties of UHPC

Following Figure 16, to quantitatively analyse the influence of nano addition on the UHPC material hydration process, the reference intensity (RIR or K), or matrix flushing is adopted in the current study. This technique was developed by Chung [46]. To guarantee the RIR method that can be used as a quantitative method, all phases in the sample being analysed must be known, otherwise the method is at best semi quantitative. Secondly, to improve accuracy of the results, as many of the variables as possible (the RIRs and the I_{rel} values) should be determined with the experimental set up used for specimen analysis.

Assuming n phases exists in the sample, the equation to calculate the weight fraction of a certain phase x is:

$$W_x = I_x / K_x (\sum_{i=1}^n I_i / K_i) \quad (10)$$

where W_x is the weight fraction of phase x , I_x is the intensity (or intensity sum) of phase x in XRF analysis. K_x is the relative intensity (or RIR) for phase x which can be found in PDF in XRF analysis.

Table 6 gives the measurement of intensity (PI) and full width at the half maximum (FWHM) of all Ca(OH)₂ peaks detected at 28 days, the intensity sum (IS) of Ca(OH)₂ is also listed for UHPC with and without nano material addition. It is noted for control sample without nano material addition, CH phase intensity sum is 33.7. For all UHPC samples with nano-material addition, intensity sum decreases.

According to Equation 10, the intensity sum of a phase is proportional to its weight fraction in the sample. Based on this concept, it is noted given the same weight dosage nano material was mixed in UHPC, the weight fraction of CH was significantly influenced by the nano material type. Nano-TiO₂ and Nano-SiO₂ had lower intensity sum of CH which indicated more prominent pozzolanic reaction between CH and nano material. The concrete strengths should be higher than the other two UHPCs with Nano-CaCO₃ and Nano-Al₂O₃ additions. This assumption is confirmed with the compressive strength curve shown in Figure 4 where UHPC with Nano-TiO₂ addition has the highest compressive strength (less CH in the paste and more CSH gel formed) while UHPC with Nano-Al₂O₃ has the lowest compressive strength.

Table 6: Calcium Hydroxide (CH) measurement based on XRD analysis at 28 days

Phase	d (Å)	Control			NC			NS			NA			NT		
		PI (cps)	FWHM	IS	PI (cps)	FWHM	IS	PI (cps)	FWHM	IS	PI (cps)	FWHM	IS	PI (cps)	FWHM	IS
CH	4.90	22	0.22		24	0.14		21	0.18		23	0.26		23	0.12	
	3.10	27	0.14		26	0.20		28	0.16		28	0.12		23	0.12	
	2.63	21	0.90	33.70	26	0.58	31.44	22	0.16	18.72	26	0.32	24.96	31	0.04	19.76
	1.93	18	0.24		22	0.24		11	0.12		14	0.26		17	0.44	
	1.81	17	0.06		14	0.14		28	0.16		21	0.06		17	0.26	
	1.70	14	0.06		14	0.04		19	0.06		15	0.16		11	0.10	

The influence of nano material addition on UHPC long-term hydration process is illustrated in Table 7 where XRD analysis on UHPC samples at 500 days is presented together with UHPC samples at 28 days. It is easily noted that all UHPC samples with nano material addition showed a decrease of intensity sum of CH at 500 days. UHPC samples with Nano-CaCO₃ had a most significant CH intensity sum decrement which indicates a most prominent long-term strength increment for this material.

Table 7: Calcium Hydroxide (CH) measurement based on XRD analysis at 28 and 500 days

Phase	Time (Day)	d (Å)	NC			NS			NA			NT		
			PI (cps)	FWHM	IS	PI (cps)	FWHM	IS	PI (cps)	FWHM	IS	PI (cps)	FWHM	IS
CH	28	4.90	24	0.14		21	0.18		23	0.26		23	0.12	
		3.10	26	0.20		28	0.16		28	0.12		23	0.12	
		2.63	26	0.58	31.44	22	0.16	18.72	26	0.32	24.96	31	0.04	19.76
		1.93	22	0.24		11	0.12		14	0.26		17	0.44	
		1.81	14	0.14		28	0.16		21	0.06		17	0.26	
		1.70	14	0.04		19	0.06		15	0.16		11	0.10	
	500	4.90	21	0.08		21	0.16		18	0.48		18	0.18	
		3.10	26	0.30		22	0.16		25	0.08		24	0.04	
		2.63	24	0.18	18.16	22	0.30	18.5	24	0.20	22.46	22	0.28	17.24
		1.93	23	0.08		17	0.12		22	0.12		15	0.16	
		1.80	18	0.04		18	0.08		18	0.20		22	0.14	
		1.70	15	0.12		14	0.11		13	0.06		14	0.10	

2.6 CONCLUSIONS

For the newly designed concrete materials with both steel fibre and nano material additions, great static strength improvement was observed. Split-Hopkinson-Pressure-Bar tests were conducted to get full understanding of the material constitutive relationships especially under dynamic loading condition. It was observed that with the same fibre reinforcement, different nano materials additions seem to have insignificant influence on the material dynamic strengths. However, material strength could be increased with the increase of nano material volume dosage. Comparing with the traditional normal strength concrete, UHPC with fibre and nano material addition has less strength increment under the same loading rate when compared with normal strength concrete. In SEM tests on post-damage UHPC samples, different damage modes at ITZ are identified, XRD and XRF analysis confirmed the filling and pozzolanic effect of nano particles addition.

REFERENCE

- [1] E. Fehling, K. Bunje, M. Schmidt, Gärtnerplatz – Bridge over River Fulda in Kassel: Multispan Hybrid UHPC-Steel Bridge, in: *Designing and Building with UHPFRC*, John Wiley & Sons, Inc., 2013, pp. 0-136.
- [2] W.J.C.Y.J.K.J.-R.C.J.S. Park, Dynamic Characteristics Evaluation of Innovative UHPC Pedestrian Cable Stayed Bridge, *Engineering*, Vol. 4 No. 12 (2012) 869-876.
- [3] M. Rebentrost, G. Wight, Perspective on UHPCs from a Specialist Construction Company, in: *Designing and Building with UHPFRC*, John Wiley & Sons, Inc., 2013, pp. 189-208.
- [4] C. Wu, D.J. Oehlers, M. Rebentrost, J. Leach, A.S. Whittaker, Blast testing of ultra-high performance fibre and FRP-retrofitted concrete slabs, *Engineering Structures*, 31 (2009) 2060-2069.

- [5] T.L.J. XIAO, STEEL-FIBRE-REINFORCED CONCRETE PANELS EXPOSED TO AIR BLAST LOADING, Proceedings of the ICE-Structures and Buildings, 134 (1999) 319-331.
- [6] X. Zhou, V. Kuznetsov, H. Hao, J. Waschl, Numerical prediction of concrete slab response to blast loading, International Journal of Impact Engineering, 35 (2008) 1186-1200.
- [7] J. Li, H. Hao, Numerical study of concrete spall damage to blast loads, International Journal of Impact Engineering, 68 (2014) 41-55.
- [8] J. Li, H. Hao, Influence of brittle shear damage on accuracy of the two-step method in prediction of structural response to blast loads, International Journal of Impact Engineering, 54 (2013) 217-231.
- [9] M. Xu, K. Wille, Fracture energy of UHP-FRC under direct tensile loading applied at low strain rates, Composites Part B: Engineering, 80 (2015) 116-125.
- [10] P. Hannant, Fibre cements and fibre concretes, in, 1978.
- [11] S. Grünewald, Performance-based design of self-compacting fibre reinforced concrete, Delft University Press Delft, The Netherlands, 2004.
- [12] J.G. MacGregor, J.K. Wight, S. Teng, P. Irawan, Reinforced concrete: mechanics and design, Prentice Hall Upper Saddle River, NJ, 1997.
- [13] J.A. Barros, V.M. Cunha, A.F. Ribeiro, J. Antunes, Post-cracking behaviour of steel fibre reinforced concrete, Materials and Structures, 38 (2005) 47-56.
- [14] H. Li, H.-g. Xiao, J. Yuan, J. Ou, Microstructure of cement mortar with nano-particles, Composites Part B: Engineering, 35 (2004) 185-189.
- [15] B.-W. Jo, C.-H. Kim, G.-h. Tae, J.-B. Park, Characteristics of cement mortar with nano-SiO₂ particles, Construction and Building Materials, 21 (2007) 1351-1355.
- [16] Y. Qing, Z. Zenan, K. Deyu, C. Rongshen, Influence of nano-SiO₂ addition on properties of hardened cement paste as compared with silica fume, Construction and Building Materials, 21 (2007) 539-545.
- [17] X. Liu, L. Chen, A. Liu, X. Wang, Effect of Nano-CaCO₃ on Properties of Cement Paste, Energy Procedia, 16, Part B (2012) 991-996.
- [18] A. Nazari, S. Riahi, The effects of SiO₂ nanoparticles on physical and mechanical properties of high strength compacting concrete, Composites Part B: Engineering, 42 (2011) 570-578.
- [19] A. Nazari, S. Riahi, The effects of zinc dioxide nanoparticles on flexural strength of self-compacting concrete, Composites Part B: Engineering, 42 (2011) 167-175.
- [20] A. Nazari, S. Riahi, The effect of TiO₂ nanoparticles on water permeability and thermal and mechanical properties of high strength self-compacting concrete, Materials Science and Engineering: A, 528 (2010) 756-763.
- [21] A. Nazari, S. Riahi, The effects of ZrO₂ nanoparticles on physical and mechanical properties of high strength self compacting concrete, Materials Research, 13 (2010) 551-556.
- [22] A. Nazari, S. Riahi, The effects of limewater on flexural strength and water permeability of Al₂O₃ nanoparticles binary blended concrete, Journal of Composite Materials, 45 (2011) 1165-1172.
- [23] A. Nazari, S. Riahi, The effects of ZnO₂ nanoparticles on split tensile strength of self-compacting concrete, Journal of Experimental Nanoscience, 7 (2012) 491-512.
- [24] A. Najigivi, A. Khaloo, A. Irajizad, S. Abdul Rashid, Investigating the effects of using different types of SiO₂ nanoparticles on the mechanical properties of binary blended concrete, Composites Part B: Engineering, 54 (2013) 52-58.
- [25] C. Buzea, I.I. Pacheco, K. Robbie, Nanomaterials and nanoparticles: Sources and toxicity, Biointerphases, 2 (2007) MR17-MR71.

- [26] S. Marais, R. Tait, T. Cloete, G. Nurick, Material testing at high strain rate using the split Hopkinson pressure bar, *Latin American Journal of Solids and Structures*, 1 (2004) 219-339.
- [27] B. Hopkinson, A method of measuring the pressure produced in the detonation of high explosives or by the impact of bullets, *Proceedings of the Royal Society of London. Series A*, 89 (1914) 411-413.
- [28] H. Kolsky, An investigation of the mechanical properties of materials at very high rates of loading, *Proceedings of the Physical Society. Section B*, 62 (1949) 676.
- [29] R. Davies, A critical study of the Hopkinson pressure bar, *Philosophical Transactions of the Royal Society of London. Series A. Mathematical and Physical Sciences*, (1948) 375-457.
- [30] M.L. Hughes, J. Tedesco, C. Ross, Numerical analysis of high strain rate splitting-tensile tests, *Computers & structures*, 47 (1993) 653-671.
- [31] Q.M. Li, H. Meng, About the dynamic strength enhancement of concrete-like materials in a split Hopkinson pressure bar test, *International Journal of Solids and Structures*, 40 (2003) 343-360.
- [32] T. Lok, P. Zhao, G. Lu, Using the split Hopkinson pressure bar to investigate the dynamic behaviour of SFRC, *Magazine of Concrete Research*, 55 (2003) 183-191.
- [33] S. Timoshenko, J.N. Goodier, *Theory of Elasticity*, by S. Timoshenko and J. N. Goodier,... 2nd Edition, McGraw-Hill book Company, 1951.
- [34] C.E.-I.d. Béton, E.-I.C.f. Concrete, CEB., *Concrete Structures Under Impact and Impulsive Loading: Synthesis Report : Contribution À la 26e Session Plénière Du C.E.B.*, Dubrovnik - Septembre 1988, CEB, Secrétariat Permanent, 1988.
- [35] L.J. Malvar, J.E. Crawford, Dynamic increase factors for concrete, in, *DTIC Document*, 1998.
- [36] B. Hughes, A. Watson, Compressive strength and ultimate strain of concrete under impact loading, *Magazine of concrete research*, 30 (1978) 189-199.
- [37] P. Bischoff, S. Perry, Compressive behaviour of concrete at high strain rates, *Materials and structures*, 24 (1991) 425-450.
- [38] X. Chen, L. Xu, S. Wu, Influence of Pore Structure on Mechanical Behavior of Concrete under High Strain Rates, *Journal of Materials in Civil Engineering*, (2015) 04015110.
- [39] T. Nicholas, Tensile testing of materials at high rates of strain, *Experimental Mechanics*, 21 (1981) 177-185.
- [40] C.A. Ross, J.W. Tedesco, S.T. Kuennen, Effects of strain rate on concrete strength, *ACI Materials Journal*, 92 (1995).
- [41] R. Chen, Y. Liu, X. Guo, K. Xia, F. Lu, Dynamic Tensile Properties of Steel Fiber Reinforced Concrete, in: T. Proulx (Ed.) *Dynamic Behavior of Materials*, Volume 1, Springer New York, 2011, pp. 37-42.
- [42] A.M. Weidner, *Dynamic Properties of Concrete and Fiber Reinforced Concrete at Room and Elevated Temperatures*, Department of Civil and Environmental Engineering, University of Utah, 2013.
- [43] J. Roncero, S. Valls, R. Gettu, Study of the influence of superplasticizers on the hydration of cement paste using nuclear magnetic resonance and X-ray diffraction techniques, *Cement and Concrete Research*, 32 (2002) 103-108.
- [44] K.L. Scrivener, T. Füllmann, E. Gallucci, G. Walenta, E. Bermejo, Quantitative study of Portland cement hydration by X-ray diffraction/Rietveld analysis and independent methods, *Cement and Concrete Research*, 34 (2004) 1541-1547.
- [45] M. Reda, N. Shrive, J. Gillott, Microstructural investigation of innovative UHPC, *Cement and Concrete Research*, 29 (1999) 323-329.

[46] F.H. Chung, Quantitative interpretation of X-ray diffraction patterns of mixtures. I. Matrix-flushing method for quantitative multicomponent analysis, *Journal of Applied Crystallography*, 7 (1974) 519-525.

Statement of Authorship

Article Name: Effects of Steel Fibres on Dynamic Strength of UHPC

Su, Y., Li, J., Wu, C., Wu, P. and Li, Z.X. 2016. Effects of steel fibres on dynamic strength of UHPC. *Construction and Building Materials*, 114, pp.708-718.

Status: Published

Su, Y. (candidate)

Contribution: helped conduct tests, processed and analysed test data and prepared manuscript

I hereby certify that the statement of contribution is accurate.

Signed..... Date 27/08/2016

J, L.

Contribution: supervised research and tests, provided critical manuscript evaluation and acted as corresponding author.

I hereby certify that the statement of contribution is accurate and I give permission for the inclusion of the paper in the thesis.

Signed..... Date 24/8/2016

Wu, C.

Contribution: helped design and conduct tests.

I hereby certify that the statement of contribution is accurate and I give permission for the inclusion of the paper in the thesis.

Signed..... Date 24/08/2016

Wu, P.

Contribution: provided critical manuscript evaluation.

I hereby certify that the statement of contribution is accurate and I give permission for the inclusion of the paper in the thesis.

Signed..... Date 2016.8.24

Li, Z.X.

Contribution: provided critical manuscript evaluation.

I hereby certify that the statement of contribution is accurate and I give permission for the inclusion of the paper in the thesis.

Signed..... Date Aug 25, 2016

CHAPTER 3: EFFECTS OF STEEL FIBRES ON DYNAMIC STRENGTH OF UHPC

Yu Su^{1,2}, Jun Li^{1,2}, Chengqing Wu^{1,2,*}, Pengtao Wu¹, Zhongxian Li¹

¹TCU-UA (Tianjin Chengjian University-University of Adelaide) Joint Research Centre on
Disaster Prevention and Mitigation

²School of Civil, Environmental and Mining Engineering, the University of Adelaide, SA,
Australia 5005

ABSTRACT

In modern civil engineering, steel fibres are widely used as reinforcement in the design of high performance concrete material. The addition of steel fibres in the concrete matrix can greatly improve the material ductility and durability as well as the impact and abrasion resistance. The performance of steel fibre reinforced concrete changes with varying concretes, fibre geometries, distribution, orientation and densities. In the recent study, an innovative ultra-high performance concrete material with nano-material addition is developed. In the mix design of this UHPC material, steel fibre is taken as an important composite. Great improvement of static compressive strength and split tensile strength had been obtained. In the current research, Split-Hopkinson-Pressure-Bar (SHPB) tests are conducted on this UHPC material to investigate its dynamic properties. Different types of steel fibres including two kinds of micro fibres and two kinds of twisted fibres are mixed in the UHPC. In total, 80 UHPC samples were tested in Swinburne University of Technology in 2011 and 190 specimens were tested in the Central South University of China in 2013. The influence of steel fibre addition on the dynamic strength of UHPC is presented and it is found that steel fibres have prominent influence on the concrete dynamic strength but insignificant impact on the Dynamic Increase Factor (DIF) curves.

3.1 INTRODUCTION

The concept of using fibres as material reinforcement is not new. Fibres have been used as reinforcement since the mighty time of ancient Roman. Horsehair was added into mortar and straw to build mud bricks in that time. Modern version of concrete fibres did not come into use until 1960s when steel fibres, glass fibres and synthetic fibres took the stage. Use of fibre

in concrete matrix can reduce the concrete permeability and enhance its crack control ability. Fine fibres control opening and propagation of microcracks as they are densely dispersed in cement matrix. Longer fibres control larger cracks and contribute to increase the final strength of fibre reinforced concrete [1].

Investigation of the influence from varying fibre reinforcement type on the concrete performance had been conducted in the recent studies. Riguard et al. [2] studied post-cracking behaviour of high performance concrete containing glass fibres, and the relationship between tensile strength and strain was extracted. Accelerated aging tests in 50 degree water were also conducted and the durability and ductility of such concrete material were verified. Zheng et al. [3] discussed characteristics of various synthetic fibres and the behaviour of concrete reinforced with each of these fibres, and they reviewed research concerning the performance of synthetic fibre-reinforced concrete based on polyethylene (PE), polypropylene (PP), acrylics (PAN), poly (vinyl alcohol) (PVA), polyamides (PA), aramid, polyester (PES) and carbon reinforcements. Alani and Beckett [4] presented results concerning the punching shear failure of a 6.00 m × 6.00 m × 0.15 m synthetic fibre reinforced ground supported slab, and they concluded that the punching shear failure values obtained were comparable to values reported for the steel fibre slabs under similar conditions.

Among all fibre types, steel fibres are known to have higher modulus of elasticity than the concrete matrix which means they can enhance the load carrying capacity, thus increase tensile strength of the material. Concrete with steel fibre reinforcement has better impact, shatter and abrasion resistance. Nowadays steel fibres are widely used as reinforcement in industrial floor slabs, standard reinforcing cage for tunnel segments, shotcrete and prefabricated concrete products. Ye et al. [5] experimentally investigated the mechanical behaviour of concrete reinforced by hybrid different shapes of steel fibres. The largest fracture energy and bending toughness were obtained with hybrid-fibres, where the volume ratio of long ultra-fine fibre was 1.5%, and the ratio of long end-hooked fibre was 0.5%. The hybrid-fibres had generated positive intermixing effect. Kim et al. [6] examined the effects of twisted steel fibre on concrete flexural toughness, and three types of twisted fibre with different lengths and diameters were considered. Ryu et al. [7] found that concrete with twisted fibre reinforcement exhibited significantly improved mechanical characteristics compared to control concrete containing conventional straight fibre. Bindiganavile and Banthia [8] pointed out that under both static and low-rate impact loads, the predominant failure mode of steel fibre reinforced concrete material was the steel fibre pull-out. To

increase the bonding between the concrete and steel fibre material, Xu et al. [9] proposed spiral shaped steel fibres, and the impact tests had demonstrated that fibre reinforced concrete specimens reinforced with this spiral shaped fibres displayed the largest ultimate compressive strength, the largest post-failure strength and the largest energy-absorption capacity amongst specimens reinforced with seven other types of fibres tested.

For steel fibre reinforced concrete, the most important factors affecting the concrete properties are fibre aspect ratio (ratio of steel fibre length over diameter) and volume fraction. Increasing fibre aspect ratio helps increasing the probability of heterogeneous distribution and flocculation in concrete. Fibre volume fraction significantly affects the workability of concrete. Yazıcı et al. [10] tested hooked-end bundled steel fibres reinforced concrete, and the influence of different aspect ratios and fibre volumes were discussed. They noted that split tensile strength, flexural strength of SFRC are improved with increasing aspect ratio and fibre volume fraction. Wang et al. [11] conducted experimental analysis on effect of fibre aspect ratio on mechanical properties of steel fibre reinforced concrete, and the results revealed that the aspect ratio had an optimal value for strengths in every concrete batch. Beyond this value, the addition of steel fibres into concrete may have an effect of increasing the ductility rather than the strengths.

In modern society, with the rising of terrorism activities, construction material concerning infrastructure protection is under fast developing. Ultra-high Performance Concrete (UHPC) of which an important composite is steel fibre is now widely investigated by government agencies and universities. Different from conventional commercial concrete, UHPC has unique material composites: typically fine-grained sand, silica fume, small steel fibers, and special blends of high-strength Portland cement. UHPC is characterized with remarkable ductility, durability and strength properties [12]. First use of ultra-high strength concrete in civil construction was in Canada. The Shawnessy Light Rail Transit (LRT) Station, constructed during fall 2003 and winter 2004, forms part of a southern expansion to Calgary's LRT system and is the world's first LRT system to be constructed with ultra-high performance concrete [13]. Later applications of this material on pedestrian bridge in Germany [14], a cable stayed bridge in Korea [15] and a series of pedestrian bridge in New Zealand [16] have impressed the world with its great mechanical performance and durability. In the recent years, UHPC had been used in structural elements to resist extreme earthquake effects [17], and explosive loads [18, 19].

In a more recent study, taking advantage of nano material technology, novel UHPC material with different steel fibre reinforcement and nano material addition was developed. From static compressive tests and the split tensile tests, it was noticed that the newly designed UHPC material has significantly improved mechanical strength which indicates its potential utilization in protective engineering against impact and explosive loads. However, before such application, it is necessary to get fully understanding of material dynamic behaviour which is different from its quasi-static performance [20, 21]. Split-Hopkinson-Pressure-Bar tests were carried out on 80 UHPC samples in Swinburne University of Technology in 2011 and 190 specimens in the Central South University of China in 2013. Four different types of steel fibres, namely micro fibre MF06, MF15 and twisted fibre TF03, TF05 were mixed in the UHPC. Through the experimental tests, influence of fibre type (twisted fibre and straight micro fibre), fibre length (6 mm micro fibre and 15 mm micro fibre), aspect ratio and fibre fraction volume (0.5% MF15, 1.0% MF15 and 2.5% MF15) on the UHPC performance can be obtained. Dynamic Increase Factor Curves which are important describing the material under high loading rate are generated based on the test results, and the influence of different fibre material addition is discussed.

3.2 UHPC SAMPLE PREPARATION

In the current research, the complete mix proportion of UHPC is shown in Table 8. It can be noted in the UHPC composites, coarse aggregates are replaced with silica fume. For conventional commercial concrete, aggregates, which account for 60 to 75 percent of the total volume of concrete, are divided into two distinct categories, i.e. fine and coarse aggregates. Fine aggregates generally consist of natural sand or crushed stone with most particles passing through a 3/8 inch (9.5 mm) sieve. Coarse aggregates are any particles greater than 0.19 inch (4.75 mm), but generally range between 3/8 and 1.5 inches (9.5 mm to 37.5 mm) in diameter. Gravels constitute the majority of coarse aggregate used in concrete with crushed stone making up most of the remainder.

In UHPC, ultra-fine particle silica fume (0.15-0.20 μm) instead of coarse aggregates is added to Portland concrete to improve its properties, in particular its compressive strength, bond strength, and abrasion resistance. These improvements stem from both the mechanical improvements resulting from addition of a very fine powder to the cement paste mix as well as from the pozzolanic reactions between the silica fume and free calcium hydroxide in the paste. The addition of silica fume can also reduce the permeability of concrete material to

chloride ions and thus protect the steel reinforcement against corrosion [22]. The workability of UHPC in coastal areas where the environment is chloride rich can be improved.

Table 8: Mix proportion of UHPC (unit: kg)

52.5 Cement	750			
Silica Fume	225			
Silica Flour	190			
River Sand	1030			
Superplasticizer	16			
Water	190			
Water/Binder	25.30%			
Nano Particles	21.7			
MF15	191	-	-	-
MF06	-	191	-	-
TF03	-	-	191	-
TF05	-	-	-	191

In the present study, nano particles nano-CaCO₃ at a constant volume fraction are added into the UHPC specimens. It was reported in the previous study that inclusion of nano size particles into the concrete matrix favours its mechanical performance. Jo et al. [23] experimentally investigated properties of cement mortars with nano-SiO₂ addition. The experimental results showed that the compressive strengths of mortars with nano-SiO₂ particles were all higher than those of mortars containing silica fume at 7 and 28 days. Liu et al. [24] added nano-CaCO₃ into the cement paste and the experimental results showed that NC had no effect on water requirement of normal consistency of cement. However, with the increase of nano-CaCO₃ content, the flowability decreased and the setting time of fresh cement paste was shortened. Flexural strength and compressive strength increased with the addition of nano-CaCO₃ at the age of 7 days and 28 days.

The inclusion of nano-CaCO₃ into the UHPC matrix in the current study is based on two considerations. Firstly, nano-CaCO₃ is proved to be effective in increasing concrete mechanical performance. Secondly, nano-CaCO₃ is a widely used nano addition and its relatively low price promised its potential application in practical civil designs.

Fibre reinforcement including four different steel fibres, i.e. MF06, MF15, TF03 and TF05 as shown in Figure 17 are mixed in the concrete material.

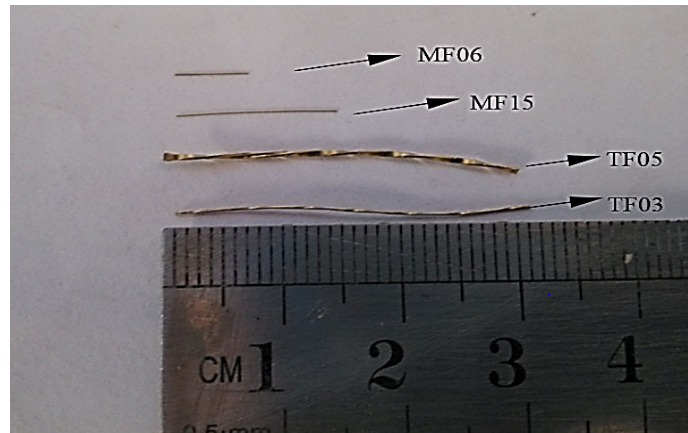


Figure 17: Different types of steel fibres

The mechanical properties and dimensions of the steel fibres are listed in Table 9.

Table 9: Material Properties of Fibres

Type	Elastic Modulus GPa	Tensile Strength MPa	Diameter mm	Length mm	Aspect ratio
MF06	210	4295	0.12	6	50
MF15	210	4295	0.12	15	125
TF03	210	1500	0.3	30	100
TF05	210	1500	0.5	30	60

All UHPC samples were produced by mixing the silica fume, fine sand and powder materials which consisted of cement and nanoparticles, in a laboratory concrete mixer. They were firstly dry mixed for 5 minutes before any water addition. 70% water was then added and mixed for 3 minutes to fluidise the mix. Superplasticizer was added before the other 30% water was finally mixed. The mixing process was then continued for another 5 minutes before steel fibres were added and manually dispersed in order to avoid clumping and guarantee the fibres were uniformly distributed and randomly oriented.

Wooden moulds as shown in Figure 18 are prepared for curing of UHPC. The specimens were firstly cured in a humid room for 24 hours and the temperature was controlled to be 20 ± 5 °C. The specimens were then demoulded and cured in hot water at a temperature of 90 °C for another 48 hours. At last, the specimens were placed in a room again at the ambient temperature until the commencement of the tests. Prior to any tests, samples were properly levelled, sanded, polished, cleaned and dried to attain smooth surfaces.



Figure 18: Concrete wooden moulds

After proper curing, the UHPC samples were drilled out using automatic core drilling machine. The specimens used for static compression test were 100 mm cubes, and the samples used in the static split tensile tests and the following SHPB tests were cylinders with 75 mm diameter with 37 mm or 75 mm height.

3.3 STATIC TESTS

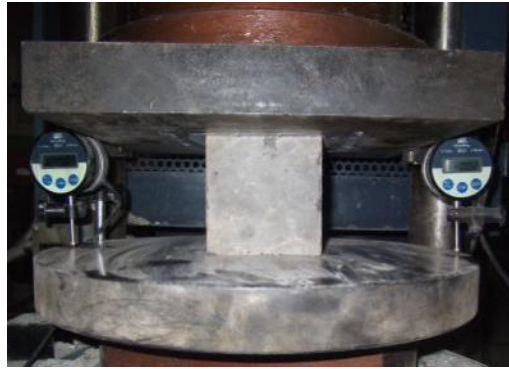
Uniaxial compression tests and split tensile tests were conducted to determine static uniaxial compressive strength and split tensile strength of UHPC.

3.3.1 Uniaxial compression test

The experiments were carried out on a number of 100 mm*100 mm*100 mm cubes using a 3000 kN capacity computer-controlled electromechanical servo hydraulic pressure testing machine as shown in Figure 19a. Testing procedure conformed to the China Standard GB/T 50081-2002. Figure 19b illustrates the testing setup. At both sides of the loading plate, there was an axially oriented LVDT to record the test data. In total there were 68 specimens tested.



(a) YAW-3000 computer controlled servo pressure testing machine



(b) Testing sample and LVDT installation

Figure 19: Testing set-up for compression tests of cubic specimens

Static stress-strain curves representing all four kinds of samples are shown in Figure 20. It can be clearly observed that with the addition of different steel fibres in the UHPC, the static performance varies significantly. UHPC with 2.5% MF15 has the highest static strength around 150 MPa which is about 30% higher than the lowest strength obtained in UHPC with 2.5% TF05 reinforcement.

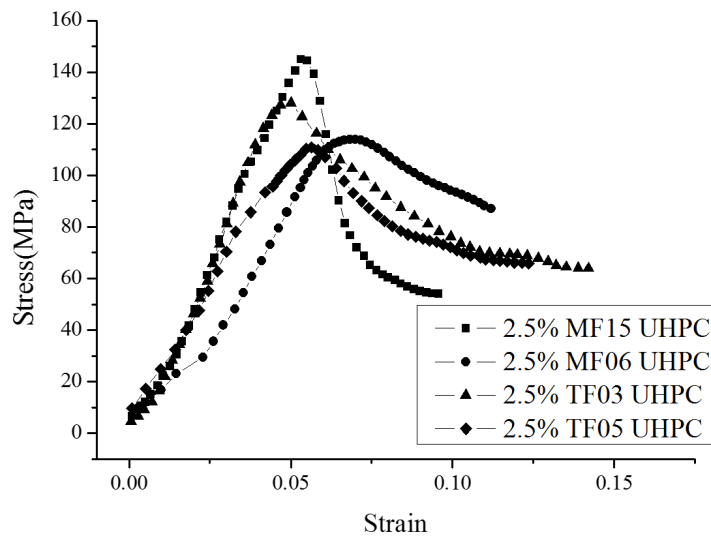


Figure 20: Stress-strain curves from quasi-static compressive tests

For the two specimens reinforced by twisted steel fibres as shown in Figure 21a, it is noted TF03 (aspect ratio $L/D=100$) has a higher compressive strength around 130 MPa while TF05 (aspect ratio $L/D=60$) has a relatively lower strength around 110 MPa. Given a same volume fraction, TF03 with a smaller diameter means a larger number of fibres in the matrix and thus can effectively resisting the cracking and improve the concrete strength.

For the two specimens reinforced by micro steel fibres as shown in Figure 21b, it is easy to see that when the volume fraction is fixed, the fibre aspect ratio exerts significant influence on the stress–strain plots. Compared to smaller aspect ratio (MF06 in which $L/D=50$), the peak strain decreases markedly but the compressive strength and elastic modulus (slope of initial straight line) increase for the larger aspect ratio (MF15 in which $L/D=125$) case. Such observations can be attributed to the fact that fine fibres MF06 control opening and propagation of microcracks as they are densely dispersed in cement matrix, and longer fibres MF15 control larger cracks and contribute to increase the final strength of FRC.

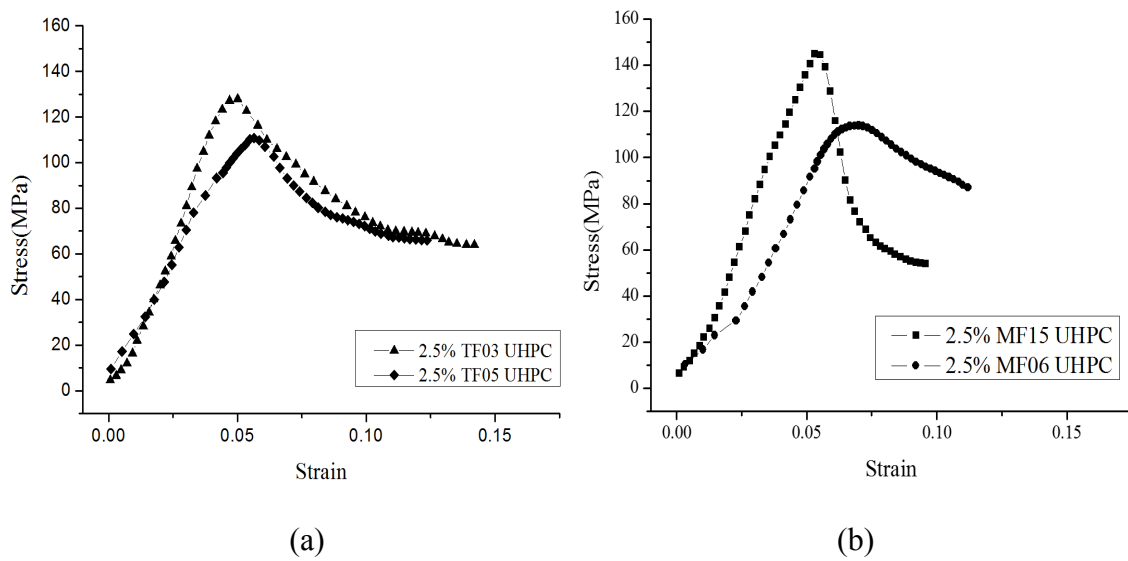


Figure 21: Influence from fibre aspect ratio on UHPC compressive strength

The influence of fibre volume fraction is illustrated in Figure 22. Three fibre volume fractions, i.e. 0.5%, 1.0% and 2.5% are studied in the uniaxial compression test, and it can be noticed from the stress strain curve that material peak compressive strength is increasing with fibre volume fraction. Furthermore, the material peak strain and ductility are also favoured with an increasing fibre volume fraction. The results indicate that to obtain a better performance of UHPC material, a reasonably higher fibre volume fraction is essential given that the concrete workability can still be satisfied.

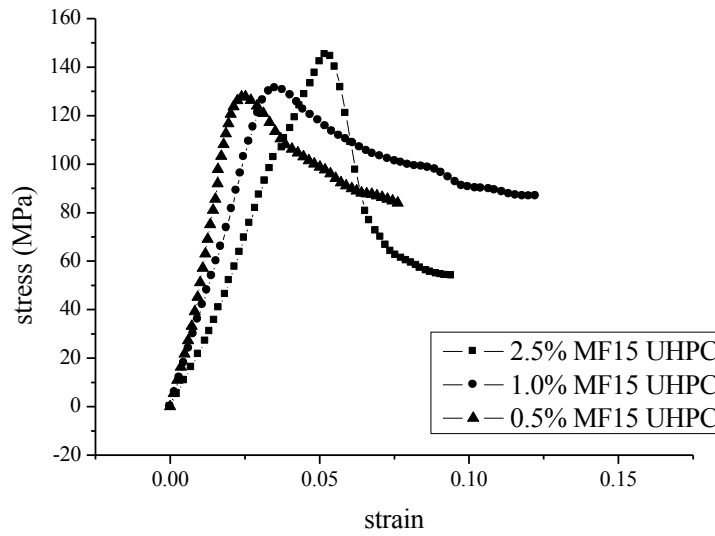


Figure 22: Compressive stress-strain curves for different fibre volume fractions

The static compressive strengths for UHPC with different fibre reinforcements are averaged and listed in Table 10.

Table 10: Experimental results of different formula UHPC under static compressive load

Fibre type	MF15	MF06	TF03	TF05
Strength (MPa)	145.12	114.51	132.29	113.05

3.3.2 Split tensile test

Split tensile test were conducted on UHPC cylinder specimens with dimension of 75 mm diameter * 37 mm height as shown in Figure 7. The test concrete cylinder was placed horizontally between the loading surfaces of compression testing machine (Figure 23a). The compression load was applied diametrically and uniformly along the length of cylinder until the failure of the cylinder along the vertical diameter (Figure 23b). In order to generate a uniform loading distribution and minimise the concentration of the high compressive stresses near the points of application. Two strips of plywood were placed between the specimen and loading plates of the testing machine.

Test stops until the concrete cylinder splits into two halves along the vertical diameter plane. The split tensile failure is induced by the indirect tensile stress form Poisson's effect.



(a) Test setup

(b) Failure specimen

Figure 23: Split tension tests

The split tensile strength was calculated based on Equation (12):

$$\sigma = \frac{2P}{\pi DL} \quad (12)$$

where P is the load at failure; D and L are the diameter and length of the specimen respectively.

Figure 24 shows the static split tensile stress strain curve of two micro fibre reinforced UHPC. It is seen again that aspect ratio has positive influence on the material mechanical performance. Compared with MF06 reinforced UHPC, UHPC with MF15 reinforcement has higher peak tensile strength and higher ductility which indicates a better energy absorption ability.

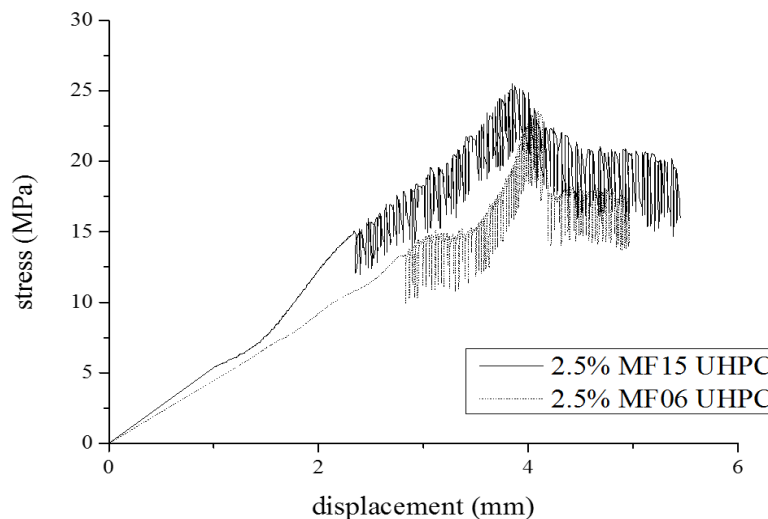


Figure 24: Stress-strain curves from static split tensile tests

The influence of volume fraction on UHPC split tensile strength is shown in Figure 25. It is observed that a slightly increased tensile strength is obtained in 1.0% MF15 UHPC

comparing with 0.5% MF15 sample. A drastically increased strength is observed from 2.5% MF 15 UHPC. Generally speaking, the ductility is also increasing with the fibre volume fraction.

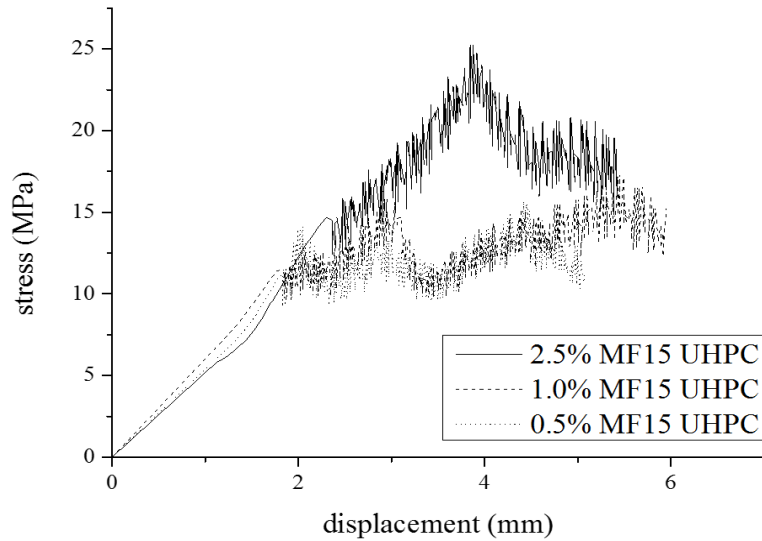


Figure 25: Tensile strength of UHPC with different fibre volume fractions

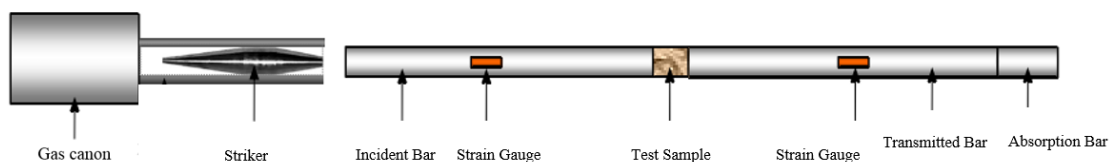
The static split tensile strengths for UHPC with different fibre reinforcements are then averaged and listed in Table 11.

Table 11: Split tensile strength of different formula UHPC under static load

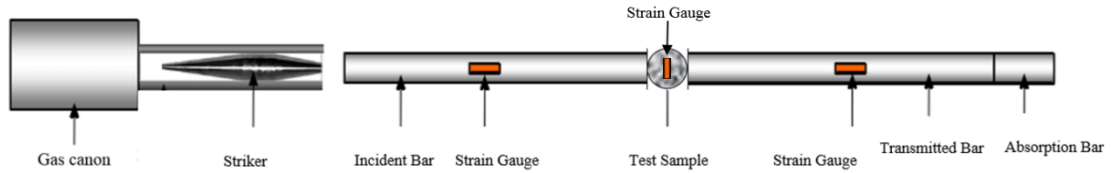
Fibre type	MF15	MF06	TF03	TF05
Strength (MPa)	22.2	20.5	13.5	15.0

3.4 SHPB TESTING PROGRAM

The dynamic tests were conducted on SHPB test machine with 75 mm diameter. The experimental system of SHPB is sketched in Figure 26.



(a) SHPB compression test setup



(b) SHPB split tensile test setup

Figure 26: SHPB experimental system

In SHPB tests, the specimen was placed between the ends of two straight bars, called the incident bar and the transmitted bar. At the end of the incident bar (some distance away from the specimen, typically at the far end), a stress wave was created which propagates through the bar toward the specimen. This wave was referred to as the incident wave, and upon reaching the specimen, split into two smaller waves. One of them, the transmitted wave, travelled through the specimen and into the transmitted bar, causing plastic deformation in the specimen. The other wave, called the reflected wave, is reflected away from the specimen and travels back down the incident bar. Strain gages were then placed on the bars to measure strains caused by the waves. Assuming deformation in the specimen is uniform, the stress and strain can be calculated from the amplitudes of the incident, transmitted, and reflected wave. Figure 27 shows typical waves in SHPB compression test.

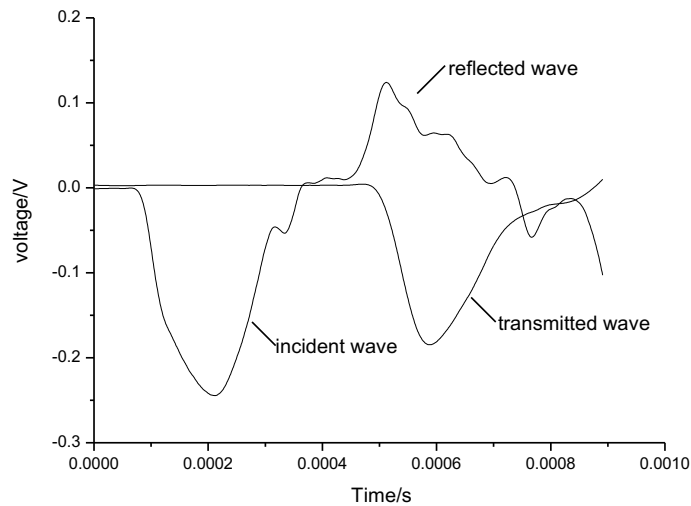


Figure 27: Typical waveform of compression test

Based on one dimensional stress wave propagation theory, the stress, strain and strain rate in SHPB test can be calculated using the following equations.

$$\sigma(t) = E \left(\frac{A}{A_s} \right) \varepsilon_T(t) \quad (13)$$

$$\varepsilon(t) = \int_0^T \dot{\varepsilon}(t) dt \quad (14)$$

$$\dot{\varepsilon}(t) = -\frac{2c_0}{L} \varepsilon_R(t) \quad (15)$$

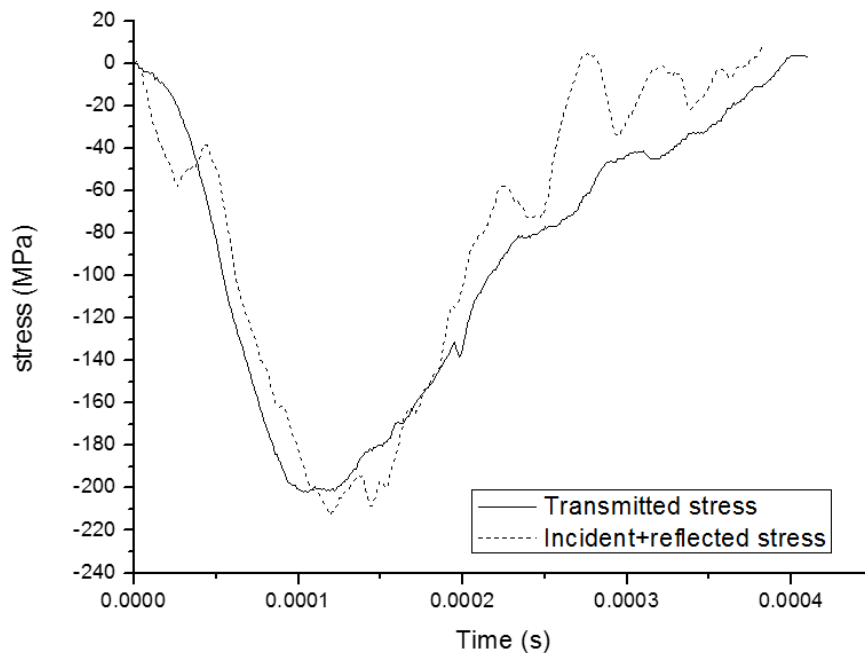
where E , A and C_0 are Young's modulus, cross-sectional area and elasticity wave velocity of the SHPB bar; A_s and L are cross sectional area and length of the test samples; ε_T and ε_R are incident strain and reflective strain.

Prior to the dynamic testing, it is critical to conduct longitudinal stress equilibrium check. Equation 5 is used to calculate the stress balance.

$$\sigma_T = \sigma_I + \sigma_R \quad (16)$$

where σ_T is the transmitted stress; σ_I is the incident stress and σ_R is the reflected stress.

Figure 28 shows typical stress equilibrium check on UHPC samples with 2.5% TF03 fibre reinforcement. The strain rates displayed in the figures are the highest strain rate reached in the SHPB tests. It can be concluded that under the highest strain rate, specimen reached stress balance which verified the accuracy of SHPB tests conducted in the present research.



2.5% TF03 (strain rate 76.31 s^{-1})

Figure 28: Stress equilibrium checks

3.4.1 SHPB – Compression

Dynamic compression test results are discussed in this section. Figure 29 shows the failure modes of UHPC samples after the tests. It can be observed that under impact loads, different fibres addition has prominent influence on the samples failure modes. UHPC specimen with 2.5% MF15 fibre addition only has some visible cracks at the edge. However, UHPC sample with shorter length micro fibre MF06 exhibits extensive cracks. For the two samples reinforced by twisted fibres TF03 and TF05, more extensive cracks can be found on the TF05 sample which indicates the larger aspect ratio of length to diameter has positive influence on the crack control of UHPC.

From the dynamic compression tests, it can be concluded that fibre length and aspect ratio both have impact on the dynamic failure modes of UHPC sample, with the increase of fibre length or aspect ratio, the damage resistance of UHPC material increases. It can also be found that among all four steel fibres, MF15 has the best crack confinement ability in the dynamic compressive test.



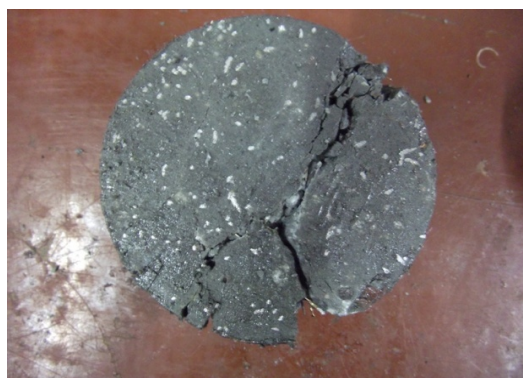
(a) 2.5% MF15



(b) 2.5% MF06



(c) 2.5% TF03



(d) 2.5% TF05

Figure 29: Failure patterns of different type fibre

Figure 30 compares the dynamic compressive stress-strain curves obtained from all four UHPC specimens. Under the strain rate of 60 s^{-1} , UHPC with 2.5% MF15 fibre reinforcement has the highest dynamic strength which is about 200 MPa, UHPC with 2.5% TF05 fibre reinforcement has the lowest strength which is about 145 MPa. For UHPC specimens have the same type of reinforcements, it can be found that MF15 performs better than MF06, and TF03 performs better than TF05. It can be concluded that the increase of fibre length and aspect ratio favours the dynamic strength of UHPC material.

Under the strain rate of 80 s^{-1} , it is worth noting that although all four materials experience strength increase during the strain rate boost, UHPC with TF05 which always has the lowest dynamic strength seems insensitive than the other three materials, however a better ductility can be noticed for this material with increased strain rate.

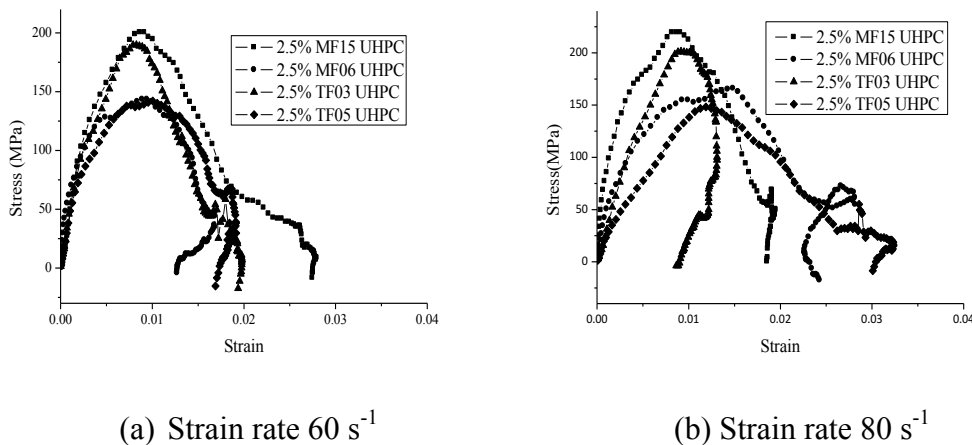


Figure 30: Comparison of stress-strain curves at different strain rates of different type fibre

Figure 31 plots the dynamic strengths of UHPC materials with different fibre reinforcement. It can be noticed that UHPC with MF15 fibre reinforcement can reach the highest strength exceeding 225 MPa at the strain rate of 93 s^{-1} . Micro fibre reinforcement is more sensitive to the strain rate effect which can be noticed from the slope of the fitted trend curves. For all UHPC materials, when the strain rate exceeds 80/s, although strength increase can still be noticed in the UHPC material, the rate of strength increase gradually slows down. This can be seen from the convex trend curve shown the figure.

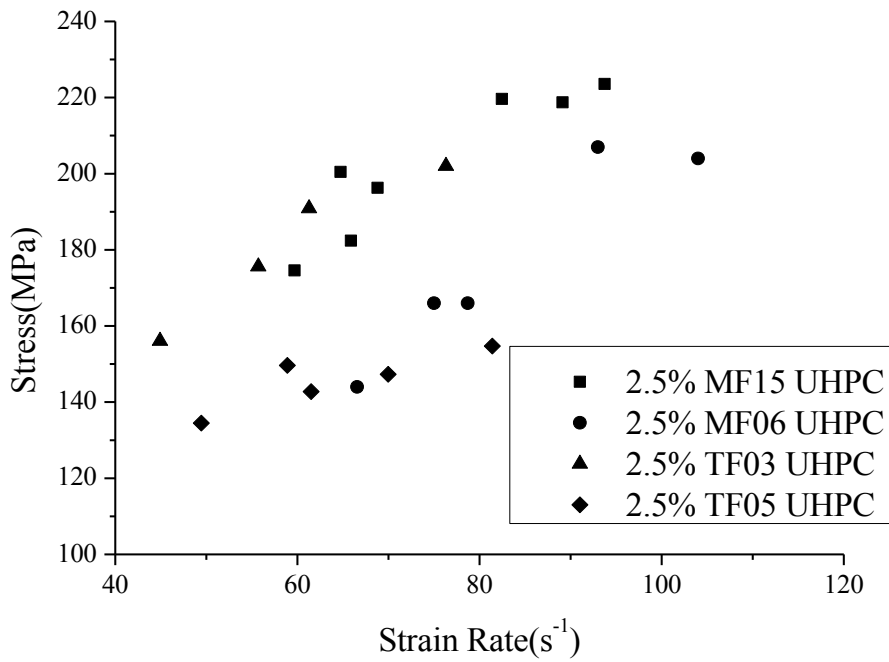


Figure 31: Strain rate-stress curves of UHPC with various types of fibres

Dividing by the static compressive strength, dynamic increase factors (DIF) curves for all these four materials are obtained and shown in Figure 32. All UHPC specimens displayed a prominent strength enhancement under high strain loading condition, and a highest DIF of about 1.8 is obtained under strain rate of around 100 s⁻¹ for UHPC with MF06 reinforcement.

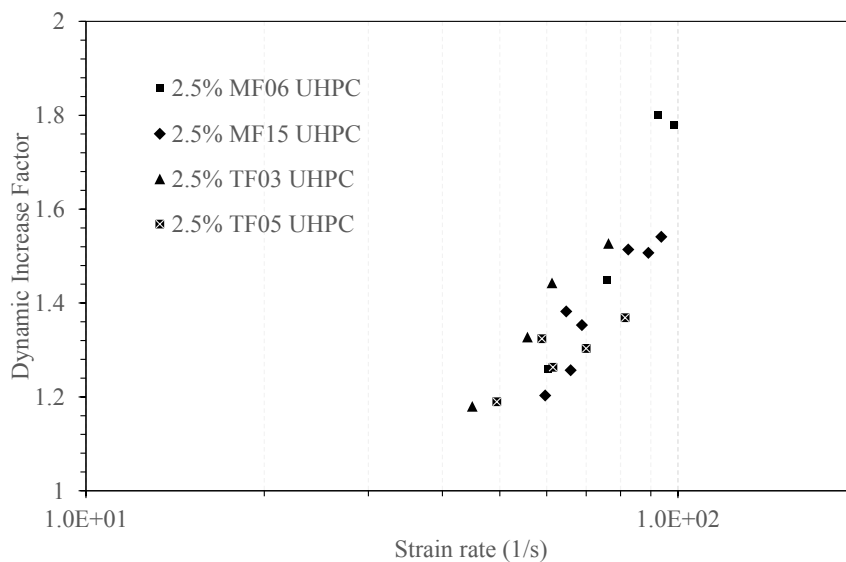


Figure 32: Dynamic increase factor curves of UHPC with various types of fibres

Comparison with conventional concrete without fibre reinforcement and nano addition is made. DIFs for normal strength concrete ($f_c=52.5$ MPa) are obtained from empirical formulae proposed by Malvar et al. [21].

For normal strength concrete compressive strength:

$$DIF = \frac{f_c}{f_{cs}} = \begin{cases} \left(\frac{\dot{\epsilon}}{\dot{\epsilon}_s}\right)^{1.026\alpha} & \text{for } \dot{\epsilon} \leq 30s^{-1} \\ \gamma_s \left(\frac{\dot{\epsilon}}{\dot{\epsilon}_s}\right)^{1/3} & \text{for } \dot{\epsilon} > 30s^{-1} \end{cases} \quad (17)$$

where f_c is the dynamic compressive strength at $\dot{\epsilon}$; f_{cs} is the static compressive strength at $\dot{\epsilon}_s$; $\dot{\epsilon}$ is the strain rate in the range of 30×10^{-6} to 300 s^{-1} ; $\dot{\epsilon}_s$ is the static strain rate 30×10^{-6} ; $\log \gamma_s = 6.156 \alpha - 2$; $\alpha = 1/(5 + 9f_{cs}/f_{co})$; $f_{co} = 10$ MPa.

It can be seen from the comparison shown in Figure 33 that normal strength concrete has constantly higher DIF values than UHPC material with different steel fibre enhancement. There are several possible explanations to such observation. Firstly, steel is known to be a more homogenous material with less defects than concrete. It was reported that the DIF of steel with ultimate strength of 860 MPa is lower than 1.1 at a strain rate of 10 s^{-1} . Previous studies [25, 26] revealed that the strain rate sensitivity of steel is decreasing with the increase of steel strength, and in the current study, the tensile strengths for the micro fibre and twisted fibre are 4295 MPa and 1500 MPa, respectively. They are expected to have even lower strain rate sensitivity. With the inclusion of the steel fibre material, UHPC can have a low strength enhancement under high strain rate loading. Secondly, it was reported [27] that the presence of moisture in concrete appears to have a significant effect on the strength enhancement under high strain rate loading. It was found that strength increases in wet concrete greater than those exhibited by dry concrete. UHPC material in the current study contains reactive powder ingredients which greatly reduce the water with in the concrete matrix and thus has a lower strain rate sensitivity than normal strength concrete. Finally, it is known that the crack velocity in concrete material increases with strain rate. Under similar strain rate loading, fibre reinforced UHPC has a slower crack expansion than its normal strength counterpart and this results in a lower strength enhancement.

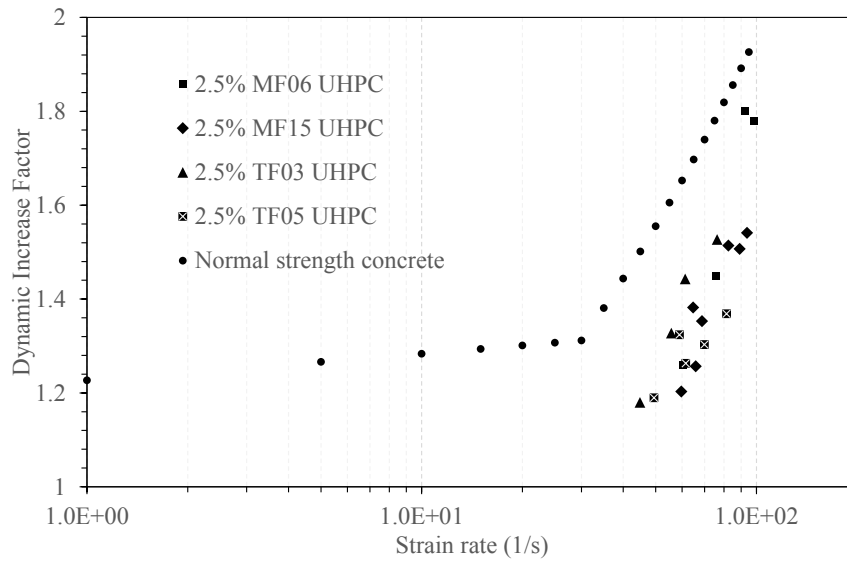
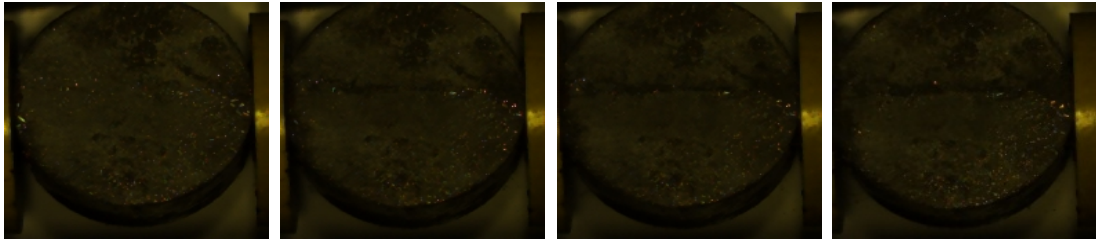


Figure 33: Dynamic increase factors of UHPC and normal strength concrete

As shown in Figure 33, a sharp increase in the slope of DIF curve happens at transition strain rate of 30 s^{-1} for normal strength concrete. Although without sufficient data, it can be predicted that such transition strain rate for UHPC material is higher than normal strength concrete. One possible explanation is that such transition stems from the increased lateral inertia effect, and in UHPC material, dispersed fibre material held together the concrete and reduced the lateral expansion which will postpone the sharp transition.

3.4.2 SHPB – Tension

Results of SHPB tests on the UHPC dynamic tension are shown in this section. Figure 34 shows the damage modes of the UHPC specimens with different steel fibre reinforcement, and influence from different fibre volume fraction is also investigated. It can be seen that 2.5% MF15 reinforced UHPC has narrower crack than 2.5% MF06 reinforced UHPC, and 2.5% TF03 reinforced UHPC has fewer cracks than 2.5% TF05 reinforced UHPC. Generally speaking, higher fibre aspect ratio helps resisting the crack extension. For the three UHPC samples reinforced by micro fibre, it is noticed that when the volume fraction is low at 0.5%, clear compressive cracks can be seen at both end of the sample. Such compressive concrete failure is not seen in high volume fraction UHPC specimens, and with the increase of the fibre dosage, the expansion of the crack is confined.



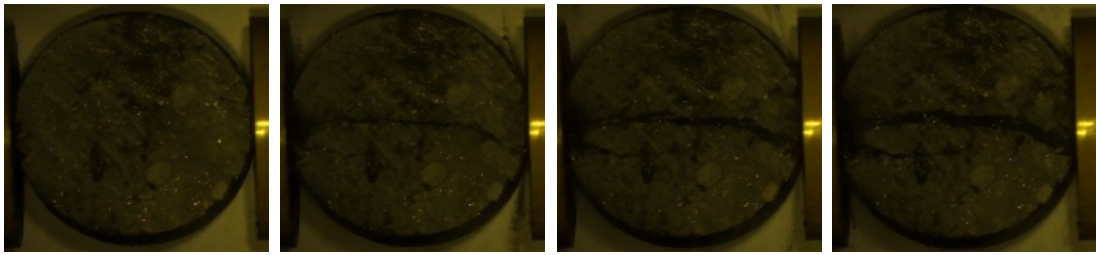
$t=0\mu s$

$t=155\mu s$

$t=310\mu s$

$t=465\mu s$

2.5% MF15



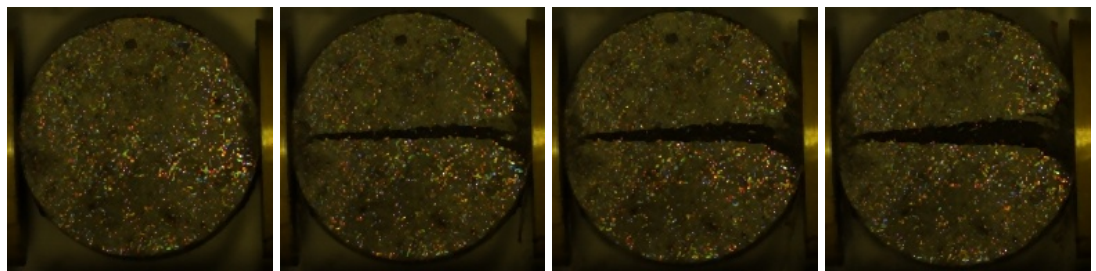
$t=0\mu s$

$t=155\mu s$

$t=310\mu s$

$t=465\mu s$

2.5% MF06



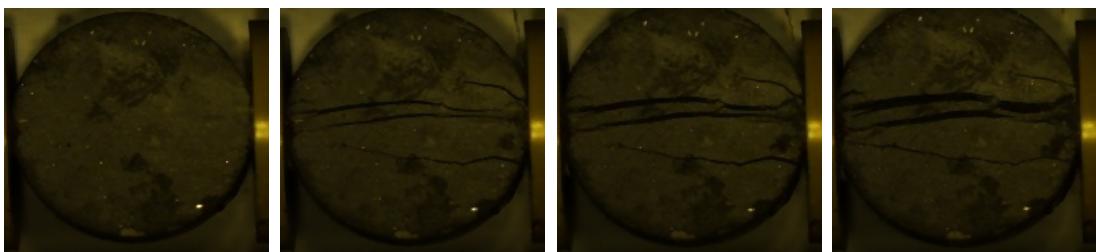
$t=0\mu s$

$t=155\mu s$

$t=310\mu s$

$t=465\mu s$

2.5% TF03



$t=0\mu s$

$t=155\mu s$

$t=310\mu s$

$t=465\mu s$

2.5% TF05

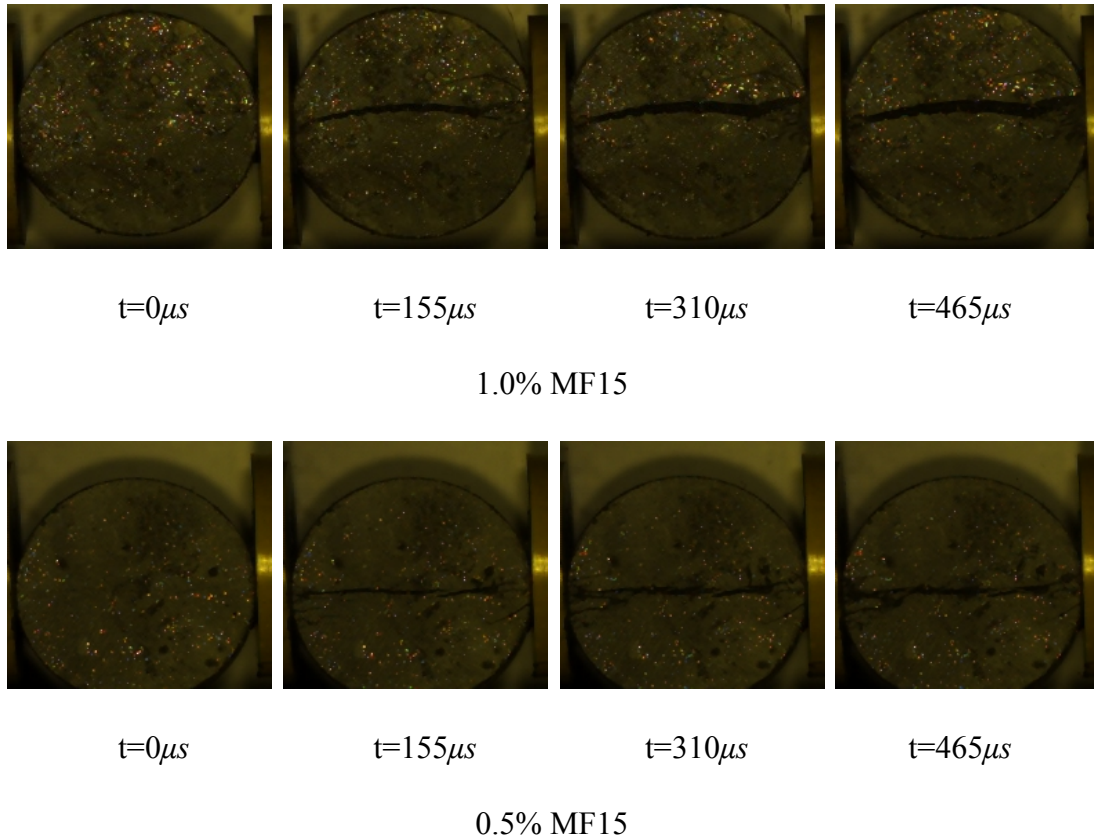


Figure 34: Damage modes of UHPC specimens under SHPB tension test

DIF values for materials with different steel fibres reinforcement are shown in Figure 35. It is noticed that under tensile tests, the twisted fibre reinforced UHPC outperforms the UHPC sample with micro fibre reinforcement.

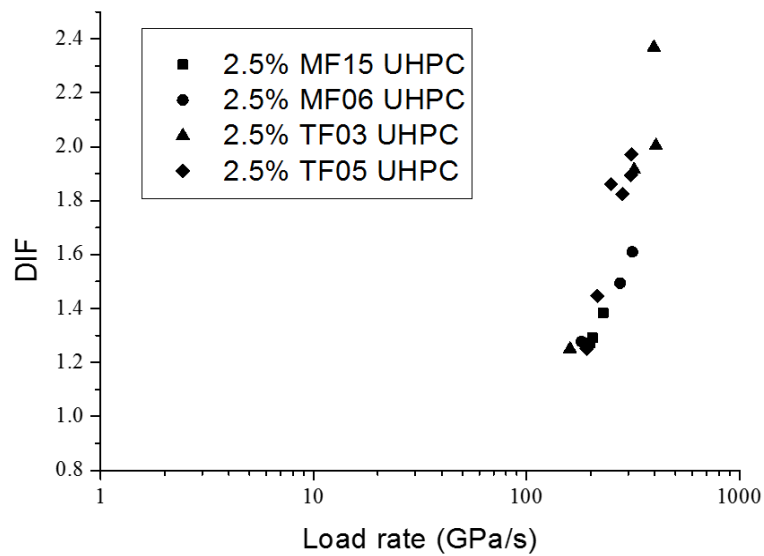


Figure 35: Dynamic increase factors of UHPC with different types of fibres in SHPB tests

Figure 36 shows the DIF values for UHPC material with the same steel fibre type, i.e. MF15 but different volume fractions including 0.5%, 1.0%, and 2.5%. It is noticed that increase of the steel fibre volume fraction gives opposite contribution to the DIF value. The highest value of DIF is obtained in UHPC with 0.5% MF15 which is about 1.85 at around 200 s^{-1} . As discussed above, steel material is less sensitive to the high strain rate loading and UHPC material with higher dosage of steel fibre can have less strength enhancement.

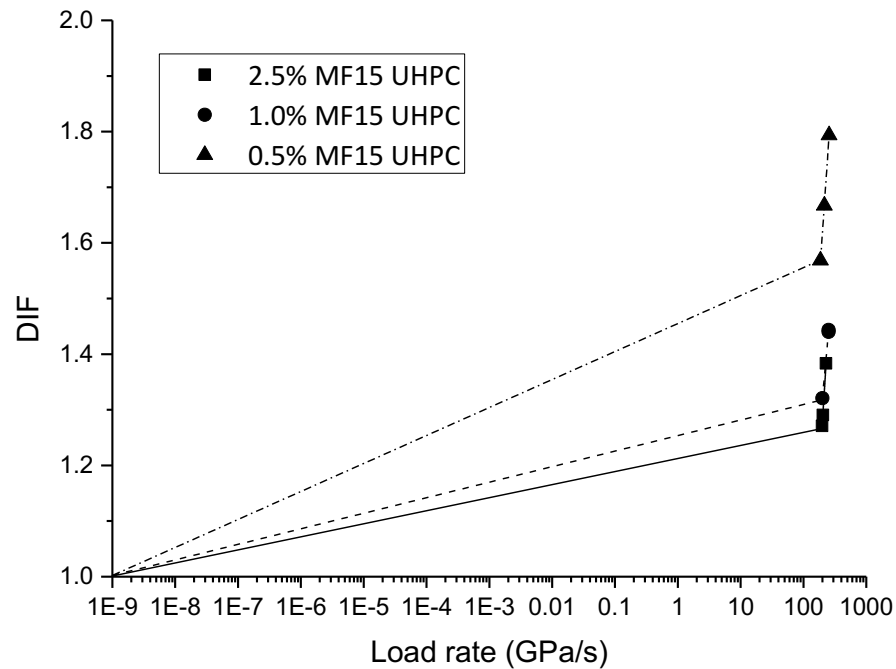


Figure 36: Dynamic increase factors influenced by the volume of MF15 in Split Tension SHPB tests

3.5 CONCLUSIONS

Split-Hopkinson-Pressure-Bar (SHPB) tests of newly developed UHPC materials are carried out. Test results are discussed and compared with static test results in the present study. Influence of different fibre reinforcements including micro steel fibre and twisted steel fibre as well as fibre aspect ratio and fibre volume fraction on the dynamic property of UHPC is investigated. The test results showed the newly designed UHPC materials have outstanding mechanical performance and ductility. The UHPC material with micro fibre reinforcement generally gives better dynamic strength when compared with the twisted fibre reinforced UHPC specimen. The increase of fibre length and aspect ratio has positive impact on the material dynamic strength. Fibre volume fraction increase favours the UHPC material performance. In the SHPC compression tests, the micro fibre reinforced UHPC is more

sensitive to the strain rate while in the SHPB tensile test twisted fibre reinforced UHPC has higher loading rate sensitivity. Comparing with normal strength concrete, UHPC material developed in the current study has relatively low sensitivity to the loading rate.

ACKNOWLEDGEMENTS

The research presented in this paper jointly supported by the National Natural Science Foundation of China under Grants 51278326 and 51238007, and the National Key Technology R&D Program of the Ministry of Science and Technology of China (2012BAJ07B05), the ARC Discovery Grant DP140103025, is gratefully acknowledged.

REFERENCES

- [1] A.M. Brandt, Fibre reinforced cement-based (FRC) composites after over 40 years of development in building and civil engineering, *Composite Structures*, 86 (2008) 3-9.
- [2] S. Rigaud, G. Chanvillard, J. Chen, Characterization of Bending and Tensile Behavior of Ultra-High Performance Concrete Containing Glass Fibers, in: G. Parra-Montesinos, H. Reinhardt, A.E. Naaman (Eds.) *High Performance Fiber Reinforced Cement Composites 6*, Springer Netherlands, 2012, pp. 373-380.
- [3] Z. Zheng, D. Feldman, Synthetic fibre-reinforced concrete, *Progress in Polymer Science*, 20 (1995) 185-210.
- [4] A.M. Alani, D. Beckett, Mechanical properties of a large scale synthetic fibre reinforced concrete ground slab, *Construction and Building Materials*, 41 (2013) 335-344.
- [5] B. Daio, S. Hu, Y. Ye, S. Yang, Z. Liu, Mechanical Behavior of Ultra-High Performance Concrete Reinforced with Hybrid Different Shapes of Steel Fiber, in: *CICTP 2012*, pp. 3017-3028.
- [6] S.H. Kim, G.S. Ryu, K.T. Koh, Flexural Behavior Characteristics of UHPC According to Twisted Steel Fiber, *Advanced Materials Research*, 652 (2013) 1499-1504.
- [7] G.S. Ryu, S.H. Kim, G.H. Ahn, K.T. Koh, Evaluation of the Direct Tensile Behavioral Characteristics of UHPC Using Twisted Steel Fibers, *Advanced Materials Research*, 602 (2013) 96-101.
- [8] V. Bindiganavile, N. Banthia, Polymer and Steel Fiber-Reinforced Cementitious Composites under Impact Loading? Part 1: Bond-Slip Response, *ACI Materials Journal*, 98 (2001).
- [9] Z. Xu, H. Hao, H. Li, Experimental study of dynamic compressive properties of fibre reinforced concrete material with different fibres, *Materials & Design*, 33 (2012) 42-55.
- [10] Ş. Yazıcı, G. İnan, V. Tabak, Effect of aspect ratio and volume fraction of steel fiber on the mechanical properties of SFRC, *Construction and Building Materials*, 21 (2007) 1250-1253.
- [11] Z.L. Wang, J. Wu, J.G. Wang, Experimental and numerical analysis on effect of fibre aspect ratio on mechanical properties of SFRC, *Construction and Building Materials*, 24 (2010) 559-565.
- [12] C. Wu, D.J. Oehlers, M. Rebstroff, J. Leach, A.S. Whittaker, Blast testing of ultra-high performance fibre and FRP-retrofitted concrete slabs, *Engineering Structures*, 31 (2009) 2060-2069.

- [13] V. Perry, D. Zakariassen, First use of ultra-high performance concrete for an innovative train station canopy.
- [14] E. Fehling, K. Bunje, M. Schmidt, Gärtnerplatz – Bridge over River Fulda in Kassel: Multispan Hybrid UHPC-Steel Bridge, in: *Designing and Building with UHPFRC*, John Wiley & Sons, Inc., 2013, pp. 0-136.
- [15] W.J.C.Y.J.K.J.-R.C.J.S. Park, Dynamic Characteristics Evaluation of Innovative UHPC Pedestrian Cable Stayed Bridge, *Engineering*, Vol. 4 No. 12 (2012) 869-876.
- [16] M. Rebentrost, G. Wight, Perspective on UHPCs from a Specialist Construction Company, in: *Designing and Building with UHPFRC*, John Wiley & Sons, Inc., 2013, pp. 189-208.
- [17] G.J. Parra-Montesinos, S.W. Peterfreund, S.-H. Chao, Highly damage-tolerant beam-column joints through use of high-performance fiber-reinforced cement composites, *ACI Structural Journal*, 102 (2005).
- [18] J. Magnusson, M. Hallgren, Reinforced high strength concrete beams subjected to air blast loading, in: *Structures under shock and impact VIII*, Wit Press, 2004, pp. 53-62.
- [19] M. Zhang, M. Sharif, G. Lu, Impact resistance of high-strength fibre-reinforced concrete, *Magazine of Concrete research*, 59 (2007) 199-210.
- [20] C.A. Ross, J.W. Tedesco, S.T. Kuennen, Effects of strain rate on concrete strength, *ACI Materials Journal*, 92 (1995).
- [21] L.J. Malvar, J.E. Crawford, Dynamic increase factors for concrete, in, DTIC Document, 1998.
- [22] R.J. Detwiler, C.A. Fapohunda, J. Natale, Use of supplementary cementing materials to increase the resistance to chloride ion penetration of concretes cured at elevated temperatures, *ACI Materials Journal*, 91 (1994).
- [23] B.-W. Jo, C.-H. Kim, G.-h. Tae, J.-B. Park, Characteristics of cement mortar with nano-SiO₂ particles, *Construction and Building Materials*, 21 (2007) 1351-1355.
- [24] X. Liu, L. Chen, A. Liu, X. Wang, Effect of Nano-CaCO₃ on Properties of Cement Paste, *Energy Procedia*, 16, Part B (2012) 991-996.
- [25] H. Fu, M. Erki, M. Seckin, Review of effects of loading rate on reinforced concrete, *Journal of structural engineering*, 117 (1991) 3660-3679.
- [26] L.J. Malvar, Review of static and dynamic properties of steel reinforcing bars, *ACI Materials Journal*, 95 (1998).
- [27] C.A. Ross, D.M. Jerome, J.W. Tedesco, M.L. Hughes, Moisture and strain rate effects on concrete strength, *ACI Materials Journal*, 93 (1996).

Statement of Authorship

Article Name: Development of novel ultra-high performance concrete: from material to structure

Su, Y., Wu, C., Li, J., Li, Z.X., and Li, W.G.

Status: Submitted to *Construction & Building Materials*

Su, Y. (candidate)

Contribution: helped conduct tests, processed and analysed test data and prepared manuscript

I hereby certify that the statement of contribution is accurate.

Signed..... Date 27/08/2016

Wu, C.

Contribution: supervised research and tests, provided critical manuscript evaluation and acted as corresponding author.

I hereby certify that the statement of contribution is accurate and I give permission for the inclusion of the paper in the thesis.

Signed..... Date 24/08/2016

Li, J.

Contribution: helped design and conduct tests.

I hereby certify that the statement of contribution is accurate and I give permission for the inclusion of the paper in the thesis.

Signed..... Date 24/8/2016

Li, Z.X.

Contribution: provided critical manuscript evaluation.

I hereby certify that the statement of contribution is accurate and I give permission for the inclusion of the paper in the thesis.

Signed..... Date Aug 25, 2016

Li, W.G.

Contribution: provided critical manuscript evaluation.

I hereby certify that the statement of contribution is accurate and I give permission for the inclusion of the paper in the thesis.

Signed..... Date 24/08/2016

CHAPTER 4: DEVELOPMENT OF NOVEL ULTRA-HIGH PERFORMANCE CONCRETE: FROM MATERIAL TO STRUCTURE

Yu Su¹, Chengqing Wu^{2,*}, Jun Li², Zhong-Xian Li³, Wengui Li²

¹School of Civil, Environmental and Mining Engineering, the University of Adelaide, SA 5005, Australia

²Centre for Built Infrastructure Research, School of Civil and Environmental Engineering, University of Technology Sydney, NSW 2007, Australia

³Tianjin Key Laboratory of Civil Structure Protection and Reinforcement, Tianjin Chengjian University, Tianjin 300384, China

ABSTRACT

This paper investigates effects of nanoscale materials and steel fibres on properties of ultra-high performance concrete (UHPC). Different types of steel fibres including twisted steel fibre (TF), waved steel fibre (WF), and micro steel fibre (MF) together with different kinds of nano materials including Nano-CaCO₃, Nano-SiO₂, Nano-TiO₂ and Nano-Al₂O₃ are studied in the present research. Material compressive stress–strain relationships, strain energy absorption, the flexural tensile strength and fracture energy absorption of UHPC with different nanoscale materials and steel fibres were compared and discussed. Scanning Electron Microscope (SEM) tests were carried out on hydrated UHPC samples and effects of nano material additions were investigated. Laboratory static bending tests and field blast tests on structural components made of selected UHPC material composition were carried out, and the results highlighted the material ductility and blast resistant capacity of UHPC material developed in the present study.

KEYWORDS: Ultra-high performance concrete (UHPC); nano materials; steel fibre; Field blast tests.

4.1 INTRODUCTION

The rising of terrorism threats has promoted fast development of new construction materials to enhance the resistance of buildings and infrastructures against blast loads. As a notable representative, ultra-high performance concrete (UHPC) which is characterized with remarkable ductility, durability and strength properties has now been widely investigated by government agencies and universities. Differing from conventional concrete, UHPC is a mix of reactive powder concrete (RPC) with a small volume percentage of short steel fibre materials [1], [2], [3]. UHPC inherits positive aspects of RPC and it is equipped with improved characteristics as a result of fibre addition. Its high strength and ductility makes it an ideal construction material for bridge decks, storage halls, thin-wall shell structures, and other infrastructure against seismic, impact and blast loads. Blast testing was conducted on UHPC slabs [4], [5] and test results were compared with control samples made with normal strength concrete. It was concluded that combination of high strength concrete with steel fibre can significantly increase blast resistance of structural components. Impact response of UHPC material through drop weight tests was experimentally investigated [6], and direct comparisons were made with conventional normal strength fibre reinforced concrete. Results indicated that UHPC was approximately two times stronger than normal strength fibre reinforced concrete. Thus UHPC is of a tremendous potential to be used in construction industry and it has drawn intensive interests by many researchers in recent years [7], [8], [9], [10], [11].

For UHPC, one of the most important factors affecting the concrete properties is steel fibre characteristics including shape of steel fibre, fibre aspect ratio (ratio of fibre length over diameter) and fibre volume fraction [12], [13]. While large fibre aspect ratio and volume fraction are recognized to be beneficial to material mechanical performance, it is also observed that the probability of heterogeneous distribution and fibre flocculation increases with fibre aspect ratio, and fibre volume fraction significantly affects concrete workability. Besides straight fibre material, deformed steel fibres such as end-hooked, waved and spiral steel fibres can be used to enhance anchorage properties with surrounding matrix so as to improve performance of concrete [1], [8],[14]. Considerable experimental and analytical studies have been conducted to investigate influence of steel fibre characteristics on performance of concrete material [14], [15], [16].

Recently there has been a growing interest in use of nanoscale materials in concrete to improve its performance [17], [18], [19], [20], [21], [22], [23], [24], [25], [26]. Material mixing technology and influence of curing or drying condition on the performance of UHPC were investigated in [27], [28], [29], [30]. With development of nano technology, researchers noticed that addition of nanoscale size particles results in significantly improved material properties without much change of the material composition. Studies concerning properties of cement mortars with Nano-SiO₂ addition were carried out [20], and the experimental results showed that the compressive strengths of mortars with Nano-SiO₂ particles were all higher than those of mortars containing silica fume at 7 and 28 days. They concluded that it was plausible to add Nano-SiO₂ particles in order to make high-performance concrete. Liu et al. [31] added Nano-CaCO₃ into the cement paste and they observed a decreased flowability and shortened setting time of fresh cement paste, and they also noticed that compressive strength of UHPC increased with addition of Nano-CaCO₃ at ages of 7 days and 28 days. Similar observations were also made through experimental studies shown in [32], [33]. Camiletti et al. [34] pointed out that Nano-CaCO₃ accelerated the cement hydration process through nucleation, and also acted as an effective filling material. Through the use of micro- and Nano-CaCO₃, more environmentally friendly UHPC can be produced by reducing its cement factor, while achieving enhanced engineering properties. These studies proved that nanoscale materials exhibited much finer particles and high pozzolanic reactivity that could be used to improve the performance of matrix so as to enhance material properties of UHPC.

In the present study, influence of nanoscale materials and steel fibres on performance of UHPC was investigated. Different percentage of twisted, waved and micro steel fibres were incorporated in the mix design. Nano-CaCO₃, Nano-SiO₂, Nano-TiO₂ and Nano-Al₂O₃ were used as nanoscale additives with contents of 3.0% by weight of cement. The compressive tests were carried out to obtain stress strain curves of the specimens and four point bending tests were conducted to get flexural tensile strength of the UHPC specimens. The influence of steel fibres and nanoscale materials on the performance of UHPC is compared and discussed. The selected UHPC composition was used in the structural component construction. In the subsequent field blast tests, the blast resistance of these components were studied.

4.2 EXPERIMENTAL PROGRAM

4.2.1 Materials

The main properties of materials used in producing UHPC in this study are presented in the following. To ensure consistency of concrete for all UHPC, the cement used in all mixes was Type SR Sulphate Resisting cement (namely 42.5 Grade) conforming to Chinese standard GB175-2007 [35]. As for aggregates, natural sand was used and the aggregate size was between 0.16 mm and 2.5 mm, the specific gravity is 2.58 g/cm³. Silica fume was used as a reactive material involving in the hydration of cement which is commonly adopted in reactive powder concrete (RPC) formulation, and silica flour was used to fill in the voids which exist between the cement paste and aggregate matrix. To accelerate cement hydration process and provide even better filling effect at nanoscale, four types of nano-particles including Nano-CaCO₃, Nano-SiO₂, Nano-Al₂O₃, and Nano-TiO₂ were used. The average particle size was determined from a Brunauer–Emmett–Teller (BET) surface area measurement i.e. 40-80 nm for CaCO₃, 20 nm for SiO₂, 30 nm for TiO₂ and 20 nm for Al₂O₃, and the specific surface area was more than 4 m²/g for CaCO₃, 230-300 m²/g for SiO₂, 77.55 m²/g for TiO₂ and 180 m²/g for Al₂O₃.

Three types of steel fibres including twisted steel fibre (TF) with diameter 0.4 mm and length 35 mm, waved steel fibre (WF) with diameter 0.5 mm and length 30 mm, and micro steel fibres (MF) with diameter 0.12 mm and lengths 6 mm and 12 mm, were incorporated into mix design of self-compacting concrete. Figure 37 shows the different types of steel fibres used in this study. The mechanical properties of steel fibres are listed in Table 12. Volume fraction of the steel fibres varied from 1% to 2.5%. The dosage was determined on the basis of a series of preliminary tests, which confirmed that a reasonable increase in fibre content resulted in enhanced concrete performance.

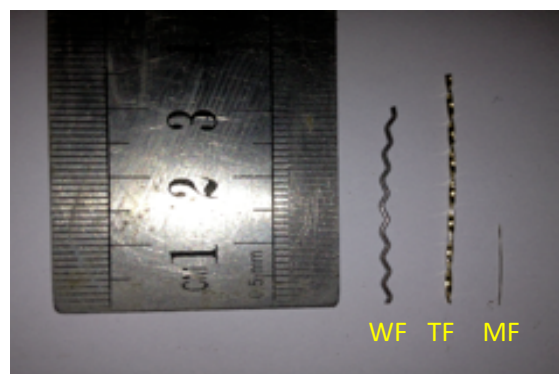


Figure 37: Different types of steel fibres

Table 12: Material properties of steel fibres

Fibre Types	Nominal Diameter (mm)	Length (mm)	Fibre aspect ratio (L/D)	Volume fraction (%)	Tensile strength (MPa)
Twisted steel fibre TF1	0.4	35	87.5	1	1480
Twisted steel fibre TF2	0.4	35	87.5	2	1480
Waved steel fibre WF	0.5	30	60	1	>800
Micro steel fibre MF06	0.12	6	50	2.5	>4000
Micro steel fibre MF12	0.12	12	100	2.5	>4000

4.2.1.1 Mix design

The mixture proportions of UHPC are reported in Table 13. A total of five series of mixtures (plain concrete and four kinds of nano materials) were prepared in the laboratory trials. Five “ref” mixtures without fibre addition were used as control specimens. As seen from the table, except for the steel fibres all ingredients were kept constants. The same water to binder ratio (water/binder=0.163) and the same weight of aggregates (with the sand percentage of 40% by weight), and a constant content of silica fume, silica flour and binder were used for all the mixtures. For the mixtures with steel fibres and nano-particles, the rows TF, WF, MF06 and MF12 were mixed with Nano-CaCO₃, Nano-SiO₂, Nano-Al₂O₃, and Nano-TiO₂ particles by the cement replacement of 3%, 1%, 2% and 3% (63.1 kg, 21.7 kg, 45.4 kg and 63.1 kg) by weight, respectively. The dosages of TF are 1% and 2% (79 kg and 158 kg) by volume, the dosages of WF, MF06, and MF12 are 1%, 2.5% and 2.5% (79 kg, 191 kg, 191 kg) by volume, respectively.

Table 13: Mix proportions of UHPC (unit: kg/m³)

Constituents	Plain	Nano-CaCO ₃					Nano-SiO ₂					Nano-TiO ₂					Nano-Al ₂ O ₃									
	Ref	Ref	1	2	3	4	5	Ref	1	2	3	4	5	Ref	1	2	3	4	5	Ref	1	2	3	4	5	
42.5 SR Cement	750	750					750					750					750									
Silica fume	225	225					225					225					225									
Silica Flour	190	190					190					190					190									
River Sand	1030	1030					1030					1030					1030									
Superplasticizer	16	16					16					16					16									
Water	190	190					190					190					190									
Water/Binder	16.3%	16.3%					16.3%					16.3%					16.3%									
Nano Particles	-	21.7					21.7					21.7					21.7									
MF06	-	-	191	-	-	-	-	-	191	-	-	-	-	-	-	191	-	-	-	-	-	191	-	-	-	-
MF12	-	-	-	191	-	-	-	-	-	191	-	-	-	-	-	-	191	-	-	-	-	-	191	-	-	-
TF	-	-	-	-	79	158	-	-	-	-	79	158	-	-	-	-	79	158	-	-	-	-	79	158	-	
WF	-	-	-	-	-	-	79	-	-	-	-	-	79	-	-	-	-	-	79	-	-	-	-	-	79	

Concrete mixtures were prepared in a laboratory concrete mixer. “Plain/Ref” mixture was plain concrete with neither nano material nor steel fibres additions. All mixtures were mixed in dry condition for five minutes, and for another three minutes after adding approximate 70% water. Then superplasticizer was added before adding the remaining 30% water. The fibres were added after the mixing process continued for another 5 minutes. The fibres were manually dispersed and added to the mixer in order to avoid fibre clump. Slumps of fresh concrete were determined immediately to evaluate the workability. The concrete mixture and slump tests were conducted according to GB 2419-81 [36] to ensure consistency of concrete for all concrete specimens with and without nanoscale additives.

Cubic specimens with dimension of 100 mm × 100 mm × 100 mm were made for uniaxial compressive tests and 100 mm × 100 mm × 400 mm beam specimens were made for flexural tensile tests. After being cured in the humid room at a temperature of 20 ± 5 °C for 24 hours, the specimens were demolded and then cured in hot water at a temperature of 90⁰ C for 48 hours. Then the specimens were cured in the first curing room again until they were tested. Both surfaces of the samples were properly levelled, sanded, polished, cleaned and dried to attain smooth surfaces before testing.

4.2.2 Material Testing

The test matrix devised for the material study was intended to cover a range of the basic behaviours of UHPC with and without different nanoscale additives. The types of tests performed can generally be grouped into two. Firstly, uniaxial compression tests which focused on the compressive strength, modulus of elasticity, compressive failure behaviours of

UHPC specimens and effect of nanoscale additives were carried out. Secondly, four-point bending tests were conducted to obtain flexural tensile strength of UHPC specimens with and without nanoscale additives. Totally, 97 specimens were tested including 68 cubic specimens for compressive tests and 29 beam specimens for flexural tensile tests.

4.2.2.1 Compressive testing

Quasi-static compressive tests were conducted on a 3000 kN computer-controlled electromechanical servo hydraulic pressure testing machine with standard procedures conforming to the Chinese standard GB/T 50081-2002. Figure 38 shows a cubic specimen that was prepared for testing. All specimens were loaded via the hydraulically controlled machine at constant loading rate until failure. To measure axial displacements in the specimens, two axial oriented LVDTs were located at each side of the loading plate.

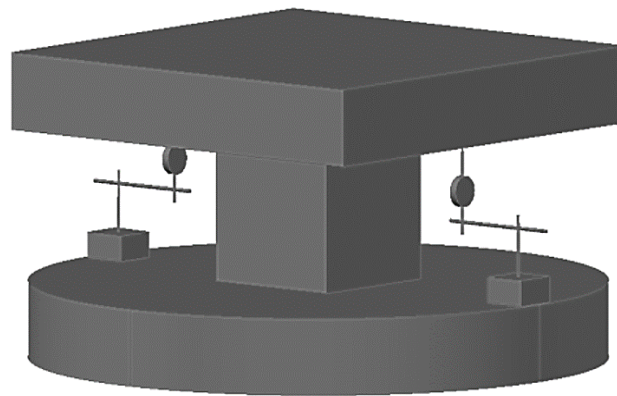


Figure 38: Testing set-up for compression tests of cubic specimens

4.2.2.2 Flexural Tensile Tests

Beam specimens with dimension of 100 mm × 100 mm × 400 mm were tested to study the effect of the nano-particles and steel fibers on their flexural tensile strengths. The beam specimens were tested with a four-point bending loading configuration, and the space between load points is 1/3 of the clear span which generates a region of no shear. As shown in Figure 39, instrumentation for beam tests included LVDTs at mid-span and at the supports to measure deflection, as well as strain gauges along the depth of the beam at mid span to generate an experimental curvature profile.

The same hydraulic testing machine as shown in Figure 39 was used in these bending tests, and the testing procedures conformed to the Chinese standard GB/T 50081-2002 [37]. In the tests, the specimens were subjected to pure bending between two loading points which were spacing at 100 mm. The specimens were supported by two metallic rollers spacing at 300 mm. Figure 39 shows setup of the flexural bending tests.

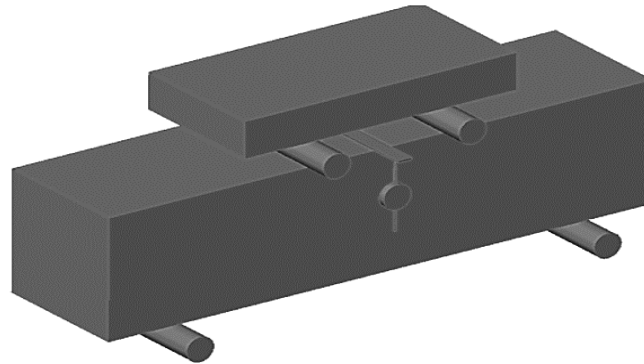


Figure 39: Setup of the flexural tensile tests

4.3 RESULTS AND DISCUSSIONS

4.3.1 Compressive tests

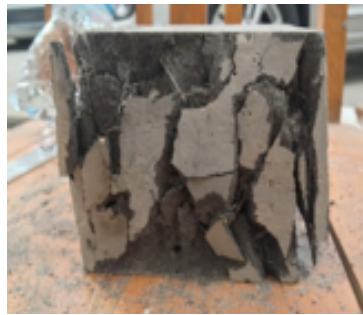
The static compressive tests for UHPC specimens with and without nano-additives were conducted. Figure 40 shows the failure patterns of the plain and fibre reinforced concrete specimens. It was observed that failure of plain concrete specimen occurred in a brittle manner. When steel fibres were mixed into cement, the specimens maintained their integrity and showed excellent crack control ability. This is because the steel fibres can bridge over the cracks and retard crack extension leading to high material ductility. The crack control ability increases with fibre volume fraction as evidenced in the comparison among samples with different fibre volume fractions. The specimen with 1 Vol-% fibres had the most severe damage while addition of 2.5 Vol-% steel fibre provided exceptional crack control capacity in the sample.



No fibre



2.5% steel fibre



1.0% steel fibre



2.0% steel fibre

Figure 40: Failure of specimens from the compression tests

4.3.1.1 Results from compression tests

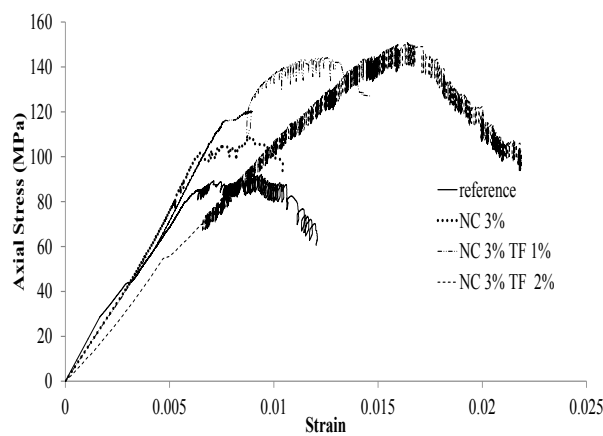
A summary of the results from all of the compressive tests is shown in Table 14. It can be seen that when there is no steel fibre reinforcement, UHPC specimens with nano-additives displayed about 10% increase in peak stress as compared to the specimens without nano-additives.

When steel fibres were mixed, nano-additives had less impact on the material strengths. For UHPC with 1 Vol-% TF reinforcement, there was an average 12% strength increment except for the specimens with Nano-TiO₂ addition. However, there was only slight strength increase for other fibre reinforced UHPC specimens (1 Vol-% WF, 2.5 Vol-% MF06 and 2.5 Vol-% MF12) after nano additions. It is therefore generally concluded that although nano-additives can increase the compressive strength of UHPC without fibre reinforcement, they have insignificant influence on the compressive strength of fibre reinforced UHPC specimens.

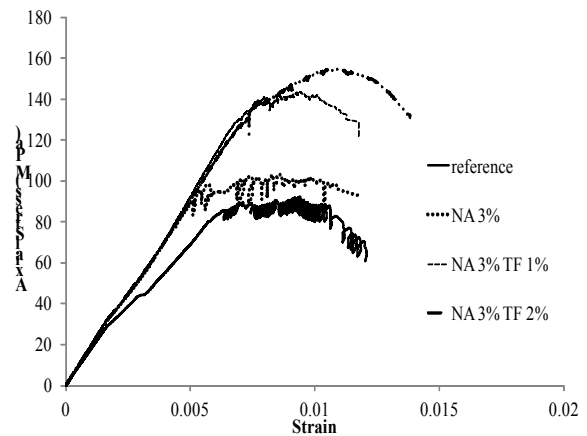
Table 14: Compression strength of UHPC with different nano-additives (unit: MPa)

Fibre Nano	NO	TF1	TF2	WF	MF06	MF12
NO	90.1	126	-	140.4	150.6	168.1
CaCO₃ 3%	108.4	144.3	150.9	136	137.3	-
SiO₂ 1%	107.2	142.3	131.2	139.2	152.5	139.1
TiO₂ 2%	95.7	124.1	160.8	136.9	156.1	168.3
Al₂O₃ 3%	103.1	143.4	154.6	144.5	155.1	169.4

The compressive stress strain curves of UHPC specimens (1 Vol-% TF and 2 Vol-% TF) with four different nano-particles (Al₂O₃, CaCO₃, TiO₂, SiO₂) are presented in Figure 41 and all samples were picked up from the specimens at 7 days. After addition of steel fibres in these four types of UHPC, significant changes occurred in the ascending and descending portions of the stress-strain curves. All these results well quantified the effect of steel fibres on material ductility enhancement. Increasing steel fibres from 1 Vol-% to 2 Vol-% affects the strain capacity and elastic deformation capability of the matrix in the pre-yielding zone considerably.



(a) Nano-CaCO₃



(b) Nano-Al₂O₃

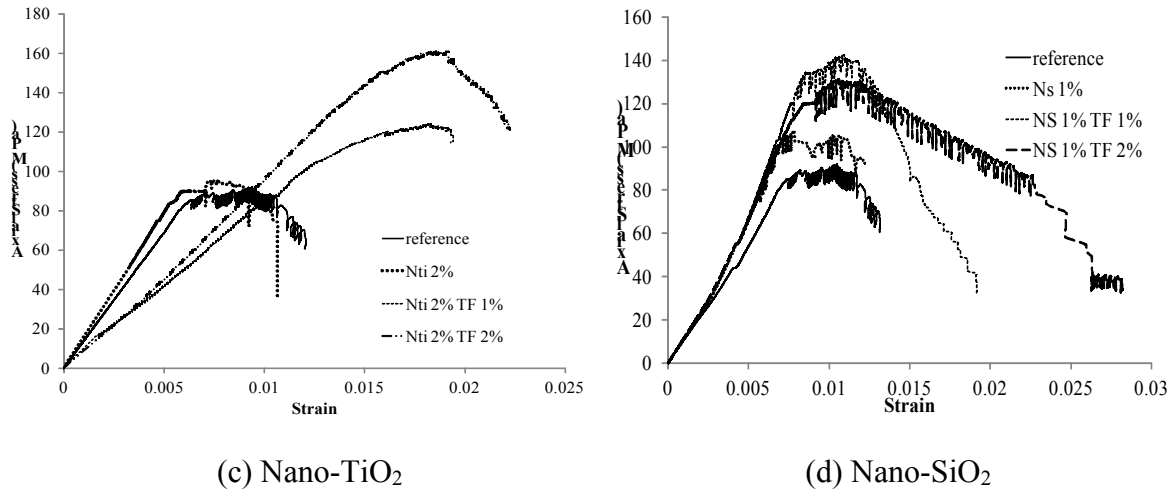


Figure 41: Comparison of compressive stress-strain curves of UHPC specimens (1 Vol-% TF and 2 Vol-% TF) with mixtures of (a) Nano-CaCO₃, (b) Nano-Al₂O₃ (c) Nano-TiO₂ and (d) Nano-SiO₂

The area under stress-strain curve of a specimen is a measure of energy absorption capacities of the material. Table 15 lists typical strain energy density of UHPC with and without fibre reinforcement and different nano-particles. As shown, the energy absorption capacity of UHPC without any steel fibre has the smallest strain energy density. Steel fibre volume dosage plays an important role in material energy absorption. As can be noted from UHPC with 2% TF, its energy absorption is higher than UHPC with 1% TF. When the same volume dosage of steel fibres was mixed, the strain energy density increased with the fibre aspect ratio as seen from the comparison between 2.5 Vol-% MF06 and 2.5 Vol-% MF12.

Table 15: Compression strain energy of UHPC with nano-additives (unit: MJ/m³)

Fibre Nano	NO	TF1	TF2	WF1	MF06	MF12
NO	0.73	2.01	---	1.30	4.51	3.07
CaCO₃ 3%	0.73	1.39	1.24	1.30	2.67	3.38
SiO₂ 1%	0.85	1.61	2.63	1.10	3.30	2.94
TiO₂ 2%	0.71	1.90	4.42	3.33	3.14	5.45
Al₂O₃ 3%	0.92	1.13	1.46	1.31	3.25	3.42

4.3.2 Flexural Tensile Tests

It is well known that adding steel fibres will increase specimen toughness and the results of this study are no exception, but whether adding nano-particles will also contribute to toughness is under investigation in this section.

In the present study, four point bending experiments on the UHPC specimens were performed. Mid-span deflections were recorded and flexural tensile strength and fracture energy were calculated for different specimens with varying nano-particles.

Figure 42 shows a comparison of failure modes of the UHPC specimens. As shown, for the specimen without fibres, the initial crack initiated from the beam bottom due to tensile stress, and then the specimen was split into two parts when the crack propagated towards the top. On the other hand, the fibre reinforced UHPC specimens remained load carrying capacity after the first crack generated. Specimens with 2.5 Vol-% MF12 showed the greatest peak load and a very ductile behaviour after formation of major crack, and bridging effects of steel fibres helps the beam to sustain external loads until the fibres were slowly pulled out. Specimens with 1 Vol-% WF showed the lowest toughness of all three specimens which was possibly due to the fibre low tensile strength and low volume dosage.



(a) No fibre

(b) MF12 2.5%



(c) WF 1 Vol-%

(d) TF 2 Vol-%

Figure 42: Failure modes of the UHPC specimens in flexural tension tests

Typical load-deflection curves of the UHPC specimens are shown in Figure 43 as expected, the load-displacement curve of the UHPC specimen without fibre reinforcement is linear up to the maximum and then failed in a brittle manner with a sudden drop, almost no material ductility can be observed. For UHPC specimens with the same nano-additives (Nano- Al_2O_3), their peak load and material ductility both increased with fibre volume dosage from 1 Vol-% TF to 2 Vol-% TF. Similar observation were noted for other UHPC samples with Nano- CaCO_3 and Nano- TiO_2 . Given a same volume dosage of TF fibre addition, and addition of Nano- Al_2O_3 gives the best load and ductility enhancement.

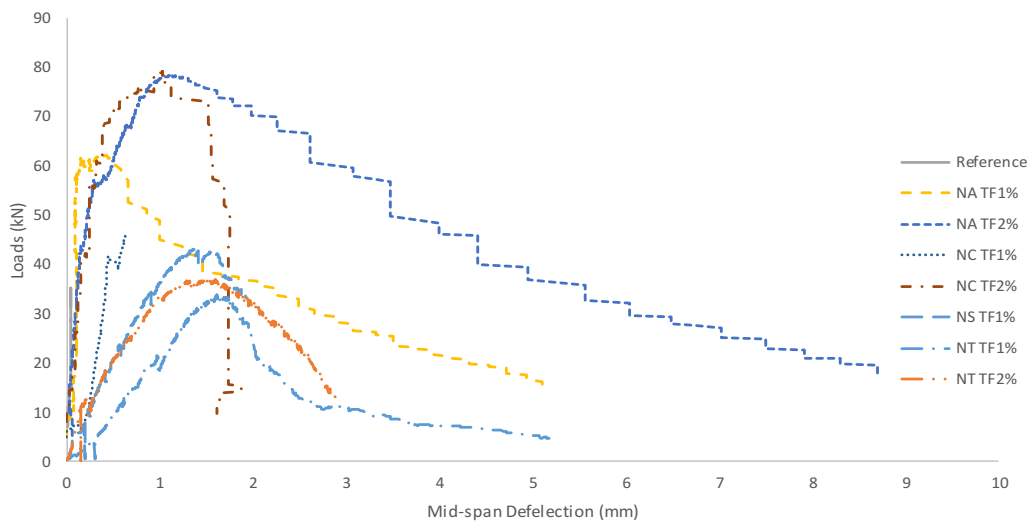


Figure 43: Flexural tensile tests results

Based on four point bending tests, flexural tensile strength was calculated from Equation (18):

$$\sigma = \frac{3F(L-L_i)}{2bd^2} \quad (18)$$

where F is the total load as indicated in Figure 7; L is the distance between two supports at bottom; L_i is the length of the loading span; b and d are the width and depth of the specimen, respectively.

Table 16 lists the data of the flexural tensile strength of UHPC specimens with different nano-additives. It is very interesting to note that the specimens containing 1 Vol-% WF have similar flexural tensile strength when comparing with non-fibre reinforced UHPC specimens (10.8 MPa versus 10.6 MPa). The addition of WF fibre in UHPC was not effective because 1 Vol-% WF fibre with low tensile strength could not provide prominent bridge effects after crack initiates.

On the contrary, the inclusion of MF fibres was useful for developing higher tensile strength. As mentioned in the previous sections, MF fibre had higher tensile strength, also, its volume percentage was larger. All of these guaranteed that MF fibres could provide effective bridging effect and postpone the final failure of the UHPC specimens. Comparing MF06 with MF12, it was noted given a constant fibre volume dosage, fibre aspect ratio gave positive impact on material flexural tensile strength, and this positive effect was also observed in material compressive strength tests.

Table 16: Flexural tensile testing results (unit: MPa)

Fibre Nano	NO	TF1	TF2	WF	MF06	MF12
NO	10.6	14.9	-	10.8	28.1	31.3
CaCO₃ 3%	12.1	14.9	23.7	11.0	20.3	34.2
SiO₂ 1%	13.0	13.0	-	9.5	17.0	26.2
TiO₂ 2%	12.3	10.2	11.1	12.4	22.4	21.9
Al₂O₃ 3%	12.4	18.7	23.5	13.2	21.4	36.1

As proposed by Bazant [38], the fracture energy may be uniquely defined as the energy required for crack growth in a specimen. The fracture energy was calculated from the following equations

$$P_0 = \frac{4M_0}{S} \quad (19)$$

$$W_F = W_0 + 2P_0\mu_0 \quad (20)$$

where μ_0 is the maximum mid-span displacement; S is the distance between two supports at bottom; M_0 is the moment caused by the self-weight of the specimen; W_0 is the work done by the applied force which is the area enclosed by the load-deflection curve. The fracture energy can be then obtained from equation (4)

$$G_f = \frac{W_F}{A} \quad (21)$$

where A is the cross sectional area of the specimen.

By using the equations (2) to (4), the fracture energies of all specimens were calculated and listed in Table 17, fibre material again showed positive effects on increasing the fracture energy of UHPC. The addition fracture energy gained from fibre bridging effect which not only can delay the crack propagation but also can resist the friction and interlock at the crack surface.

Similar fracture energy was noticed for the specimens using different nano-particles. However, for the fibre reinforced UHPC specimens, the values from specimens with different nano additions fluctuated significantly showing that the nano-particles influenced the fracture energy of steel fibre reinforced specimens more than non-fibre reinforced specimens.

Table 17: Fracture energy of UHPC with different nano-particles (unit: J/m³)

Fibre Nano	NO	TF1	TF2	WF	MF06	MF12
NO	110.8	5029.1	--	3959.8	22931.2	32551
CaCO₃ 3%	--	7033.3	13031.9	2812.2	4809.6	38773.1
SiO₂ 1%	987.6	5624.1	--	1781.4	7179.5	16466.7
TiO₂ 2%	219.4	6988	7566.1	4268.7	13746.5	17715.8
Al₂O₃ 3%	877.8	17060.8	39538.3	4601	17186.3	45024.3

4.4 MICROSCOPY ANALYSIS

Morphology of the samples was observed by Scanning Electron Microscopy (SEM) in using LEO 1550 Scanning Electron Microscope. UHPC samples with and without nano material addition were scanned after SHPB split tensile tests. Pictures of matrix taken from the SEM tests are listed in Figure 44.

In Figure 44a, large number of well-developed calcium hydroxide Ca(OH)_2 plates are observed implying that without nano particles addition, the air voids of the hardened UHPC are relatively large and plate-shaped Ca(OH)_2 has enough space to grow. In UHPC with nano particles addition as shown in Figure 44b, very dense structure with quite few small sized air pores is observed, and the main hydration product is the foil-like fine C-S-H gel, and also there is almost no plate-shaped Ca(OH)_2 . These observations confirm the pozzolanic effect of nano material in generating additional C-S-H gel which is the fundamental source for concrete strength, in addition, the nano-scale filling effect from the nano material is also beneficial for a material strength enhancement.

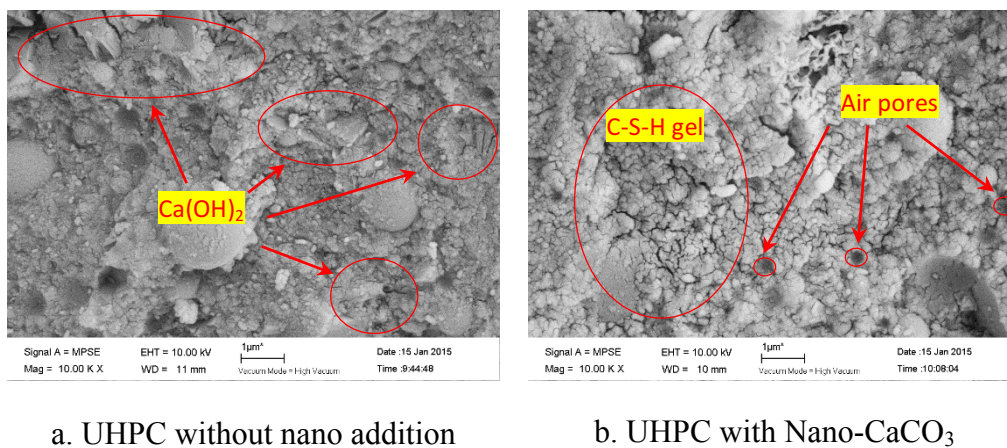


Figure 44: Pictures of mortar matrix from SEM analysis

4.5 LABORATORY AND FIELD BLAST TESTS ON UHPC COMPONENTS

UHPC material has promising practice applications in the protective structural design due to its exceptional mechanical properties. In the present study, structural components were casted in the laboratory with selected material composition discussed above. Static bending tests and field blast tests were carried out so as to further investigate the performance of UHPC material.

4.5.1 Specimen geometry

As shown in Figure 45, these specimens had a square cross-section of 200 mm \times 200 mm and a span of 2500 mm. The longitudinal reinforcement consisted of 8 Φ 16 mm screw thread rebars, the yield stress and ultimate strength of these rebars were 1350 MPa and 1600 MPa, respectively). The transverse reinforcement consisted of Φ 8 mm plain roller ties with a yielding strength of 300 MPa. The clear concrete cover was kept as a constant of 35 mm.

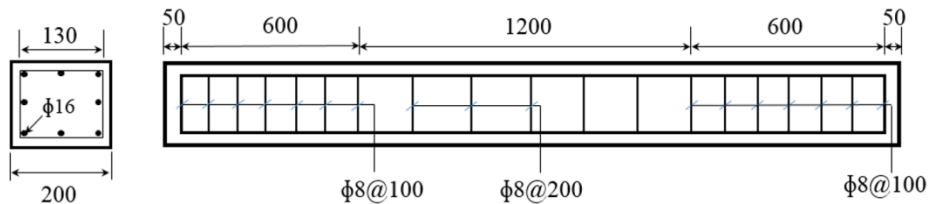


Figure 45: Specimen configuration and reinforcement

4.5.2 UHPC component subjected to static bending

In these series of tests, two UHPC materials were used to cast the components, UHPC material with 2.5 Vol-% TF fibre reinforcement and 3% Nano- CaCO_3 addition was used to cast Component-1 while UHPC material with 2.5 Vol-% MF12 fibre reinforcement and 3% Nano- CaCO_3 addition was used to case Component-2, and the dimension and reinforcement are shown in Figure 46. It is worth noting that, so as to yield a comparative study, the volume fraction of TF fibre was increased to 2.5%.

The instrumentation and test setup are shown in Figure 46. Electrical resistance strain gauges were used to measure the strain of the concrete. Five strain gauges were located on the side surface of the components at mid-span to measure strain at different heights. In addition, displacement measurement device was bonded on the concrete at the compressive chord level. The LVDT was placed at mid-span and at the loading point to measure deflection. Finally, load cell bonded to the actuator was used to measure the load applied to the component.

Steel roller supports were installed at a distance of 50 mm from both ends of the component. Load was applied through hydraulically actuated jack at mid-span, displacement controlled loading was adopted at a speed of 1/1500 of the specimen span length (2400 mm) per minute. The loading process was continued until the component was observed to soften.

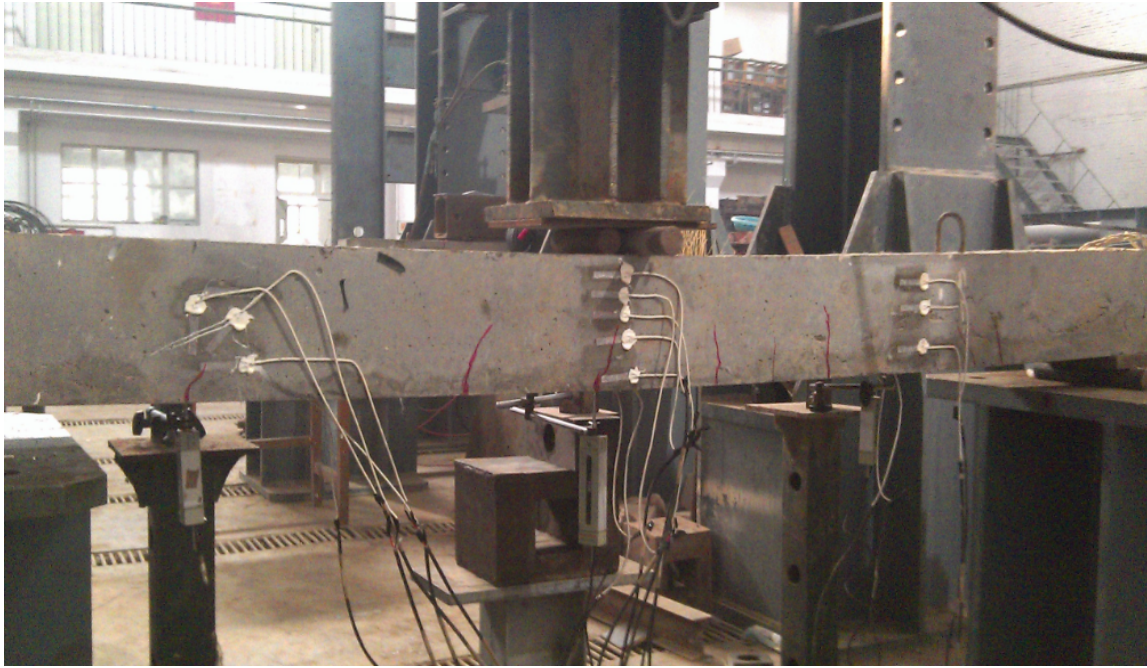
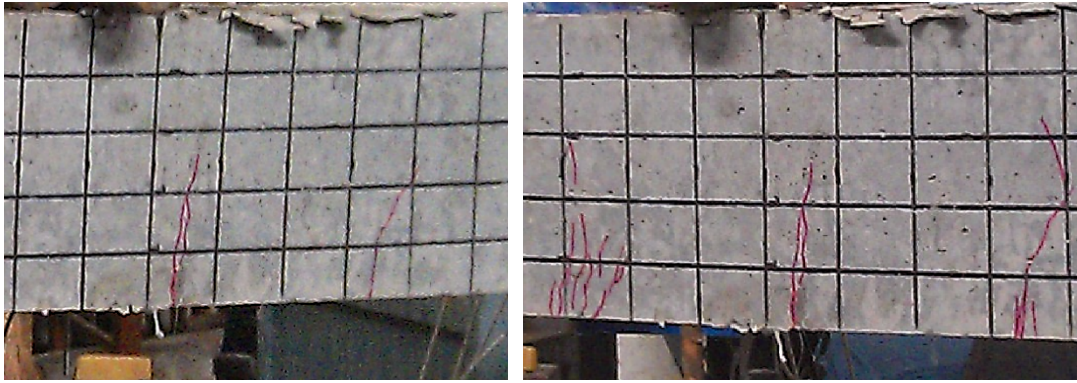


Figure 46: Instrumentation and setup in the static bending tests

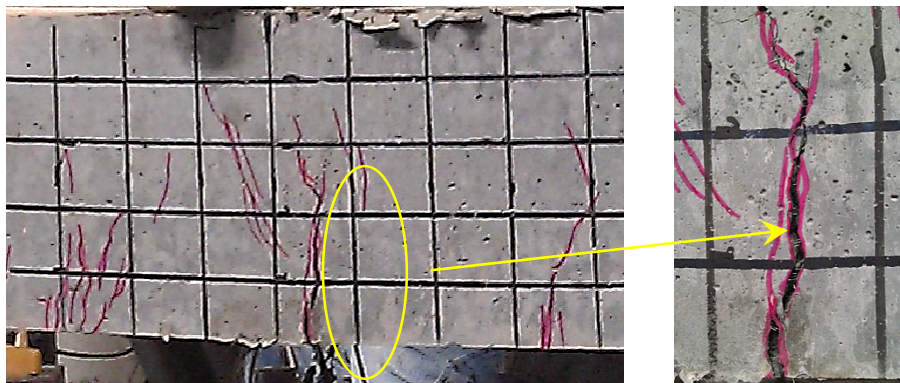
At the beginning of the test, the load increased linearly and no cracks was observed. After audible signal, first crack initiated at mid-span where the maximum bending moment and tensile stress located, and followed by several micro cracks distributed sparsely. As the testing continued after first cracking, more micro cracks appeared between the existing cracks, most of these cracks propagated towards the upper surface, and the crack width was not visually widened. As the testing further progressed, the steel fibres at the bottom of the mid-span were gradually pulled out from the matrix due to the load carried by these fibre was larger than the bonding strength between the UHPC matrix and the fibre.

After reaching the peak load, the first fibre (fibres) was pulled out from the matrix, the load carried by this fibre was distributed to surrounding fibres, and this process increased the load and stress on nearby fibres. As the external load further increased, the first crack became significantly wider leading to structural softening and the eventually, the structural failure. The whole process of the bending tests was illustrated in Figure 47.



(a) First crack

(b) Multi-cracks



(c) Further cracking before yielding

Figure 47: Crack propagation on the UHPC component under bending

Load deflection curve for Component-1 and 2 are shown in Figure 48. The mid-span deflection until the initiation of cracks increased linearly and was proportional to load. After the initial cracking, deflection increased nonlinearly until the maximum load was reached. It is seen that UHPC with MF addition showed better ductility and preserved loading capacity even after 45 mm mid-span deflection, on the other hand, UHPC with TF fibre addition showed less ductility. The difference can be ascribed to the fibre aspect ratio, in the present study, MF12 fibre had larger aspect ratio than TF fibre (100 versus 87.5), and under tensile loads, fibre with larger aspect ratio had better bonding with the matrix and therefore better ductility was achieved.

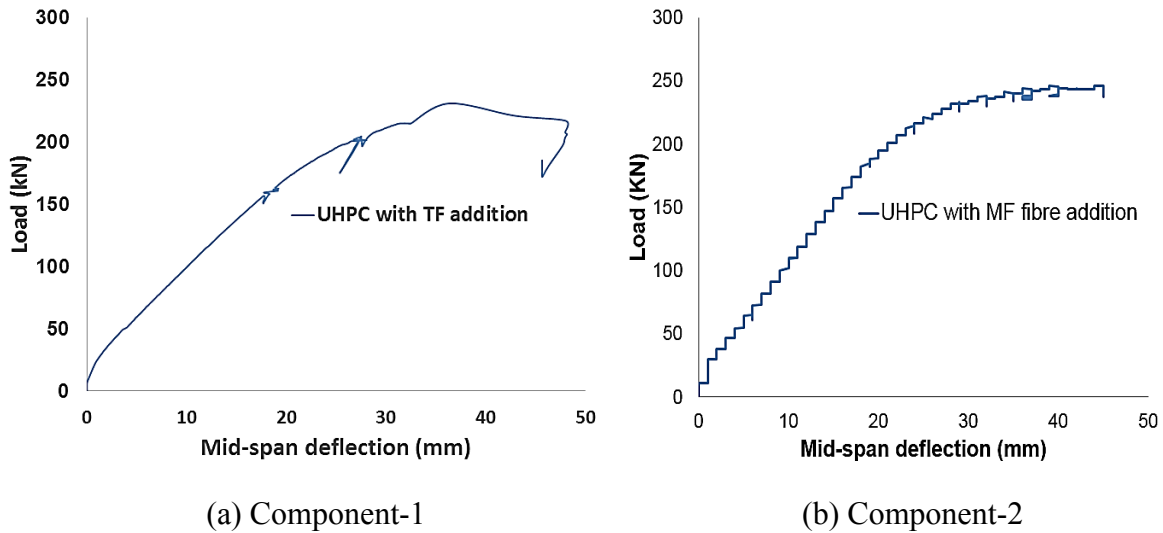


Figure 48: Load deflection curve

4.5.3 UHPC component subjected to blast loads

After conducting the static bending tests, the material composition with better ductility (2.5 Vol-% MF12 with Nano-CaCO₃) was chosen to cast the columns for field blast tests. In the field tests, the columns were placed on the steel frame with LVDTs installed on the column bottom surface, the pressure transducers were installed on the steel support close to the column upper surface. It is worth noting that in such test setup, the blast load recorded by the pressure sensor would be larger than the actual blast load on the column due to the larger stiffness of the steel support. The pressure transducer has a sampling rate of 0.2 MHz, and the LVDT had stroke length of -150 mm to +150 mm.

After the recording instruments were connected, the whole frame was lowered into the ground and the gap between the column and the frame was sealed with rubber sheets so as to protect the instruments underneath from the blast wave. The pneumatic jack at one end of the column provided constant 1000 kN axial force during the blast test. Cylindrical emulsion explosive charge was placed at 1.5 m height above the specimen. The field blast test instrumentation and setup is shown in Figure 49.

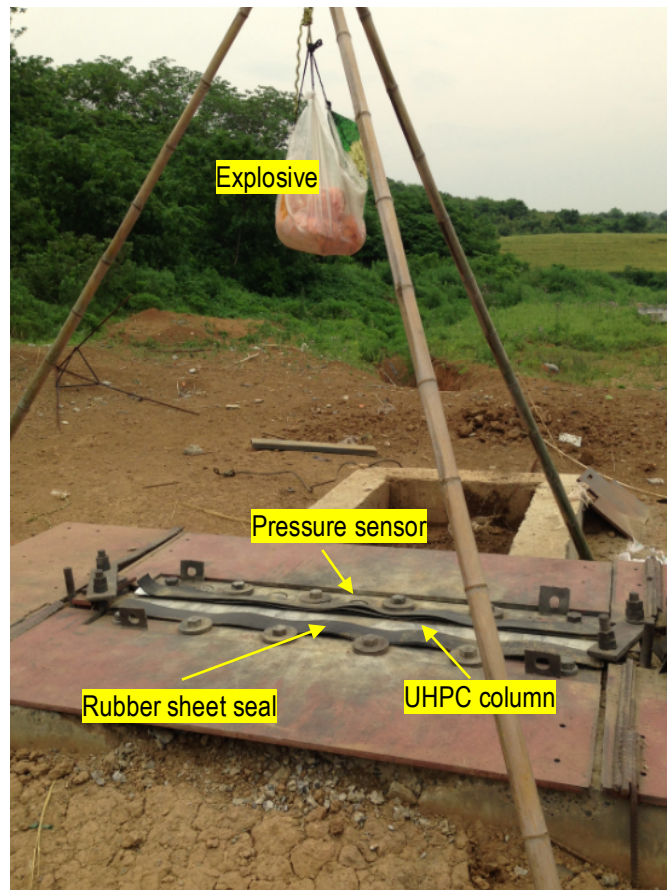


Figure 49: Field blast test setup

UHPC column was tested under blast scenarios with 17.5 TNT equivalences. For comparative purpose, one high strength concrete (HSC) column was tested under 17.5 kg TNT equivalence blast loads. In the material composition of high strength concrete column, no steel fibre material and nano additives were mixed.

Blast overpressure time histories are shown in Figure 50, and it is seen that empirical predictions from UFC 3-340-2 [39] slightly underestimated the peak blast pressure on the column which could be possibly caused by the charge shape effect.

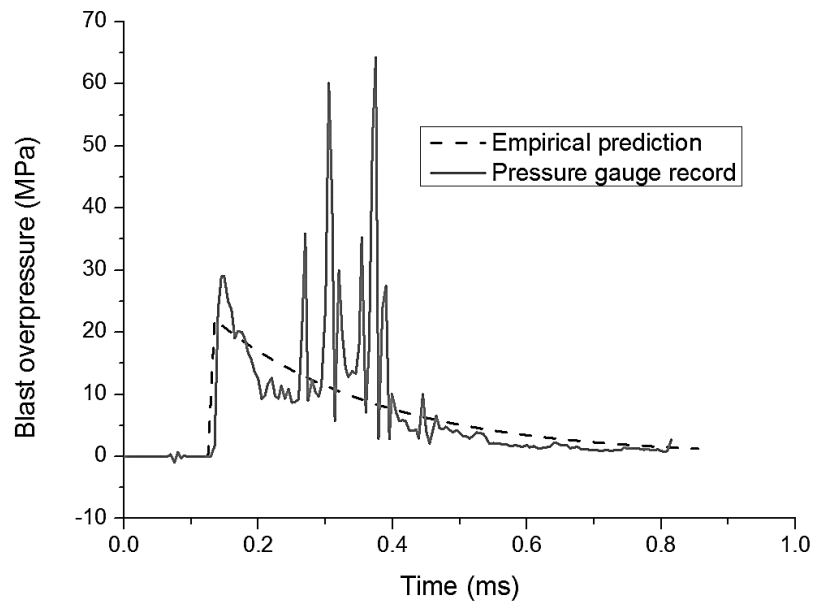


Figure 50: Blast pressure time-histories

Under the blast pressure from 17.5 kg TNT equivalence, HSC column failed in a complex mode as shown in Figure 51a. Material failure on the upper surface can be possibly caused by two reasons, firstly, due to size limitation, three dimensional blast wave propagated towards the free edge in the column width direction, and multiple reflection occurred in the corner area which caused the material failure; secondly, after the blast loading phase, column entered into free vibration phase in which the maximum compressive strain exceeded material capacity. Besides material failure on the upper surface, shear cracks were clearly seen on the column.

For UHPC column under the same blast load, almost no damage was observed except some hairline cracks as shown in Figure 51b. The steel fibres provided bridging effect after crack opening and retarded crack propagation.



(a) HSC Specimen with 1000 kN axial load under 17.5 kg charge weight loading



(b) UHPC Specimen with 1000 kN axial load under 17.5 kg charge weight loading

Figure 51: Structural column performance after field tests

4.6 CONCLUSIONS

Based on compressive tests and four point bending tests on UHPC samples, the present study investigates the effects of incorporating nano-additive and different fibre types on performance of ultra-high performance concrete. According to the compressive test results, UHPC specimens with different fibre types showed better performance than specimens without fibre reinforcement in terms of stress-strain relationship, compressive strength and strain energy density. Among fibre reinforced specimens, the specimens with 2.5% MF12 fibres showed the greatest improvement in the compressive tests.

The results obtained in the four point bending test indicated that the fibre reinforced UHPC beams outperformed the non-fibre reinforced beams in terms of the ductility, flexural tensile strength and the fracture energy. In contrary to the conclusion of the compressive test, the use of nano-additives affected more on the fracture energy of fibre reinforced UHPC beams than non-fibre reinforced UHPC beams. Microscopy analysis explains the effects of nano-material in promoting the cement hydration process.

Reinforced UHPC components with selected material composition were tested under three point bending, crack propagation process was recorded and discussed and it was observed that fibre aspect ratio was influential on structural ductility.

The field blast tests results demonstrated that columns built with UHPC material had exceptional blast resistance capability, while high strength concrete column failed in a brittle mode. UHPC column showed almost no damage, while HSC column failed in brittle mode, and UHPC column showed energy-absorbing flexure response without much mid-span deflection.

ACKNOWLEDGEMENTS

The research presented in this paper jointly supported by ARC DP160104661, the Key Projects of Tianjin Science and Technology Support Plan 14ZCZDSF0016, and The National Basic Research Programme 2015CB058002, is gratefully acknowledged.

REFERENCES

- [1] F. Aslani, S. Nejadi, Creep and shrinkage of self-compacting concrete with and without fibers, *Journal of Advanced Concrete Technology*, 11 (2013) 251-265.
- [2] R. Deeb, A. Ghanbari, B.L. Karihaloo, Development of self-compacting high and ultra high performance concretes with and without steel fibres, *Cement and concrete composites*, 34 (2012) 185-190.
- [3] P. Groth, D. Nemegeer, The use of steel fibres in self-compacting concrete, in: *International RILEM symposium on self-compacting concrete*, 1999, pp. 497-507.
- [4] C. Wu, D.J. Oehlers, M. Rebstrost, J. Leach, A.S. Whittaker, Blast testing of ultra-high performance fibre and FRP-retrofitted concrete slabs, *Engineering Structures*, 31 (2009) 2060-2069.
- [5] J. Li, C. Wu, H. Hao, An experimental and numerical study of reinforced ultra-high performance concrete slabs under blast loads, *Materials & Design*, 82 (2015) 64-76.
- [6] V. Bindiganavile, N. Banthia, B. Aarup, Impact response of ultra-high-strength fiber-reinforced cement composite, *ACI Materials journal*, 99 (2002).
- [7] L.P. de Oliveira, J.C. Gomes, L. Bernardo, M. Ramos, Evaluation of dry mortar ratio as mix design parameter for steel fibre reinforced self compacting concrete, *Construction and Building Materials*, 40 (2013) 642-649.
- [8] B. Miao, J.C. Chern, C.A. Yang, Influences of fiber content on properties of self-compacting steel fiber reinforced concrete, *Journal of the Chinese Institute of Engineers*, 26 (2003) 523-530.
- [9] S. Ghanbarpour, H. Mazaheripour, S. Mirmoradi, A. Barari, The effect of type and volume fraction (VF) of steel fiber on the mechanical properties of self-compacting concrete, *Journal of Engineering, Design and Technology*, 8 (2010) 247-256.
- [10] J. Li, C. Wu, H. Hao, Blast Resistance of Newly Developed Ultra-High Performance Concrete Columns, in: *International Conference on Protective Structures (ICPS3)*, Newcastle, Australia, 2015.
- [11] D.-Y. Yoo, J.-J. Park, S.-W. Kim, Y.-S. Yoon, Combined effect of expansive and shrinkage-reducing admixtures on the properties of ultra high performance fiber-reinforced concrete, *Journal of Composite Materials*, 48 (2014) 1981-1991.
- [12] Ş. Yazıcı, G. İnan, V. Tabak, Effect of aspect ratio and volume fraction of steel fiber on the mechanical properties of SFRC, *Construction and Building Materials*, 21 (2007) 1250-1253.
- [13] Z. Wang, J. Wu, J. Wang, Experimental and numerical analysis on effect of fibre aspect ratio on mechanical properties of SRFC, *Construction and Building Materials*, 24 (2010) 559-565.
- [14] J. Ambroise, S. Rols, J. Pera, H. Reinhardt, A. Naaman, Properties of self-levelling concrete reinforced by steel fibres, in: *Third International RILEM Workshop on High Performance Fiber Reinforced Cement Composites*, RILEM Publications SARL, 1999, pp. 9-17.

- [15] A.S. El-Dieb, Mechanical, durability and microstructural characteristics of ultra-high-strength self-compacting concrete incorporating steel fibers, *Materials & Design*, 30 (2009) 4286-4292.
- [16] L. Ferrara, P. Bamonte, A. Caverzan, A. Musa, I. Sanal, A comprehensive methodology to test the performance of steel fibre reinforced self-compacting concrete (SFR-SCC), *Construction and Building Materials*, 37 (2012) 406-424.
- [17] J. Belkowitz, D. Armentrout, The investigation of nano silica in the cement hydration process, *ACI Special Publication*, 267 (2009).
- [18] M. Berra, F. Carassiti, T. Mangialardi, A. Paolini, M. Sebastiani, Effects of nanosilica addition on workability and compressive strength of Portland cement pastes, *Construction and Building Materials*, 35 (2012) 666-675.
- [19] M. Jalal, M. Fathi, M. Farzad, Effects of fly ash and TiO₂ nanoparticles on rheological, mechanical, microstructural and thermal properties of high strength self compacting concrete, *Mechanics of Materials*, 61 (2013) 11-27.
- [20] B.-W. Jo, C.-H. Kim, G.-h. Tae, J.-B. Park, Characteristics of cement mortar with nano-SiO₂ particles, *Construction and Building Materials*, 21 (2007) 1351-1355.
- [21] H. Li, H.-g. Xiao, J. Yuan, J. Ou, Microstructure of cement mortar with nano-particles, *Composites Part B: Engineering*, 35 (2004) 185-189.
- [22] A. Nazari, S. Riahi, The effect of TiO₂ nanoparticles on water permeability and thermal and mechanical properties of high strength self-compacting concrete, *Materials Science and Engineering: A*, 528 (2010) 756-763.
- [23] A. Nazari, S. Riahi, The effects of ZrO₂ nanoparticles on physical and mechanical properties of high strength self compacting concrete, *Materials Research*, 13 (2010) 551-556.
- [24] A. Nazari, S. Riahi, The effects of SiO₂ nanoparticles on physical and mechanical properties of high strength compacting concrete, *Composites Part B: Engineering*, 42 (2011) 570-578.
- [25] Y. Qing, Z. Zenan, K. Deyu, C. Rongshen, Influence of nano-SiO₂ addition on properties of hardened cement paste as compared with silica fume, *Construction and Building Materials*, 21 (2007) 539-545.
- [26] F. Sanchez, K. Sobolev, Nanotechnology in concrete—a review, *Construction and Building Materials*, 24 (2010) 2060-2071.
- [27] K. Wille, A. Naaman, S. El-Tawil, G. Parra-Montesinos, Ultra-high performance concrete and fiber reinforced concrete: achieving strength and ductility without heat curing, *Materials and Structures*, 45 (2012) 309-324.
- [28] A.M. Soliman, M.L. Nehdi, Effect of drying conditions on autogenous shrinkage in ultra-high performance concrete at early-age, *Materials and Structures*, 44 (2011) 879-899.
- [29] J. Dils, V. Boel, G. De Schutter, Vacuum mixing technology to improve the mechanical properties of ultra-high performance concrete, *Materials and Structures*, (2014) 1-17.
- [30] J. Dils, G. De Schutter, V. Boel, Influence of mixing procedure and mixer type on fresh and hardened properties of concrete: a review, *Materials and Structures*, 45 (2012) 1673-1683.
- [31] X. Liu, L. Chen, A. Liu, X. Wang, Effect of Nano-CaCO₃ on Properties of Cement Paste, *Energy Procedia*, 16, Part B (2012) 991-996.
- [32] A. Nazari, S. Riahi, The effects of limewater on flexural strength and water permeability of Al₂O₃ nanoparticles binary blended concrete, *Journal of Composite Materials*, 45 (2011) 1165-1172.
- [33] A. Nazari, S. Riahi, The effects of ZnO₂ nanoparticles on split tensile strength of self-compacting concrete, *Journal of Experimental Nanoscience*, 7 (2012) 491-512.
- [34] J. Camiletti, A.M. Soliman, M.L. Nehdi, Effects of nano- and micro-limestone addition on early-age properties of ultra-high-performance concrete, *Materials and Structures*, 46 (2013) 881-898.

- [35] A. Neuberger, S. Peles, D. Rittel, Scaling the response of circular plates subjected to large and close-range spherical explosions. Part I: Air-blast loading, *International Journal of Impact Engineering*, 34 (2007) 859-873.
- [36] Chinese standard GB2419, (1981).
- [37] Chinese standard GB/T 50081, (2002).
- [38] Z.P. Bazant, *Fracture Mechanics of Concrete Structures: Proceedings of the First International Conference on Fracture Mechanics of Concrete Structures (FraMCoS1)*, held at Beaver Run Resort, Breckenridge, Colorado, USA, 1-5 June 1992, Taylor & Francis, 1992.
- [39] US Department of Defense, Structures to resist the effects of accidental explosions (UFC 3-340-02), in: *Unified Facilities Criteria*, Washington, DC, 2008.

Statement of Authorship

Article Name: Mesoscale study of novel ultra-high performance concrete under static and dynamic loads

Su, Y., Li, J., Wu, C., Wu, P., Tao, M. and Li, X.

Status: Submitted to *Materials and Design*

Su, Y. (candidate)

Contribution: helped conduct tests, processed and analysed test data and prepared manuscript

I hereby certify that the statement of contribution is accurate.

Signed..... Date 27/08/2016

Li, J.

Contribution: supervised research and tests, provided critical manuscript evaluation and acted as corresponding author.

I hereby certify that the statement of contribution is accurate and I give permission for the inclusion of the paper in the thesis.

Signed..... Date 24/8/2016

Wu, C.

Contribution: helped design and conduct tests.

I hereby certify that the statement of contribution is accurate and I give permission for the inclusion of the paper in the thesis.

Signed... Date 24/08/2016

Wu, P.

Contribution: provided critical manuscript evaluation.

I hereby certify that the statement of contribution is accurate and I give permission for the inclusion of the paper in the thesis.

Signed..... Date 20/8/24

Tao, M.

Contribution: provided critical manuscript evaluation.

I hereby certify that the statement of contribution is accurate and I give permission for the inclusion of the paper in the thesis.

Signed..... Date 24/08/2016

Li, X.

Contribution: provided critical manuscript evaluation.

I hereby certify that the statement of contribution is accurate and I give permission for the inclusion of the paper in the thesis.

Signed..... Date 20/8/25

CHAPTER 5: MESOSCALE STUDY OF NOVEL ULTRA-HIGH PERFORMANCE CONCRETE UNDER STATIC AND DYNAMIC LOADS

Yu Su¹, Jun Li², Chengqing Wu^{2*}, Pengtao Wu³, Ming Tao⁴, Xibing Li⁴

¹School of Civil, Environmental and Mining Engineering, the University of Adelaide, SA,
Australia 5005

²School of Civil and Environmental Engineering, University of Technology Sydney,
Australia

³Tianjin Key Laboratory of Civil Structure Protection and Reinforcement, Tianjin Chengjian
University, Tianjin 300384, China

⁴School of Resources and Safety Engineering, Central South University, Changsha, Hunan,
China

ABSTRACT

In this paper, a three-dimensional numerical model to study the static and dynamic behaviour of ultra-high performance steel fibre reinforced concrete is developed. Ultra-high performance steel fibre reinforced concrete is assumed to be a two-phase model consisting of concrete matrix and steel fibres. The concrete matrix is modelled with homogeneous material and the straight round steel fibres are assumed to be dispersed with random locations and orientations in the matrix. The interfacial transition zone (ITZ) effect is studied based on the single fibre pull-out tests, and parameters describing the fibre-matrix one dimensional bond-slip behaviour are obtained and discussed based on both experimental and theoretical results. After the three-dimensional model is validated with static split tensile tests, split Hopkinson pressure bar (SHPB) split tensile tests are numerically modelled and the stress-time history is interpreted in the mesoscale level. The proposed model qualitatively and quantitatively predicts the material static and dynamic behaviours, and also gives insights on the fibre reinforcement effect in the concrete matrix.

5.1 INTRODUCTION

Concrete is a widely used material in structural construction all over the world. Unreinforced concrete is a brittle material with low tensile strength and tensile strain, it is, therefore, mainly used to carry axial compressive loads. With steel bar reinforcement, concrete extends its application into the bending elements. Despite this revolutionary improvement, concrete remains brittle and weak in tensile as a material.

Fibrous material additions had been used to enhance the performance of concrete-like material since ancient time. It is well known that the addition of fibre material significantly changes the behaviour of the concrete composite, especially during the post-cracking phase. Addition of fibre material leads to substantially improved structural ductility, better hysteretic response under cyclic load reversals, better bonding of the reinforcing bars, improved resistance of the concrete cover to spalling, improved shear resistance, savings in stirrups, and overall improved energy absorption capacity of the structure [1]. Among all different types of fibre material (natural fibre, synthetic fibre, carbon fibre, glass fibre etc.), steel fibres are the most widely used in civil construction since their first development in 1960s [2].

Extensive study was carried out to understand the behaviour of steel fibre reinforced concrete (SFRC). Ezeldin and Perumalsamy [3] studied influence from fibre aspect ratio, volume fraction on the compressive stress-strain behaviour of SFRC with compressive strength ranging from 35 MPa to 85 MPa, and based on the results, a simple equation to predict the complete compressive stress-strain curve was proposed. Based on experimental study, Wecharatana and Shah [4] concluded that the post-cracking behaviour of random discontinuous fibre reinforced brittle-matrix composites can be predicted by the use of a stress–crack opening displacement relationship. Tan et al. [5] proposed an analytical method for the prediction of both the instantaneous and long-term deflections of the beams with steel fibre reinforcement. The method accounted for the enhanced cracking load and the beam stiffness, as well as the creep and shrinkage restraints due to fibres. Under dynamic loads, fibre reinforced normal strength concrete is observed to be more rate-sensitive than the unreinforced matrix, and the sensitivity increases with the fibre content [6]. It has been reported that the fibre pull-out strength increases with an increase in the loading rate [7] leading to an increased energy absorption capacity under dynamic loads [8]. Naaman et al. [9] pointed out that during the failure of SFRC, most fibres pull out rather than break, and the tensile strength of the fibres is not as important as their bond properties.

Although SFRC can be treated as homogeneous at macroscopic scale, when observed at a smaller length scale, SFRC is heterogeneous and consists of constituents including aggregate, CH crystals, C-S-H gel, water and fibre material. It is impractical to consider all the phases in the microstructure of SFRC. In general, to investigate the interfacial transition zone (ITZ) effect on the fibre bonding properties, SFRC is described as multi-phase material consisting of the cement paste, aggregates, fibres and ITZs among them. In some previous studies, the interfaces between fibres and cement paste are presumed to be perfect [10, 11], however, the existence of ITZs weakens the bonding between the fibres and concrete matrix. The bonding performance of SFRC is influenced by the fibre geometry [12-14], fibre orientation [15, 16], and also the strength of the matrix, it is therefore critical to consider the ITZ effect in the performance of SFRC.

As can be noted in the literature, the mechanical behaviour of SFRC is mainly investigated through experimental and associated analytical studies. Over the past several decades, with the development of computer power and computational mechanics, numerical simulation of material and structural behaviour under both static and dynamic conditions are becoming increasingly popular. Mao et al. [17] carried out numerical simulation of SFRC slab against blast loads based on modified concrete model, and the material strain hardening and softening phases were considered to update the concrete damage model in commercial hydro-code LS-DYNA. Wang et al. [18] proposed constitutive relationship for SFRC, and simulated the SFRC specimens under split Hopkinson pressure bar tests, and their results indicated the feasibility of the proposed numerical model for material dynamic behaviour analysis. Elastic-Plastic-Hydrodynamic model was adopted by the authors [19-21] and Wang et al. [22] to describe the material behaviour of steel fibre reinforced concrete, and reasonable correlation between the numerical results with blast tests were found in the analysis. Besides these homogeneous models, mesoscale study considering the heterogeneity of concrete under static and dynamic loads can also be found in the literature. Research was carried out on plain concrete in mesoscale under dynamic loads [23-25]. Xu et al. [26] developed an axisymmetric mesoscale model with components of fibre, aggregate and mortar to investigate the dynamic failure behaviour of SFRC material under impact loading. Fang and Zhang [27] conducted three-dimensional modelling of steel fibre reinforced concrete material under intense dynamic loading, and their model well reproduced SFRC failure under contact detonations.

In a recent study, a specifically formulated steel fibre reinforced concrete material was developed, and material tests as well as structural components tests were carried out to understand the performance of this novel material under both static and dynamic loading conditions [12, 21, 28, 29]. This material is formulated by combining Portland cement, silica fume, quartz flour, fine silica sand, high-range water reducer, water, and steel fibres. Due to its excellent mechanical characteristics, this material can be classified into the category commonly known as ultra-high performance concrete (UHPC). Its dense matrix, in combination with high performance fibre material, leads to a very low material permeability, which can also improve the durability of the structural members.

In the present paper, the bonding effect between the fibre material and matrix is investigated firstly by single fibre pull-out tests in which different fibre embedding depths are considered. The experimental results are then used to establish the bond-slip relationship in the numerical model. The numerical model is then calibrated through static split tensile tests, and SHPB tests are finally investigated with the mesoscale model.

5.2 MATERIALS AND SINGLE FIBRE PULL-OUT TEST

The material composition in the present study is listed in Table 18, and high performance steel fibre material used in the present study has a diameter of 0.12 mm and a length of 15 mm with its yielding strength of 4200 MPa. Fibre volume fraction of 2.5 Vol-% is considered.

A notable character which makes the current material distinguished from the conventional UHPC material is the addition of nanoscale particles. The addition of nano material affects material hydration process. When a small quantity of the nano-particles is uniformly dispersed in the cement paste, the nano-particles located in the cement will promote and accelerate cement hydration due to their high activity. It was reported [30] that concrete strength increases with nano content up to 4 wt.% and then decreases. In order to achieve a balance of performance and cost-effectiveness, a weight dosage of 2.5% is made in the present study.

Table 18: Mix proportions of different UHPC formula (unit: kg)

Constituents	Proportions
52.5 Cement	750
Silica Fume	225
Silica Flour	190
Sand	1030
Superplasticizer	16
Water	190
Water/Cement	25.30%
Steel Fibre	2.5 Vol-%
Nano-CaCO ₃	63.1 (2.5 wt.%)

5.2.1 Single fibre full out test

The primary reason behind the addition of fibre material into the concrete matrix is to delay and confine the crack. Although inclusion of fibre material is believed to enhance the concrete pre-cracking strength, the effect of fibre addition becomes more prominent only after the crack initiates. Fibres bridge over the cracked parts, delaying the sudden failure of brittle concrete matrix. The fibre bridging effect is primarily related to the interfacial bonding strength which governs the post-cracking material performance under external pull-out loads. It is therefore critical to understand the fibre pull-out behaviour.

In the present study, to obtain the interfacial bond properties between fibres and matrix, a series of fibre pull-out tests are conducted. As shown in Figure 52, five embedding lengths, i.e. 20 mm, 30 mm, 40 mm, 50 mm and 60 mm are considered. In the test, displacement control is adopted with a constant loading speed of 1 mm/min. Test stops when the fibre is pulled-out or fractured. The fibre lengths after pull-out and fracture are measured.

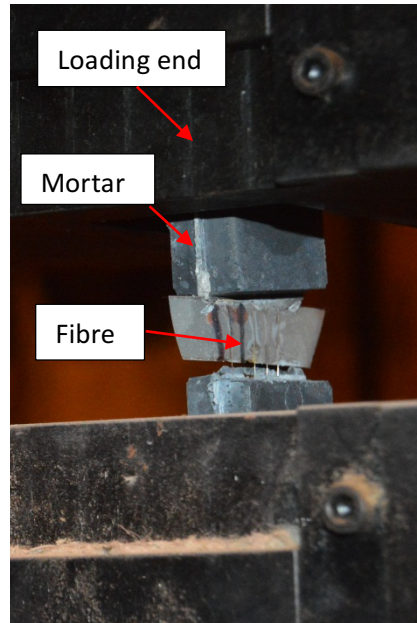


Figure 52: Setup of fibre pull-out test

Test results reveal that with the increase of fibre embedding length, the failure mode alters from fibre pull-out to fibre fracture. Figure 53 shows the load versus slip curve for the given five fibres, and it is clear the peak load increases with the embedding length, however at a cost of post-peak ductility. When the embedding length is 60 mm, the peak load reached 54 kN while the peak load is only 22 kN for fibre with embedding length of 30 mm. The descending portion of the curve is rather steep for 60 mm embedding length indicating the fibre fracture.

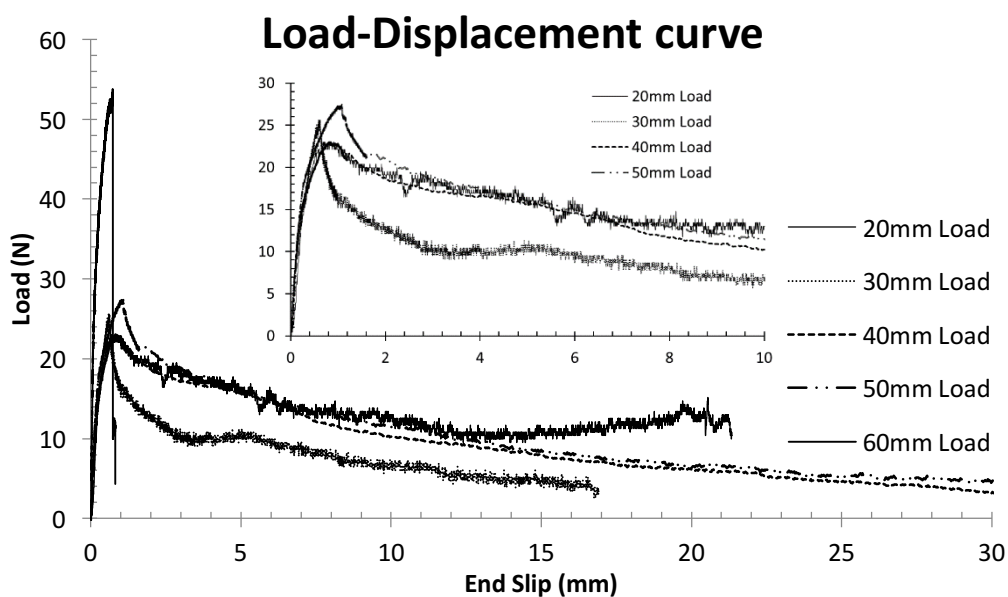


Figure 53: Load versus end-slip curves for different fibre embedding depths

For a smooth fibre with round cross-section, the whole process of fibre pull-out contains three stages as shown in Figure 54. At the initial stage, the fibre-matrix interface remains intact and the corresponding segment of the curve is almost linear; when the external force reaches a critical value, an interfacial crack is initiated at the point where the fibre penetrates the matrix and starts propagating along the interface. In this stage, interfacial frictional force in the debonded zone is working together with the adhesive force in the intact zone to resist the external force. With further increase of the external load, the frictional force increases proportionally in the debonded area, while the adhesive force in the intact zone progressively decreases. The force reaches its maximum when the embedded part of the fibre becomes too short. Full debonding occurs after the maximum force was reached. The force in the remaining segment is purely because of the frictional force between the fibre and matrix. It was found that this segment gradually decreases as the fibre is being pulled out from the matrix, but in microbond test in which the fibre-matrix contact area remains constant after the fully debonding, the recorded force is also constant.

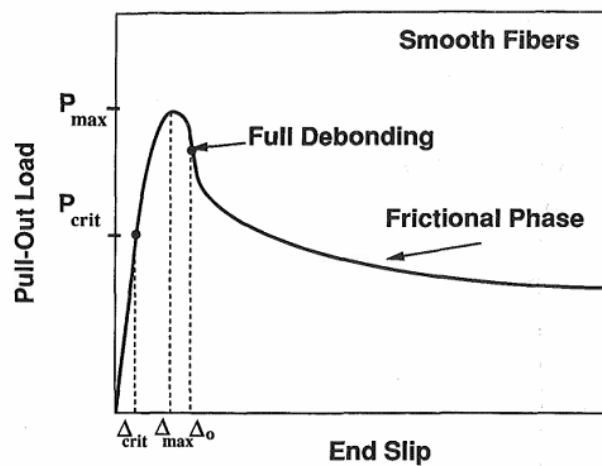


Figure 54: General fibre pull-out load versus end slip curve

Mathematical derivation of straight fibre pull-out from the matrix has been formulated by Naaman et al. [31]. Prior to end slip reaches a critical value of Δ_{crit} , the embedded fibre segment sticks with the surrounding matrix without any relative displacement. Within this stage, the pull-out load can be expressed as:

$$P = \Delta \frac{\lambda A_m E_m}{Q-2} \frac{1+e^{-\lambda l}}{1-e^{-\lambda l}} \quad (\Delta \leq \Delta_{crit}) \quad (22)$$

where $Q = 1 + \frac{A_m E_m}{A_f E_f}$, A_f and E_f are the area and elastic modulus of the fibre, respectively; A_m and E_m are the area and elastic modulus of the matrix, respectively; $\lambda = \sqrt{KQ}$ in which $K = \kappa\psi/A_m E_m$ and κ is the bond modulus, ψ is the perimeter of the fibre; and l is the fibre embedded length.

It can be noted from the above equation that there is a linear relationship between the applied force and the displacement of the fibre free end.

For debonding stage between $\Delta_{crit} \leq \Delta \leq \Delta_0$, and the fully debonded zone $\Delta \geq \Delta_0$, the theoretical solution of the pull-out load can be found in [31].

5.2.2 Numerical study of single fibre pull out test and model validation

5.2.2.1 Material model

In the numerical simulation of the single fibre pull-out tests, the matrix is modelled with solid element and material model 72 Mat_CONCRETE_DAMAGE_Rel3 in LS-DYNA. This material model uses three shear failure surfaces and includes the damage and strain rate effects. This model provides model parameter generation capability which is based solely on unconfined compression strength of the concrete. The automatic generated model parameter can also be examined and modified by the user.

For the fibre material, Material model 98 Mat_SIMPLIFIED_JOHNSON_COOK is adopted, and fibres are modelled with truss element so as to avoid computational difficulties while maintaining reasonable accuracy.

Parameters used in the current numerical model are listed in Table 19.

Table 19: Parameters used in numerical model

Material	Model in LS_DYNA	Input parameter	Value
Mortar matrix	MAT_72R3	Density	2450 kg/m ³
		Unconfined compressive strength	140 MPa
		Poisson's Ratio	0.19
Steel fibres	MAT_98	Density	7830 kg/m ³
		Young's Modulus	210 GPa
		Poisson's Ratio	0.28

5.2.2.2 Contact algorithm

It is worth noting that, in spite of the modelling efforts found in the literature [32], a more advanced and comprehensive model is still required to predictively model the fibre-matrix bonding effect, including progressive interfacial debonding, unstable crack propagation, and post-debond frictional sliding. One such approach involves using tiebreak and cohesive zone models in the finite element analysis using commercial codes such as LS-DYNA. One viable material model offered in LS-DYNA for use with cohesive zone elements is `*MAT_COHESIVE_MIXED_MODE`, which is a bilinear mixed-mode traction separation constitutive law used to model interfacial failure [33]. However, this model requires establishment of solid element for the cohesive zone which is impractical in the present study considering the extremely small fibre diameter and large fibre number.

A feasible alternative contact modelling algorithm in LS-DYNA is `Contact_1D`. This one-dimensional contact algorithm, suitable for defining one-dimensional bonding and sliding mechanism between solid elements and truss elements in LS-DYNA, has been used to simulate the bonding, debonding and sliding between the steel fibre and concrete matrix [27].

In this model, the slave node of a string of beam or truss elements, modelling the steel fibre, is forced to slide along a master line of nodes embedded in the solid mesh, which models the concrete matrix. This kinematic constraint is applied using a penalty function approach. Fictitious springs are inserted between slave nodes and their projections over the master lines. These springs produce internal forces along the rebar and are proportional to the distance between slave nodes and master lines, as shown in Figure 55.

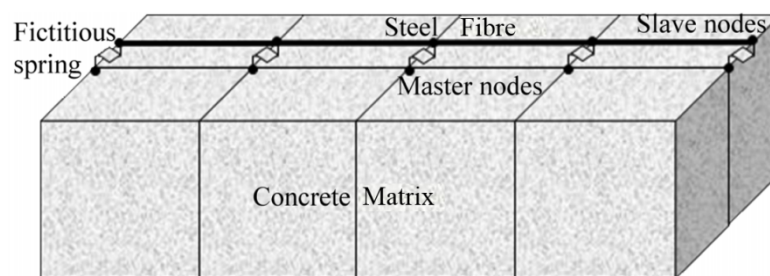


Figure 55: Fictitious spring between fibre and concrete matrix

Considering the accumulative damage, the bond between fibre and concrete is represented in a two-phase constitutive model. In the elastic range, the bonding strength is linear

proportional to the slip S . After reaching the maximum bonding strength τ_{max} , the bond shear stress will decay exponentially in the plastic range.

$$\tau = \begin{cases} G_s S, & S \leq S_{max} \\ \tau_{max} e^{-EXP \times D}, & S > S_{max} \end{cases} \quad (23)$$

where G_s is bond shear modulus, EXP is the exponent in damage curve, D is a damage parameter which is defined as the sum of the absolute values of the plastic displacement increments.

The shear force, acting on the bonding area A_s at step $n+1$ is given as:

$$f_{n+1} = \min(f_n + G_s \times A_s \times \Delta S, G_s \times A_s \times S_{max}) \quad (24)$$

Based on the above equations, the contact algorithm is defined as shown in Figure 56a:

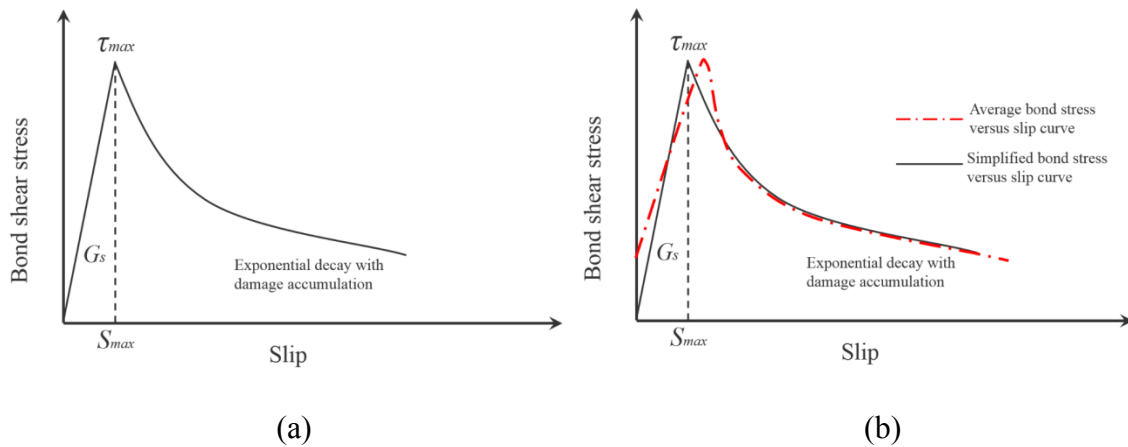


Figure 56: Bond shear stress-slip relationship for the one-dimensional slide line model

It is worth noting that this relationship is a simplified model for fibre-matrix interaction. In the real fibre pull-out test (as shown in Figure 56b), there is no relative slip between concrete and steel fibre at the very beginning, and the stress transfer mechanism between them is represented by adhesion in this stage. In the simplified model, it is assumed that slip begins at the beginning of bond stress development. The shear modulus is assumed to be constant before reaching the peak bond stress τ_{max} . This assumption yields a less accurate model for the maximum elastic slippage but provides an accurate bond modulus. However, in the numerical simulation, the importance of the bond modulus overweighs the maximum elastic slip.

5.2.2.3 Contact parameters and modelling results

In the present study, single fibre pull-out tests were carried out, and the relationship between the pull-out load and slip is now known for a given fibre, and the bond shear stress versus slip curve can be theoretically obtained. Assuming the curve is as described in Figure 5a with the linear elastic ascending branch, followed by a deteriorating frictional zone. The whole curve can thus be described by three parameters: the bond modulus G_s ; the bond strength τ_{max} or the slip S_{max} ; and the decaying frictional parameter EXP describing the deteriorating frictional zone.

When determining the bond modulus, first of all, the slope of the linear ascending portion (P/Δ as shown in Equation 1) of the pull-out curve is calculated graphically. The value of Q can be evaluated from the physical and mechanical properties of the fibre and the matrix. Only a fraction of the matrix cross-sectional area is effective if the proportion of the specimen's cross-sectional area to that of the fibre is relatively large, therefore the area of the effective matrix requires evaluation. As pointed by Naaman et al. [31], the solution is not very sensitive to the value of A_m . Once Q and the slope are known, λ in Equation 1 can be solved. Having found λ , the bonding modulus can now be solved as

$$\kappa \text{ (or } G_s) = A_m E_m K / \psi \quad (25)$$

The slip S_{max} can be approximately read graphically from the pull-out versus slip curve. The damage curve exponential coefficient EXP can be derived through the least squares fitting of the curve to the test data.

Previous study reveals that to prevent fibre fracture, the embedded length of fibre is limited by [34]:

$$L_e < \frac{\sigma_f D_f}{4\tau_{ult}} \quad (26)$$

where L_e is the maximum fibre embedded length, D_f is the fibre diameter, σ_f is the fibre tensile strength and τ_{ult} is the interfacial shear strength i.e. the IFSS.

Based on the present experimental trails, the IFSS can be calculated as 2.1 MPa.

In this simulation, the parameter used in the contact algorithm for fibre with 20 mm embedding length is shown in Table 20.

Table 20: Parameters used in the contact definition

*CONTACT_1D				
<i>ERR</i>	<i>SIGC</i>	<i>GB</i>	<i>SMAX</i>	<i>EXP</i>
6E-5 m	1.4E8 Pa	2.393E9 Pa	1.25E-3	0.2

* *ERR* is the external radius of the fibre, *SIGC* is the compressive strength of the concrete.

The comparison between the simulation and the experimental results of 20 mm embedding length is shown in Figure 57. It is seen that the simulation results coincide well with the experimental results, and the error in predicting the peak force is only 4%. The relatively accurate results indicate the effectiveness of the contact algorithm adopted in the present study.

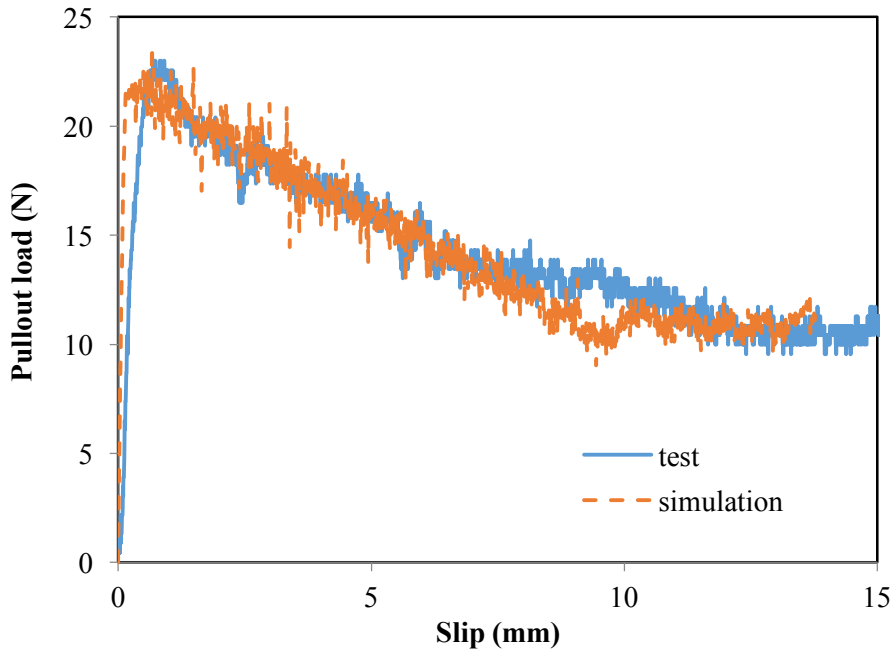


Figure 57: Comparison between test and simulation

5.3 STATIC SPLIT TENSION TEST

After calibration with the experimental study, the bonding between the fibre materials with the base matrix is determined and simulated with contact algorithm, and in this section, static split tension test is numerically studied based on the 3D mesoscale model.

Static split tensile test were conducted on cylindrical UHPC specimens with diameter of 75 mm and height of 37.5 mm as shown in Figure 58.



(a) Test setup



(b) Failure specimen

Figure 58: Split tensile tests

In the numerical model, the steel fibre is assumed to be straight in the matrix with a predefined length L and diameter D , the total number of the fibres can be determined based on the fibre volume fraction and fibre dimension. The flow chart for the 3D mesoscale model establishment is shown in Figure 59.

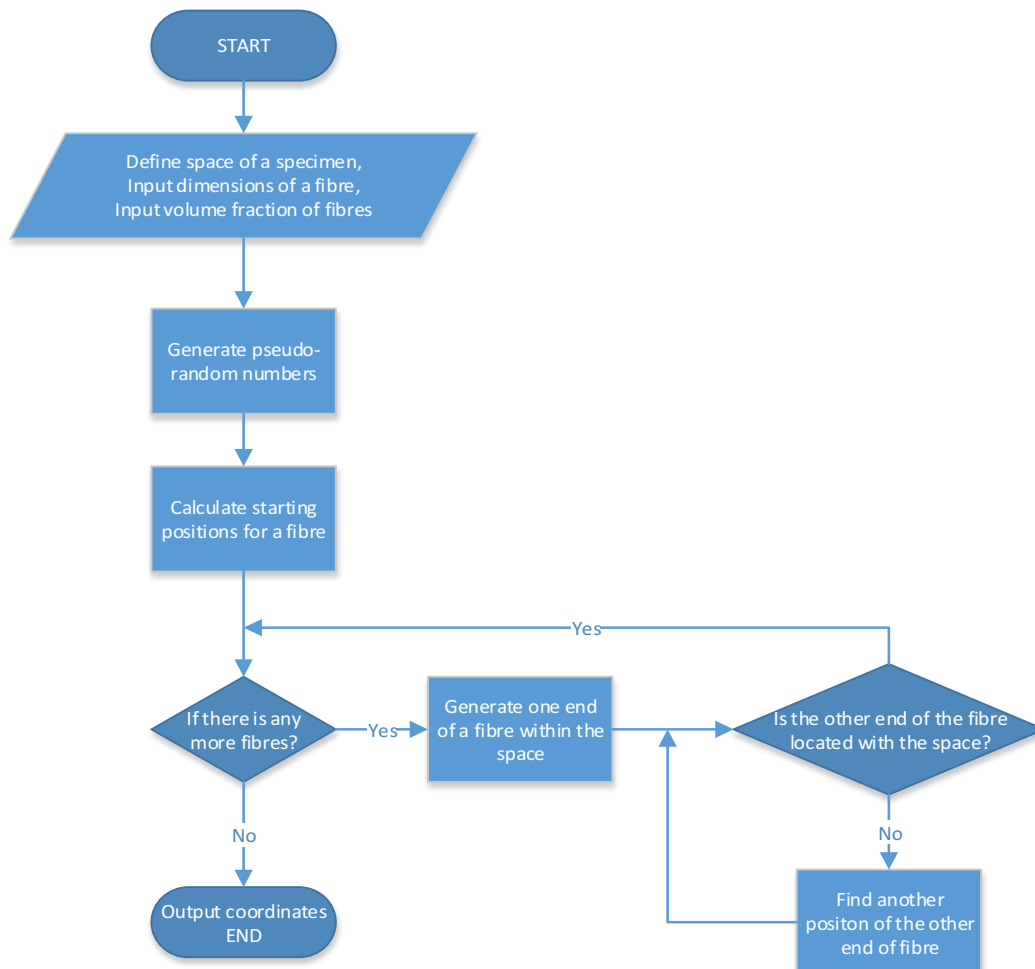


Figure 59: 3D mesoscale model establishment

The established 3D mesoscale model contains 2,664,000 solid elements for concrete matrix and 291,342 truss elements for fibre phase which are determined based on sensitivity analysis.

Comparison of the failure modes between the numerical model and experimental results is shown in Figure 60, and reasonable accurate failure is predicted by the mesoscale model. It is clearly seen that the numerical model not only captures the cracking in the mortar matrix, the bridging effect is also clearly demonstrated by the explicitly modelled steel fibres.

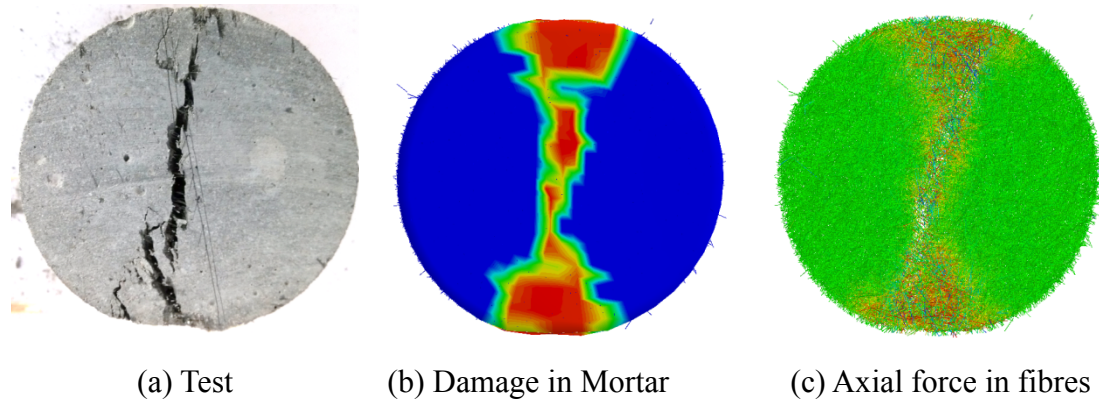


Figure 60: Comparison of the damage mode

Comparing the splitting tensile stress displacement data, it is seen the simulation results collate well with the experimental study, and the peak stress from the simulation is around 22.5 MPa while the average experimental result is around 20 MPa, and the error is 12.5%. The ascending and descending portion of the curves matches reasonably well.

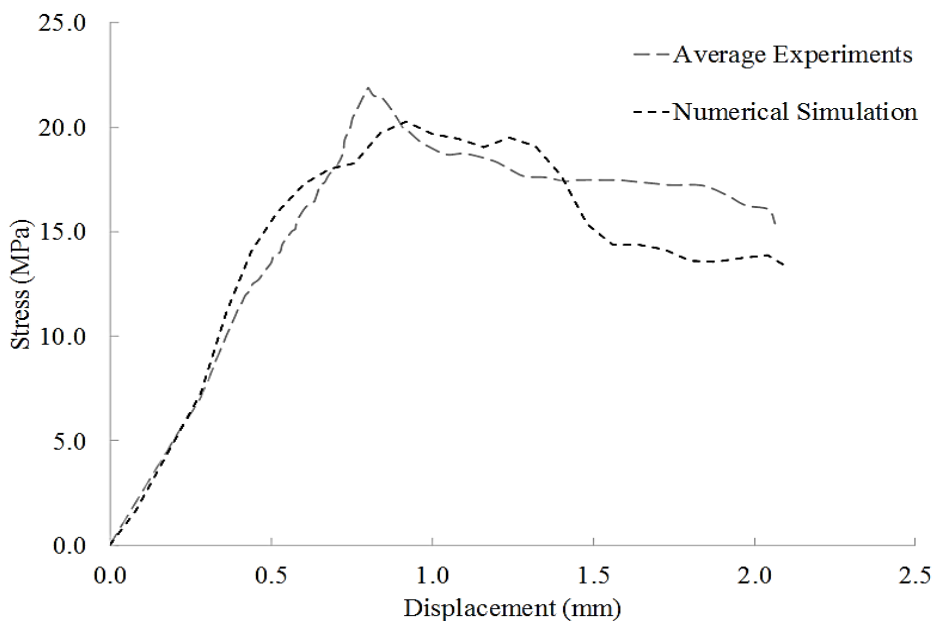


Figure 61: Split stress - Displacement curve

5.4 SPLIT HOKINSON TENSION TEST

Concrete material is strain-rate sensitive, and the reason behind is ambiguous. Ross et al. [35] pointed out that the limiting crack velocity under increased strain rate would lead to an increase in ultimate strength and deformation capacity. Toutlemonde and Rossi [36] attributed the strength gain to an intrinsic viscous stress related to free-water movement within the nanopores instead of the coarser pores initially related to the water-cement ratio of the cement paste. Suaris and Shah [37] correlated the strain-rate effects on the mechanical behaviour of concrete with the microcracking process and proposed an approach using a continuous damage concept. The strain-rate dependence of tensile microcrack growth has also been used by Bischoff and Perry [38] to explain the higher strength and compressive strain observed at high strain rates.

5.4.1 SHPB test setup

In the current study, the dynamic tests were conducted on SHPB test specimens with 75 mm diameter and 37.5 mm height. The experimental systems of SHPB compressive and split tensile tests are sketched in Figure 62. SHPB split tensile test can generate a tensile stress within the specimen by far-end compression, which is easy and convenient in instrumentation.

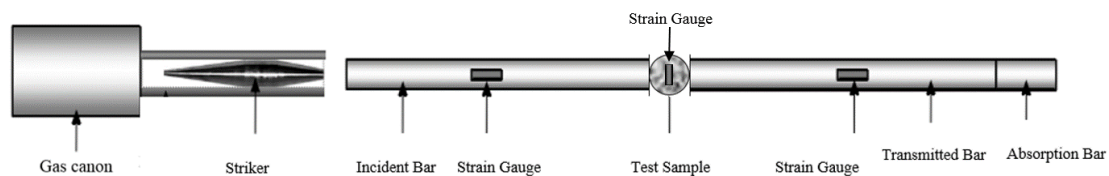


Figure 62: SHPB split tensile test setup

When the striker impacts the incident bar, a one-dimensional compressive stress wave is generated. The stress wave (incident wave) propagates along the incident bar towards the specimen. When it reaches the interface between the incident bar and the specimen, the incident wave splits into two smaller waves. One of them, the transmitted wave, travels through the specimen and into the transmitted bar, causing plastic deformation in the specimen. The other wave, called the reflected wave, is reflected away from the specimen and travels back down the incident bar. Strain gages are then placed on the bars to measure strains caused by the waves. Assuming deformation in the specimen is uniform, the stress and strain can be calculated from the amplitudes of the incident, transmitted, and reflected waves.

The SHPB split tension setup is shown in Figure 63. Both pressure bars in SHPB split tension tests have the same dimension of Ø75 mm and length of 2000 mm and the absorption bar is Ø75 mm and length of 500 mm. Strain gauges are attached at the centres of the pressure bars. The bars are made of stainless steel with Young's modulus 210 GPa, density 7830 kg/m³, elastic wave velocity 5547 m/s, and Poisson's ratio 0.3.

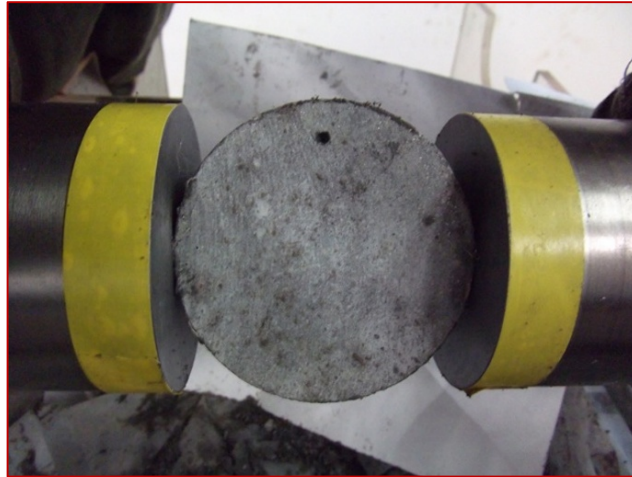


Figure 63: Set-up for SHPB split tension test

Based on the theory of one-dimensional wave propagation, the equation below is used to calculate the stress in the incident bar.

$$\sigma(t) = E \left(\frac{A}{A_s} \right) \varepsilon_T(t) \quad (27)$$

where E and A are the Young's modulus and cross sectional area of pressure bars, respectively, A_s is the cross sectional area of specimen, and ε_T is the measured transmitted strain.

The dynamic tensile force and strength of UHPC specimens in the SHPB tests are calculated by:

$$P = \sigma(t)A_p \quad (28)$$

$$\sigma(f) = \frac{P}{\pi RT} \quad (29)$$

where P is the force applied on the specimen, $\sigma(t)$ the stress in the incident bar, A_p is the cross sectional area of pressure bars, π is a circular constant, and R and T are the radius and thickness of the specimen, respectively.

5.4.2 Numerical study

From the SHPB test, the typical stress-time relationship of UHPC from SHPB split tension test can be obtained.

Previous study had revealed the material dynamic performance of this novel UHPC material, and influence of nano particles and steel fibres are discussed extensively [12, 39]. In the present paper, the focus is numerical simulation of the SHPB split tensile test based on 3D mesoscale model. The numerical model consists of incident pressure bar, UHPC specimen and transmitted pressure bar as shown in Figure 64. The striker bar is not modelled. Instead, the incident dynamic stress generated by the impact of the striker bar is directly applied to the incident bar as a stress boundary. The steel pressure bars are modelled by MAT_RIGID, and the contact between the specimen and pressure bars is modelled by CONTACT_SURFACE_TO_SURFACE with default parameters in LS-DYNA.

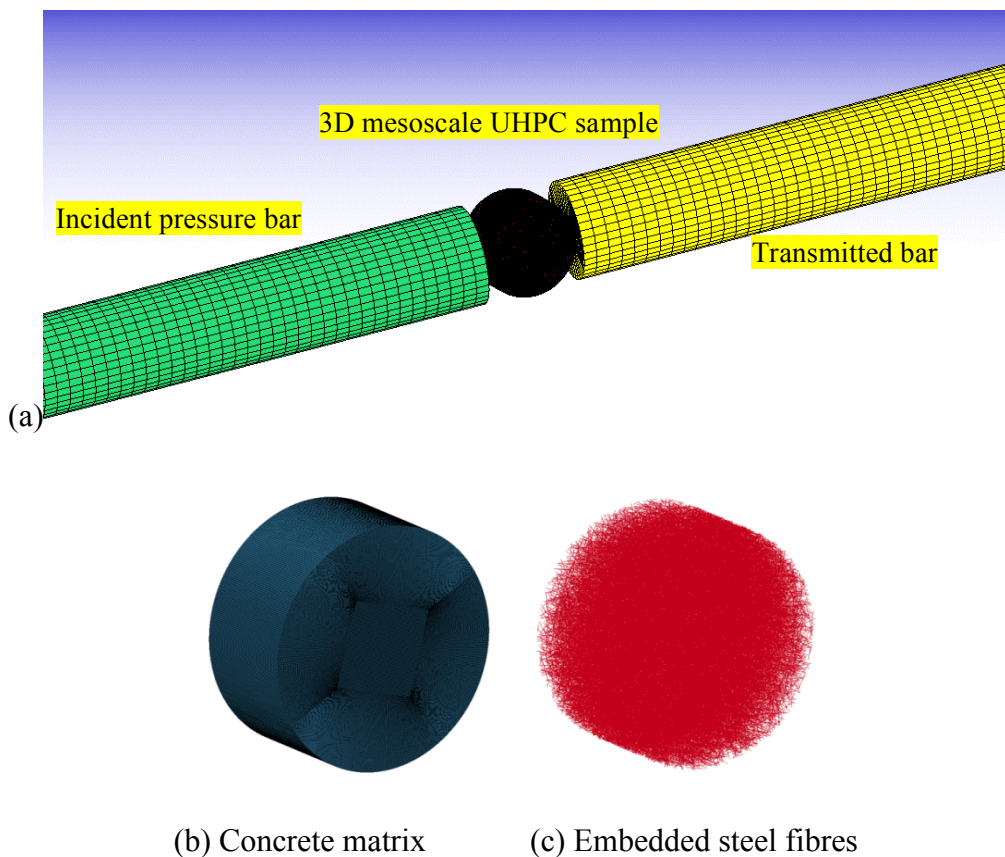


Figure 64: Finite element model of SHPB split tensile test

Adequate modelling of material under dynamic loads requires the information of strain rate effect, The dynamic increase factors of normal strength concrete under tensile loads which are obtained from formulae proposed by Malvar and Crawford [40].

$$DIF = \frac{f_t}{f_{ts}} = \begin{cases} \left(\frac{\dot{\epsilon}}{\dot{\epsilon}_s}\right)^\delta & \text{for } \dot{\epsilon} \leq 1s^{-1} \\ \beta \left(\frac{\dot{\epsilon}}{\dot{\epsilon}_s}\right)^{1/3} & \text{for } \dot{\epsilon} > 1s^{-1} \end{cases} \quad (30)$$

where f_t is the dynamic tensile strength at $\dot{\epsilon}$; f_{ts} is the static tensile strength at $\dot{\epsilon}_s$; $\dot{\epsilon}$ is the strain rate in the range of 1×10^{-6} to 160 s^{-1} ; $\dot{\epsilon}_s$ is the static strain rate 1×10^{-6} ; $\log \beta = 6\delta - 2$; $\delta = 1/(1+8f_{cs}/f_{co})$; $f_{co} = 10 \text{ MPa}$.

For normal strength concrete compressive strength:

$$DIF = \frac{f_c}{f_{cs}} = \begin{cases} \left(\frac{\dot{\epsilon}}{\dot{\epsilon}_s}\right)^{1.026\alpha} & \text{for } \dot{\epsilon} \leq 30s^{-1} \\ \gamma_s \left(\frac{\dot{\epsilon}}{\dot{\epsilon}_s}\right)^{1/3} & \text{for } \dot{\epsilon} > 30s^{-1} \end{cases} \quad (31)$$

where f_c is the dynamic compressive strength at $\dot{\epsilon}$; f_{cs} is the static compressive strength at $\dot{\epsilon}_s$; $\dot{\epsilon}$ is the strain rate in the range of 30×10^{-6} to 300 s^{-1} ; $\dot{\epsilon}_s$ is the static strain rate 30×10^{-6} ; $\log \gamma_s = 6.156 \alpha - 2$; $\alpha = 1/(5+9f_{cs}/f_{co})$; $f_{co} = 10 \text{ MPa}$.

Despite these well-established empirical equations for normal strength concrete, an analogous conclusion from normal concrete to UHPC is not adequate. With the alterations to the material composition, the failure mechanism changes, instead of progressive crack propagation and failure in normal strength concrete, fibre material in UHPC limits and confines the crack initiation and propagation which can significantly influence the inertia effect under high rate loading condition. The low water-cement ratio in UHPC also warrants a much dense micro structure with less porosity (initial defects) and water content.

In the previous study conducted by the author, the rate effect is discussed through experimental study [12]. The results on material tensile strength, in combination with relevant study by other researchers, are presented in Figure 65. The data points within the red circle are the results by the author. Generally speaking, with the increase of strain rate, the strength under tension loading also increases significantly. The increase is less pronounced with increasing concrete strength. It is clearly seen the current material has lower strain rate effect than other concrete.

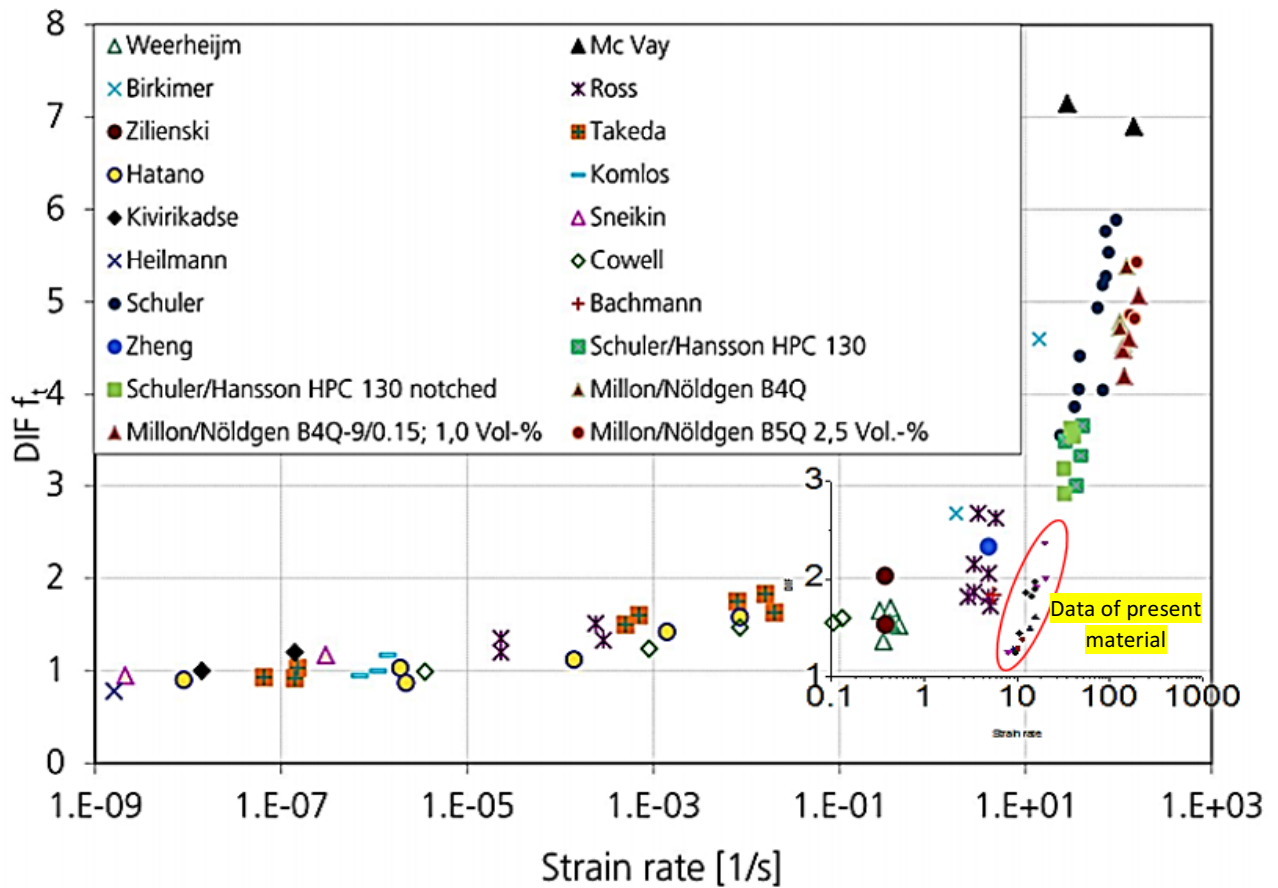


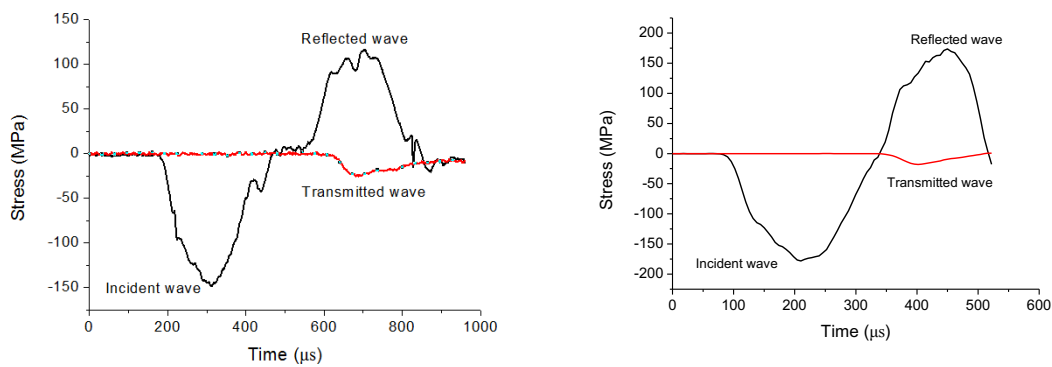
Figure 65: Dynamic Increase Factor (DIF) for the tension strength of different concretes and UHPC in comparison

Material strain rate effect is less prominent under compressive loads, and this conclusion applies to UHPC as well [12]. In the present study, the strain rate effect is considered for concrete phase only in 3D mesoscale model. The strain rate effect on the steel phase is neglected, although steel is also rate dependent material, its rate sensitivity is lower than concrete, and also decreasing with the increase of steel strength. In the present study, steel fibre has an ultra-high tensile strength 4200 MPa, its rate sensitivity is therefore much less than concrete phase which can be neglected. In addition, the previous study reveals that no additional over-proportional increase of DIF between the UHPC specimen with and without fibres [41, 42].

To provide in-depth comparison, homogenised model without modelling the steel fibres is also considered in the current study. Teng et al. [43] and Wang et al. [44] developed homogenised numerical model based on MAT_ELASTIC_PLASTIC_HYDRODYNAMIC to simulate the UHPC members subjected to dynamic loads, and their simulation results showed high accuracy when comparing with the experimental observations. Similar procedures was

also adopted when simulating blast induced UHPC member response [20]. The parameter required for the material model is tabulated effective plastic stress versus effective plastic strain curve which can be straightforwardly obtained from uniaxial compressive tests.

In the tests, two strain gauges were attached on the incident pressure bar and transmitted pressure bar, and the measured stress histories under the applied impulse are shown in Figure 66a. In the 3D mesoscale numerical simulation, stress histories of elements with the same locations as in the test are recorded for comparison, and the results are shown in Figure 66b.



(a) Experiment

(b) 3D mesoscale model

Figure 66: Comparison of stress histories from test and simulation

Figure 67 shows the results of comparison between the 3D mesoscale simulation and test data. In this case study, the strain rate experienced in the UHPC sample is 14.9/s. It can be noticed the stress-time history from the 3D mesoscale simulation coincides well with the laboratory test results, and both the peak value and softening behaviour of the UHPC sample are in good agreement.

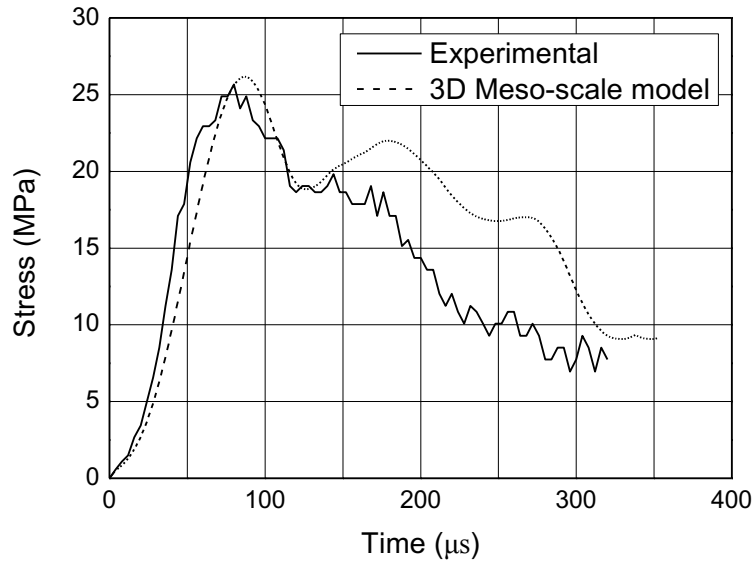
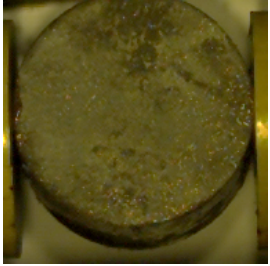
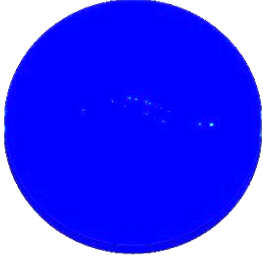
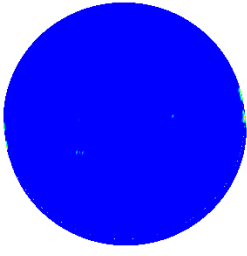
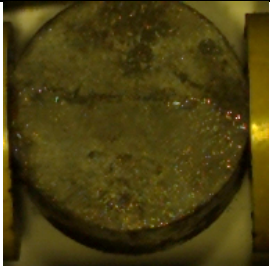
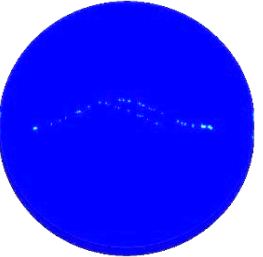
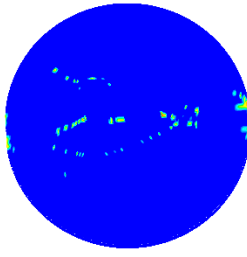
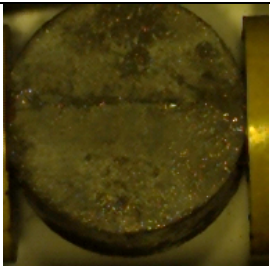
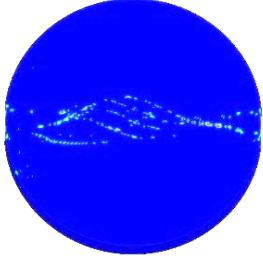
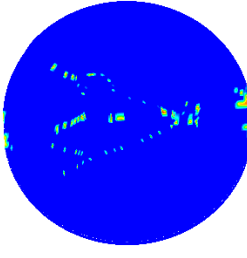
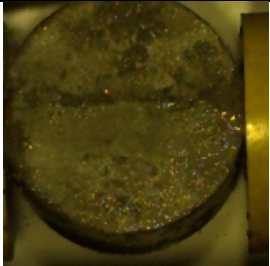
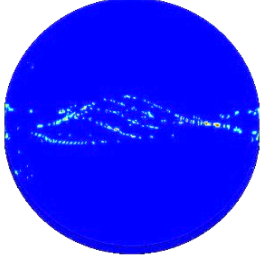
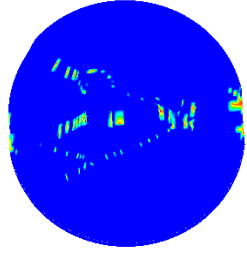


Figure 67: Comparison of stress-time curves obtained in the test and 3D Mesoscale model

In the test, the high-speed camera photography was used to record the developing of crack of the UHPC specimen. The corresponding failure patterns from the test and 3D mesoscale numerical simulation are compared in Table 4. From the comparison of the failure patterns between testing results and simulation, it can be observed that under the same loading condition at the same time, the 3D mesoscale numerical simulation results yield good agreement with the test results in terms of the crack prediction. On the other hand, the homogenised model overpredicts the sample damage although it captures the crack initiation with reasonable accuracy.

The fibre bridging effect can be interpreted by relating the crack propagation with the stress-time history curve as shown in Table 21. With wave propagation in the sample, damage accumulates and crack initiates in middle of the sample and the crack direction is parallel to the wave propagation direction. At time around 75 μs , major crack appears and there is a loss of the dynamic tensile stress, soon after that the stress increases again due to fibres bridging over the cracked parts and provide additional resistance. The fibre bridging effect prevails until the major crack reaches the sample edge at around 155 μs , and in the following stage, fibre bond-slip behaviour dominates the sample resistance. As discussed in the previous sections, after full debonding occurs, pure fictitious load acts on the interface between the fibre and concrete matrix, and this fictitious load deteriorates almost exponentially with the slip.

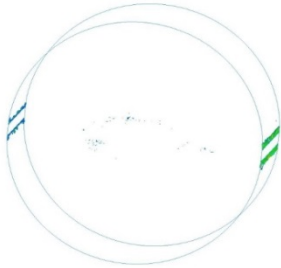
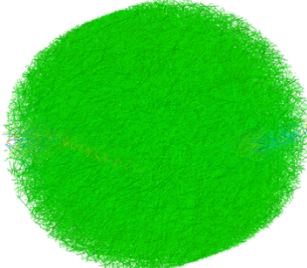
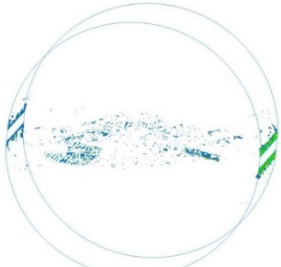
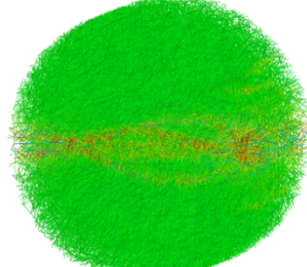
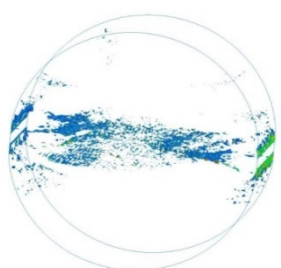
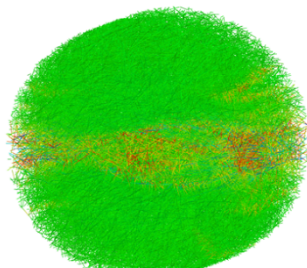
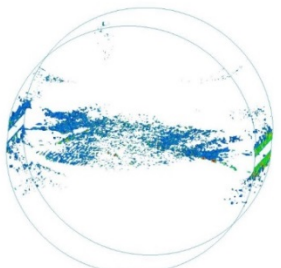
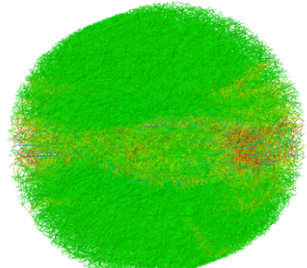
Table 21: Comparison of simulation results with high speed camera observation

Test	Mesoscale model	Homogenised model
 $T = 0 \mu s$		
 $T = 75 \mu s$		
 $T = 155 \mu s$		
 $T = 310 \mu s$		

Closer observation on the behaviours of embedded fibre is shown in Table 22. The contours in the table are axial stress with in the fibre material, and it is noted at the very beginning when micro cracks develop in the concrete matrix, there is no axial stress in the fibres; with the expanding of the microcrack, fibre axial load increases until the maximum pull-out load is reached at $t = 155 \mu s$. With explicitly modelled fibre material, the strain evolution during the dynamic loads can be clearly viewed and analysed. The relatively accurate numerical results

are promising, further study with the validated 3D mesoscale model can help ease the effort experiments which are costly and time-consuming.

Table 22: Crack and axial force development in the numerical model

<i>Cracks in Mortar</i>	<i>Axial force in fibres</i>
 <p>$T = 0 \mu s$</p>	 <p>$T = 0 \mu s$</p>
 <p>$T = 75 \mu s$</p>	 <p>$T = 75 \mu s$</p>
 <p>$T = 155 \mu s$</p>	 <p>$T = 155 \mu s$</p>
 <p>$T = 310 \mu s$</p>	 <p>$T = 310 \mu s$</p>

5.5 CONCLUSION

In the present paper, three-dimensional numerical model, considering the random distribution of steel fibres, has been proposed to investigate the behaviour of UHPC material under both static and intense dynamic loading. Random fibre distribution and orientation is considered in the model development. Fibre interaction with the concrete matrix is studied through single fibre pull-out tests, and the results are used to establish the one dimensional bond-slip contact algorithm in the three-dimensional model. Based on the proposed model, static split tensile test is simulated, and it is noted the proposed model gives good prediction of material behaviour under static load. In the simulation of the SHPB test, results from the proposed model correlate well with the experimental results, while the homogenised model without explicit modelling of steel fibres overpredicts the concrete damage. Compared with the frequently used homogeneous concrete model, the proposed 3D numerical model, considering the random distribution of steel fibres, could predict the responses of SFRC material subjected to intense dynamic loadings more realistically, especially in the post-cracking phase. The dynamic stress-time history curve is interpreted with the aid of the proposed model, and the effect from fibre reinforcement can be clearly viewed in the three dimensional model.

REFERENCES

- [1] A. Naaman, F. Alkhairi, H. Hammoud, *Fiber Reinforced Concrete*, Contract, 100 (1993) 205.
- [2] A.M. Brandt, *Fibre reinforced cement-based (FRC) composites after over 40 years of development in building and civil engineering*, *Composite Structures*, 86 (2008) 3-9.
- [3] A.S. Ezeldin, P.N. Balaguru, *Normal-and high-strength fiber-reinforced concrete under compression*, *Journal of materials in civil engineering*, 4 (1992) 415-429.
- [4] M. Wecharatana, S.P. Shah, *A model for predicting fracture resistance of fiber reinforced concrete*, *Cement and Concrete Research*, 13 (1983) 819-829.
- [5] K. Tan, P. Paramasivam, K. Tan, *Instantaneous and long-term deflections of steel fiber reinforced concrete beams*, (1994).
- [6] V. Gopalaratnam, *Properties of steel fiber reinforced concrete subjected to impact loading*, (1986).
- [7] V. Bindiganavile, N. Banthia, *Polymer and Steel Fiber-Reinforced Cementitious Composites under Impact Loading—Part 1: Bond-Slip Response*, *Materials Journal*, 98 (2001) 10-16.
- [8] W. Suaris, S.P. Shah, *Strain-rate effects in fibre-reinforced concrete subjected to impact and impulsive loading*, *Composites*, 13 (1982) 153-159.
- [9] A. Naaman, F. Alkhairi, H. Hammoud, *MECHANICAL BEHAVIOR OF HIGH PERFORMANCE CONCRETES, VOLUME 6: HIGH EARLY STRENGTH FIBER REINFORCED CONCRETE*, 1993.

- [10] V.P. Dutra, S. Maghous, A. Campos Filho, A. Pacheco, A micromechanical approach to elastic and viscoelastic properties of fiber reinforced concrete, *Cement and concrete research*, 40 (2010) 460-472.
- [11] E. Gal, R. Kryvoruk, Meso-scale analysis of FRC using a two-step homogenization approach, *Computers & Structures*, 89 (2011) 921-929.
- [12] Y. Su, J. Li, C. Wu, P. Wu, Z.-X. Li, Effects of steel fibres on dynamic strength of UHPC, *Construction and Building Materials*, 114 (2016) 708-718.
- [13] K. Holschemacher, T. Mueller, Y. Ribakov, Effect of steel fibres on mechanical properties of high-strength concrete, *Materials & Design*, 31 (2010) 2604-2615.
- [14] R.S. Olivito, F.A. Zuccarello, An experimental study on the tensile strength of steel fiber reinforced concrete, *Composites Part B: Engineering*, 41 (2010) 246-255.
- [15] S.-T. Kang, J.-K. Kim, Investigation on the flexural behavior of UHPCC considering the effect of fiber orientation distribution, *Construction and Building Materials*, 28 (2012) 57-65.
- [16] S.J. Barnett, J.-F. Lataste, T. Parry, S.G. Millard, M.N. Soutsos, Assessment of fibre orientation in ultra high performance fibre reinforced concrete and its effect on flexural strength, *Materials and Structures*, 43 (2010) 1009-1023.
- [17] L. Mao, S. Barnett, D. Begg, G. Schleyer, G. Wight, Numerical simulation of ultra high performance fibre reinforced concrete panel subjected to blast loading, *International Journal of Impact Engineering*, 64 (2014) 91-100.
- [18] Z.L. Wang, L.P. Wu, J.G. Wang, A study of constitutive relation and dynamic failure for SFRC in compression, *Construction and Building Materials*, 24 (2010) 1358-1363.
- [19] J. Li, C. Wu, H. Hao, Investigation of ultra-high performance concrete slab and normal strength concrete slab under contact explosion, *Engineering Structures*, 102 (2015) 395-408.
- [20] J. Li, C. Wu, H. Hao, An experimental and numerical study of reinforced ultra-high performance concrete slabs under blast loads, *Materials & Design*, 82 (2015) 64-76.
- [21] J. Li, C. Wu, H. Hao, Residual Loading Capacity of Ultra-High Performance Concrete Columns After Blast Loads, *International Journal of Protective Structures*, 6 (2015) 649-670.
- [22] Z.L. Wang, H. Konietzky, R.Y. Huang, Elastic-plastic-hydrodynamic analysis of crater blasting in steel fiber reinforced concrete, *Theoretical and Applied Fracture Mechanics*, 52 (2009) 111-116.
- [23] X.Q. Zhou, H. Hao, Mesoscale modelling and analysis of damage and fragmentation of concrete slab under contact detonation, *International Journal of Impact Engineering*, 36 (2009) 1315-1326.
- [24] Y. Lu, Z. Song, Z. Tu, Analysis of dynamic response of concrete using a mesoscale model incorporating 3D effects, *International Journal of Protective Structures*, 1 (2010) 197-217.
- [25] X. Wang, M. Zhang, A.P. Jivkov, Computational technology for analysis of 3D meso-structure effects on damage and failure of concrete, *International Journal of Solids and Structures*, 80 (2016) 310-333.
- [26] Z. Xu, H. Hao, H.N. Li, Mesoscale modelling of fibre reinforced concrete material under compressive impact loading, *Construction and Building Materials*, 26 (2012) 274-288.
- [27] Q. Fang, J. Zhang, Three-dimensional modelling of steel fiber reinforced concrete material under intense dynamic loading, *Construction and Building Materials*, 44 (2013) 118-132.
- [28] J. Li, C. Wu, H. Hao, Z. Wang, Y. Su, Experimental investigation of ultra-high performance concrete slabs under contact explosions, *International Journal of Impact Engineering*, 93 (2016) 62-75.
- [29] Y. Su, J. Li, C. Wu, P. Wu, Z.-X. Li, Influences of Nano-particles on Dynamic Strength of Ultra-High Performance Concrete, *Composites Part B: Engineering*.

- [30] Y. Qing, Z. Zenan, K. Deyu, C. Rongshen, Influence of nano-SiO₂ addition on properties of hardened cement paste as compared with silica fume, *Construction and Building Materials*, 21 (2007) 539-545.
- [31] A. Naaman, G. Namur, J. Alwan, H. Najm, Fiber Pullout and Bond Slip. I: Analytical Study, *Journal of Structural Engineering*, 117 (1991) 2769-2790.
- [32] Q.-S. Yang, Q.-H. Qin, X.-R. Peng, Size effects in the fiber pullout test, *Composite structures*, 61 (2003) 193-198.
- [33] S. Sockalingam, G. Nilakantan, Fiber-matrix interface characterization through the microbond test, *International Journal of Aeronautical and Space Sciences*, 13 (2012) 282-295.
- [34] L. Yang, J.L. Thomason, Development and application of micromechanical techniques for characterising interfacial shear strength in fibre-thermoplastic composites, *Polymer Testing*, 31 (2012) 895-903.
- [35] C.A. Ross, J.W. Tedesco, S.T. Kuennen, Effects of strain rate on concrete strength, *Materials Journal*, 92 (1995) 37-47.
- [36] F. Toutlemond, P. Rossi, Free water in concrete pores: an attempt of physical explanation of concrete dynamic behavior, *Special Publication*, 175 (1998) 261-280.
- [37] W. Suaris, S.P. Shah, Constitutive model for dynamic loading of concrete, *Journal of Structural Engineering*, 111 (1985) 563-576.
- [38] P. Bischoff, S. Perry, Compressive strain rate effects of concrete, in: *MRS Proceedings*, Cambridge Univ Press, 1985, pp. 151.
- [39] Y. Su, J. Li, C. Wu, P. Wu, Z.-X. Li, Influences of nano-particles on dynamic strength of ultra-high performance concrete, *Composites Part B: Engineering*, 91 (2016) 595-609.
- [40] L.J. Malvar, J.E. Crawford, Dynamic increase factors for concrete, in: *Proceedings of the 28th DDESB seminar*, Orlando, FL. ANSI Std.; 1-17., 1998.
- [41] T. Lok, P. Zhao, Impact response of steel fiber-reinforced concrete using a split Hopkinson pressure bar, *Journal of Materials in Civil Engineering*, 16 (2004) 54-59.
- [42] T. Lok, P. Zhao, G. Lu, Using the split Hopkinson pressure bar to investigate the dynamic behaviour of SFRC, *Magazine of Concrete Research*, 55 (2003) 183-191.
- [43] T.-L. Teng, Y.-A. Chu, F.-A. Chang, B.-C. Shen, D.-S. Cheng, Development and validation of numerical model of steel fiber reinforced concrete for high-velocity impact, *Computational Materials Science*, 42 (2008) 90-99.
- [44] Z. Wang, J. Wu, J. Wang, Experimental and numerical analysis on effect of fibre aspect ratio on mechanical properties of SRFC, *Construction and Building Materials*, 24 (2010) 559-565.

CHAPTER 6: CONCLUDING REMARKS AND SUGGESTIONS TO FUTURE STUDY

6.1 MAJOR FINDINGS

This thesis mainly presented experimental investigation and 3D mesoscale analysis of the behaviours of the newly developed ultra-high performance concrete. The major contributions and findings made in this research are summarized below:

- 1) With the same fibre reinforcement, different nano materials additions seem to have insignificant influence on the material dynamic strengths. However, material strength could be increased with the increase of nano material volume dosage. Comparing with the traditional normal strength concrete, UHPC with fibre and nano material addition has less strength increment under the same loading rate when compared with normal strength concrete.
- 2) The increase of fibre length and aspect ratio has positive impact on the material dynamic strength. Fibre volume fraction increase favours the UHPC material performance. In the SHPB compression tests, the micro fibre reinforced UHPC is more sensitive to the strain rate while in the SHPB tensile test twisted fibre reinforced UHPC has higher loading rate sensitivity. Comparing with normal strength concrete, UHPC material developed in the current study has relatively low sensitivity to the loading rate.
- 3) In SEM tests on post-damage UHPC samples, different damage modes at ITZ are identified, XRD and XRF analysis confirmed the filling and pozzolanic effect of nano particles addition. XRD analysis reveals the long term effects on the material strength growth from nano material addition.
- 4) Fibre interaction with the concrete matrix can be simplified as sliding contact in numerical model, and the parameters defining the contact can be obtained from through single fibre pull-out tests. It is seen from the tests results that fibre damage model is largely dependent on the embedding length, with the increasing of fibre embedding length, fibre failure alters from debonding to fracture.
- 5) 3-D mesoscale model with explicit modelling of the fibre phase and interfacial bonding can be used to study the static and dynamic material behaviour. The mesoscale model

provides more accurate results than homogeneous numerical model, and it can be used to generate supplement data for experiment and thus reduce the cost in the tests.

- 6) Field blast test on structural component made of the newly developed material had demonstrated the blast resistant capabilities, and such material has potentiality of wide application in protective design of military structures and important civilian structures.

6.2 FUTURE WORKS

Despite the exceptional material performance, the usage of steel fibre material and nano particles makes the material costly, and the major study on the next stage will further optimize the material compositions so as to improve the cost-effectiveness of ultra-high performance concrete. Moreover, with the consideration of UHPC working under coupling effects of both blast loading and fire, which frequently happen in gas explosion, future study will be conducted on improving the fire-resistance of UHPC to overcome its shortage of spalling failure in fire.